Lincoln University

Te Whare Wānaka o Aoraki

CHRISTCHURCH•NEW ZEALAND

Lincoln University Digital Thesis

SOFTWARE PROJECT ON FRACTURE DYNAMICS OF WOOD

AND ARTIFICIAL NEURAL NETWORK MODEL FOR

PREDICTION OF FRACTURE TOUGHNESS

A thesis submitted in partial fulfilment

of the requirements for the degree of

Master of Applied Science

at

Lincoln University

by Dharmasiri B Dassanayake

Lincoln University

2000

SOFTWARE PROJECT ON FRACTURE DYNAMICS OF WOOD AND ARTIFICIAL NEURAL NETWORK MODEL FOR PREDICTION OF FRACTURE TOUGHNESS

by D.B.Dassanayake

This study focussed on fracture and dynamics in wood using high speed imaging equipment, general and various types of imaging software other than the general equipment such as testing machine and related software. The C++ programming language helped to analyse and calculate data. Recorded fracture processes at experiments were highly valuable as they carry very important dynamic data rather than animation. This study clearly displayed the importance of the crack closure and extensions at fracture, which provided quantitative and qualitative data with the aid of software. Further data obtained from this study on fracture dynamics that combines the physical fracture path and relevant load or stress along the fracture path during its fracturing time events seems to be more important. But the thesis limits the analysis up to quantitative values of physical fracture such as crack length and speed separately analysed with the fracture toughness for crack initiation.

Fracture toughness at crack initiation was modelled using an Artificial Neural Network software package. It was a hard task due to the complexity of the parameters related to fracture. However, a fine model was developed drawing zero weights to about 40% of the input parameters used. The model proved that the linked (uncracked) particles or molecules of wood are highly influenced on fracture and fracture toughness. It agrees with the Weibull's weakest link theory, but changes occur according to the loading configuration used. Therefore the local volume effect as the size effect is hypothesised to distance dependent from the crack plane and the loading plane. The study shows that the fracture effectiveness of the geometry factor of the fracturing member differs according to the loading configuration. In other words, the type of the geometry factor whether the volume or the length etc., is determined by the loading configuration used in the application. Therefore, a requirement of a proper definition or categorisation of loading configuration for fracture is raised at this point. This concept is effectively confirmed by the study in crack dynamics too as it shows the low volumetric effect at high rates of loading while it is high at low rates of loading.

The study has contributed considerable new work to its field. This includes a theoretically and practically sound method of deriving length and speed of individual crack of the bunch of cracks made at any event during the fracture process recorded by a high speed camera followed by a C++ programming module and a Dbase IV database. The data accuracy was very high due to this module and the use of several general and imaging software packages too. There are valuable data left behind that can be used for computer simulation type of studies on fracture. Approximation using Artificial Neural Network method on fracture toughness was also a new method for this study, which provided a very good model.

Key words: Crack Length, Crack Speed, Catastrophic Failure, Duration of Fracture, Uncracked Volume, Network Topology, Network Training, CTDIM, NISD, CDID, GEN, Normalisation.

Contents

LIST OF FIGURES AND TABLES

Figures

Tables

**Forward to My precious daughter
Lakmini Dasssanayake**

in love

Chapter 1:   Introduction

Wood is known to be the only renewable construction material in the world. Fracture in wood beams follows certain paths that depend upon the characteristics of the wood structure made of mainly trachieds and rays in softwood species. Under normal condition a trachied is longer than a ray. Trachieds are axially elongated cells up to 10 mm long depending on the tree, with pointed ends and hexagonal structure. Rays are thinner wall (than trachieds) cells that are radially arranged. Rays are connected to trachieds through pits, which are scattered and they are inherent weak points in the structure. Wood structure has been formed to satisfy biological requirement of a tree. However in the same species the gross structure of trachieds even differs from tree to tree, depending upon how it was grown, how many branches it had, in which soil, and under which environmental or climatic conditions it was grown etc. The degree of weakness at bonds (pits) depends on other properties of wood such as density, moisture content, temperature etc.

Timber is extensively used in New Zealand for various construction purposes, and as a raw material for various products. When loads are applied on timber beam in construction for example, it experiences stresses and strains. Unknown cracks could form due to various changes in the environment, which would affect its structure and subsequently create high stresses and strains at crack tips. Therefore it can result in secondary fracture paths starting from an available crack tip. This path or crack extension or propagation occurs at a critical load level where internal energy is released. This release rate varies with the wood structure and is related to its fracture toughness, which is a measurement of timber strength. The magnitude of this property is determined by geometric and material parameters of wood. Capturing these parameters and modelling fracture strength would be useful for ensuring the safety of wood structure. Since pinus radiata is a widely used wood species in New Zealand, its fracture behaviour was investigated in this study. As can be ascertained from the above discussion, fracture mechanics of wood is a complicated subject due to its natural characteristics and variability compared with human-made materials.

In practical situations, wood beams are placed under loads for longer periods, which then experience conditions, such as forces due to wind, temperature, vibration, humidity and light as well as biological factors such as bacteria and fungi. Weak

bonds or paths in wood structure may provide easy routes for crack propagation under these conditions. Crack initiation which is the initial stage of such propagation, may be the result of a blunting and sharpening processes occurring at a crack tip or a micro crack tip, thereby affecting the elastic potential of wood. In addition to the above factors, the size of a beam is known to influence crack initiation or fracture behaviour in wood. However very little effort in this regard has been so far made on fracture of pinus radiata which is the most predominant residential construction material in New Zealand.

According to the engineering elastic beam theory, cross-sections of a beam remain unchanged (plane) under bending. It means, under applied loading or any other it is assumed that the fibres of cross-section move together without slipping when theories are applied. However shear loading is significant in wood as it has a relatively low shear strength. Another assumption is made on the neutral axis of the beam, which is the symmetrical plane of the beam perpendicular to the applied load in bending. It also remains unchanged according to the assumptions of the theory. Such assumptions may be perfectly applied for smaller beams whereas they may not be valid for larger beams. A load placed for a longer period on a beam may experience deviations in these planes from the original position. Additionally it may get adjusted or learn to adapt to situations that occur within a few years time of the original loading. This implies a possible size effect but it cannot be the only reason for this situation. Fibres in these original axis and cross-sections may displace disturbing their uniformity. Because the cross sections and the neutral axis are defined based on the perfect regular rectangular shape of a uniform beam, the irregular wood structure can affect this uniformity when applying this theory.

Multiscaleability

James Glimm and David H. Sharp of the State University of New York in their article in the Siam News states that the strength properties of a structure are mutiscale (October 1997 Siam News). It says, "At the smallest scale are the defects on the atomic scale such as inclusions, substitutions and vacancies. Macroscopic properties

2

such as strength, toughness, corrosion resistance and electrical conductivity depend crucially on structures at various length scales. The strength of a pure crystal, for example, is typically an order of magnitude greater than the strength of a poly-crystal formed from the same material, while fracture resistance and ductility are much lower. Metals then are inherently multiscale." Hence irregularity in wood structure should call for greater multiscale-ability than metal. This is an indication of the size effect and hints a need for a multiscale approach to study of fracture.

Farid Abhraham of IBM Almaden Research Centre says, "It has been believed that the complex features of fracture are a consequence of imperfections in the material. Some argue that the fracture dynamics may be universal or structure-independent, and that dynamical instability of the crack tip governs the morphology sequence of mirror, mist, and hackle. All these features are unexplained using continuum theory." [Abhraham, F, April – June 1997; 1.1]. His paper points to a requirement for considering microscopic picture of the fracturing process. When all these factors are combined together it requires considering the parallel involvement of many factors influencing wood fracture.

Background

This paragraph initially explains the necessity of the study and subsequently indicates the specific objectives related to fracture propagation and toughness.

A laboratory study was used to investigate the fracture in wood, and to model fracture toughness as well as to study the post fracture behaviour of cracks in wood under loads. The testing methods were developed in order to implement it in the laboratory environment.

Due to the anisotropy of wood structure, it is a difficult task to predict the fracture and post fracture characteristics such as the toughness and fracture path. The continuum theory, on which theoretical fracture formulations are based, assumes that the material in a representative volume is homogeneous; however wood as a heterogeneous material may not follow these assumptions due to variability of material and structural behaviour.

Some of the possible factors that can affect fracture of wood other than crack length are.

- Size
- Loading configuration (Rate of Loading /Duration of load)
- temperature
- Moisture content
- Density
- Young's Modulus
- Grain orientation and irregularity in the member, or knot distribution
- Natural frequency

For a given species used in dry conditions, predominant factors influencing fracture are size and rate of loading. Other factors will have a secondary or much less influence. Accordingly this study focussed on the two major factors, size and rate of loading, while considering other factors within the context of the experiments.

Material strength and fracture behaviour are intended study areas under the proposed experimental scheme. Fracture toughness is known to be a material property, and an expression for it has been derived for isotropic materials and has been extended to orthotropic and anisotropic materials. Under this categorization wood is orthotropic because of its symmetries along radial, tangential and longitudinal directions. However, due to the *variable structure*, fracture toughness is known to be affected by *size* and due to time dependent variability of material properties it can also be affected by rate of loading. Studies on fracture have shown variations in results obtained by different researchers and the results are in argument. For example some results differ from the results of Weibull's theory and experiments (Madsen, B., 1992). This study develops a model for fracture toughness as the strength of a pre-cracked three point bending wood beam relating to the above-mentioned factors (Pederson, Mu et al, 1999).

Fracture propagation and toughness are important in timber construction and design where wood beams are used. Time dependent deformation, known as creep, is a major problem in long term loaded wood beams used in the real world applications. The *rate of loading* tests have been used instead of duration of load (DOL) experiments because it is faster to conduct and can be interpolated into creep

4

situations. DOL experiments incur high costs due to long testing periods. Therefore rate of loading is an important factor in fact finding on creep. Hence the objectives of this investigation were developed as follows.

Objectives:

Specific objectives of the research are to

1. study the influence of size and rate of loading on crack propagation using high speed video imaging and,

2. model fracture toughness for crack initiation using Artificial Neural Network.

1. Study the influence of size and rate of loading on crack propagation using high speed video imaging

Fracture propagation (beyond crack initiation) cannot be expected to occur in a uniform fashion. If the uniformity of fracture propagation of different materials is hypothesised to be mapped onto a line as in figure 1-1, wood might fall in a range in the turbulent side. (U – uniform, T – Turbulent)

M: (propagation behaviour) $\in [0,1] \in \mathfrak{R}$

$$U \underline{\hspace{8cm}} T$$

0   1

wood
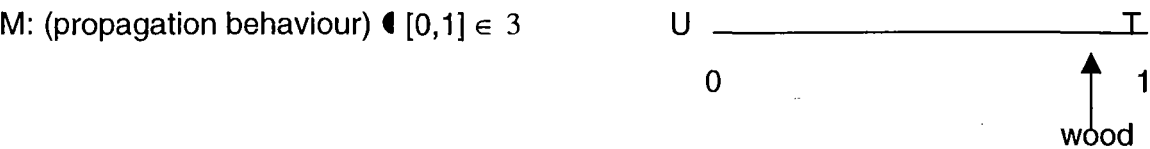
Figure 1-1 Mapping of uniformity of crack propagation

This study investigates the time to reach certain fracture states (defined in chapter 6), and crack speed and influence of size of the specimen and loading configurations on crack propagation. Video camera and a high-speed recording device were used to record the fracture process followed by processing of the images of recorded fracture to obtain relevant data.

2. Model fracture toughness for crack initiation using Artificial Neural Network.

The fracture toughness was investigated using Artificial Neural Networks (ANN). ANN is an advanced mathematical technique that is rich in parallelism and non-linearity, which is useful in establishing non-linear relationships between output data and multitude of input data. ANNs can handle many inputs simultaneously in a parallel manner. They can also be used to study the influence of individual or a group of variables while maintaining other variables constant. For these reasons, ANNs were used to study influence of material and geometric variables on fracture toughness of wood.

Chapters for Discussions and conclusions

Since this thesis consists of two themes in the area of crack dynamics and modelling of fracture toughness using ANN theory, there are two distinct sets of discussions and conclusions pertaining to each output in order to maintain the flow of the text. Therefore it was intended to include discussions and conclusions at the end of each of Chapter 5 and Chapter 8 where results of the two themes are presented.

Reference:

1.1.   Abraham, FE, "Portrait of a crack; Rapid Fracture Mechanics Using Parallel Molecular Dynamics", April – June 1997, IBM Almaden Research Centre.

1.2.   Pederson, MU, Clorius, CO, Damkidle, P, Hoffmeyer, P & Traberg, S., 1999, "Size Effect in Tension Perpendicular to the Grain", Department of Structural Engineering and Materials, Technical University of Denmark, DK 2800 Lyngby, pp. 207 – 214

1.3.   Madsen, B., 1992, Structural Behaviour of Timber, pp 128,129,153, 177, 241

Chapter 2: Literature Review (Crack Dynamics)

2.1 History

Weibull in 1939 assumed that the weak links of a material are uniformly distributed over the volume in order to explain the volume effect on the strength of a material. But he did not consider wood, which was later on, treated as a cracked material. Bohannan in 1966 showed that the Weibull's weakest link theory can be applied to wood. He experimentally showed that the length times depth fits the Weibull's theory better than the volume as the predictor of strength. Barret in 1974 reported on size effect in Douglas Fir while Tak Jee Mou in 1976 did the same on glulam blocks for tension perpendicular to grain. Size effect would differ for different wood species (Reference for this page has been extracted from Madsen, 1982).

Size of a specimen can lead to different fracture effects due to the random distribution of defects in the member. Barrett and Foschi in 1978 cited this effect in a paper presented at the First international conference on wood fracture. Pierce in 1926 who studied cotton yarn and Tucker who studied concrete in 1927 proposed the weakest link theory which originated in statistical strength theory. This concept shows that when a member is subjected to tension, a chain is as strong as its weakest link. In 1939 Weibull showed that the strength of a specimen depends on its volume assuming that weak links are uniformly distributed over the volume. He explained the strength of a weakest link system using an exponential type cumulative distribution. But he did not use wood in his experiments. Johnson in 1953 further improved his theory and Bohannan in 1966 applied the Weibull's weakest link theory to wood for the first time. According to his findings, the strength is best expressed by the length times depth rather than the volume. Barrett in 1974 reported the size effect in clear Douglas Fir specimens in his tensile tests perpendicular to grain and the combined experiments of Foschi and Barrett in 1978 showed the size effect on shear specimens.

Pederson in 1999 explained that the strength depends on height of the specimen rather than volume or height (depth) times length. The influence of volume and the

depth times length effects can be compared in order to analyse which size effect is more relevant in crack propagation.

It was also observed in our study that the Moisture Content (MC) of a specimen was randomly distributed over its surface or volume. Such variation of MC in large members was found to be higher than that for small ones. Distribution of MC can be useful for this study since it is a key factor influencing wood properties.

2.2   Fracture toughness as a requirement for crack propagation

The Linear Elastic Fracture Mechanics (LEFM) is generally applied to investigate and predict the propagation of existing cracks.   The parameter that governs crack tip strength development and crack propagation is termed stress intensity factor K.   The K is derived theoretically and is a material parameter that depends on geometry when dimensions are limited. Considering an elliptical hole of axes of 2a and 2b (a > b) in a rectangular plate (Figure 2-1), the formulae for stresses near the tip of an existing crack have been derived under the assumption a >> b.   From these formulae the following relationship (Equation 2-1) between the remote applied stress (σ) and stress intensity factor K has been derived (Pilkey, 1992).

2a - crack length σ - stress remote from the crack
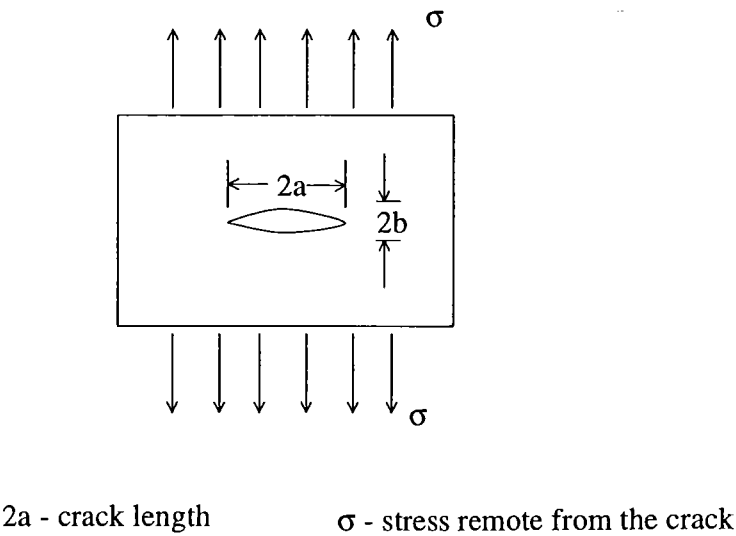
Figure 2-1: Stress applied in a member perpendicular to crack length

$$K = C\sigma\sqrt{\pi a} \qquad\qquad\qquad \textbf{[2.1]}$$

where C = constant based upon the geometry of the crack and the specimen,

K = Stress Intensity Factor

a = available crack length

As the applied stress increases, K reaches a critical magnitude (K_c) and the energy stored in the specimen is released resulting in unstable crack propagation. A flaw may propagate in one of the pure propagation modes or in mixed mode according to the orientation of the existing crack.

Therefore,

$$K \leq K_c \qquad\qquad\qquad \textbf{[2.2]}$$

where K_c - Critical Intensity Factor or **Fracture Toughness**

We intended to investigate fracture toughness of wood beams under three point bending (Figure 2-2). The general equation that calculates K for such a beam made of another material is given in Equation 2-3. We applied this equation to wood beams.

$$K = \sigma\sqrt{\pi a}\,F(\tfrac{a}{b}) \qquad\qquad\qquad \textbf{[2.3]}$$

where

b = height (depth) of the specimen

C = F(a/b), a function of (a/b) is discussed in detail in Chapter 7.

10
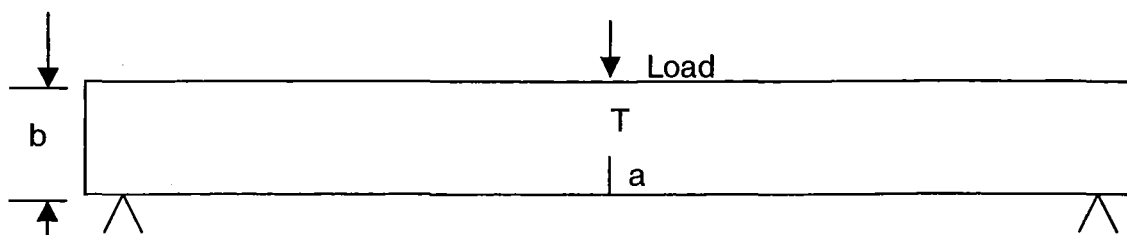
Figure 2-2– Typical bending configuration of a cracked beam: T-showing the line subjected to highest tensile stress

2.3 Duration of Load

Some bending tests carried out for notched and un-notched specimens under various loading conditions have shown important results. To calculate the nominal bending strength researchers have used the reduced cross section for notched specimens and full cross section for unnotched specimens. Those results have shown that no strength loss was observed in notched specimens while un-notched ones showed a reasonable strength reduction as rate of loading decreased. The strength would have been influenced by the stress concentration in the notched ones to maintain a similar strength level under different durations of load.

The time effect associated with rate of loading is more pronounced for wood than for other construction materials. The duration of load and rate loading experiments are time consuming and therefore are costly (Madsen, 1992).

2.3.1. Models developed for Duration Of Load (DOL)

One successful approach is to consider the DOL phenomenon as a form of damage accumulation. A function for accumulated damage can be formed using the initial or previous damage levels. This function based on logarithm or any other exponential form would be a differential equation in time and therefore the numerical values can be adapted in order to fit a set of data such as ramp loading. But some of the models show that the DOL is independent of strength whereas some other have shown that it is strength dependent (Madsen, 1992).

It is a known fact that at constant load, wet wood takes a shorter time to reach a certain deformation than dry wood. According to Nielsen (1978) wood is a cracked viscoelastic material for which the fracture mechanics concepts of wood should be formulated. This concept is referred to as damaged viscoelastic material (DVM). It has been illustrated considering a single crack of initial length $2l_o$ and crack mouth opening of δ_0 at each end of the crack (Figure 2-3). When the load is applied the crack mouth opening δ is increased while the length is left unchanged until time t_s at which δ becomes critical δ_{cr} or given in equation 2.4. This is the stage at which the length of the crack, $2l_0$, starts to increase.

$$\delta_0 < \delta < \delta_{cr}$$ [2.4]

From this starting point, the crack extends until the catastrophic failure occurs at a crack length of $2l_{cr}$ at a very high speed of crack extension satisfying the following.

$2l_0 < 2l < 2l_{cr}$ during t such that $t_s < t < t_{cat}$ [2.5]

t_s = time to crack initiation

t_{cat} = time to catastrophic failure (see Figure 2.3)
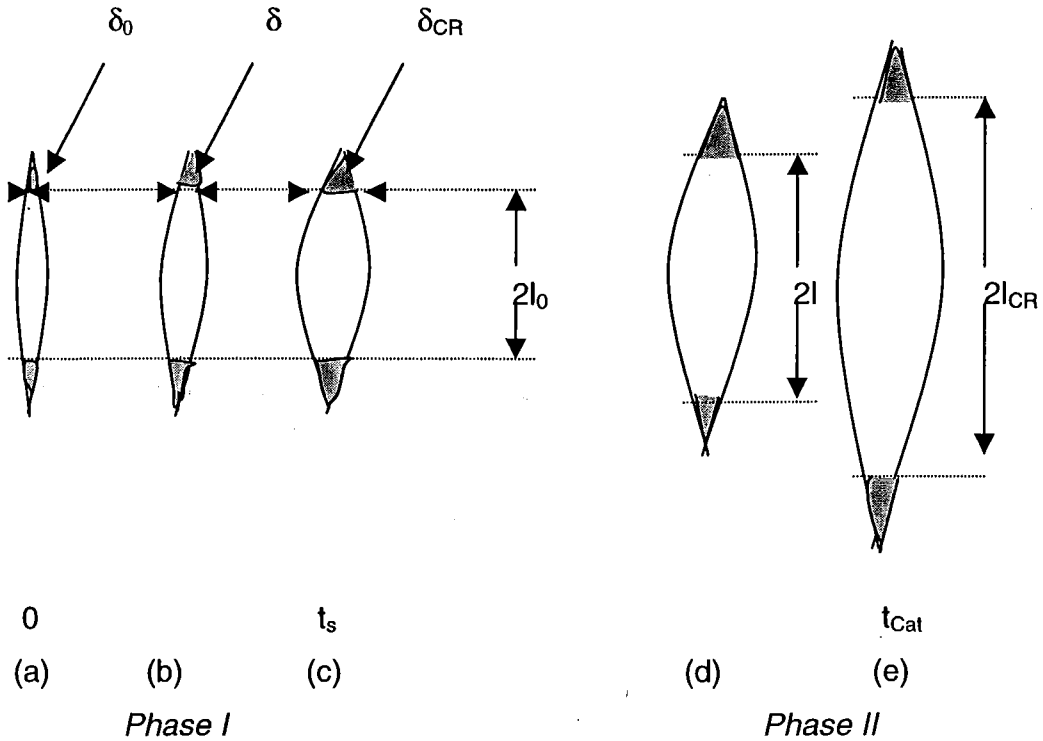
Figure 2-3: Stages of crack extension: Phase 1 – (a),(b),(c) constant crack length 2l$_0$; Phase II – (d),(e) constant mouth width δ_{CR}

High rates of loading are associated with a very short duration of load. Although the standard rates of loading conditions are much different to that of real world conditions these tests are useful because they enable In-Grade testing to be practical and economical. Under loading and environmental conditions in real (commercial) world applications, these tests take very long times and are costly; therefore rate of loading tests are usually not conducted for this reason (Madsen, 1992). Hence, tests are conducted in laboratories and adjust the data to reflect design conditions. Certain test results have shown that the strength is rate of loading dependent, which has been further, concluded by Spencer's experiments (1979). He used one thousand fifty two pieces of 3650x140x38 mm^3 Douglas Fir specimens, which were grouped to assign 8 different rates of loading, and the results are shown in the Table 2.1 and Figure 2-4. Span for all specimens were set to 2.5 m. while the load was applied at different constant rate of loading.
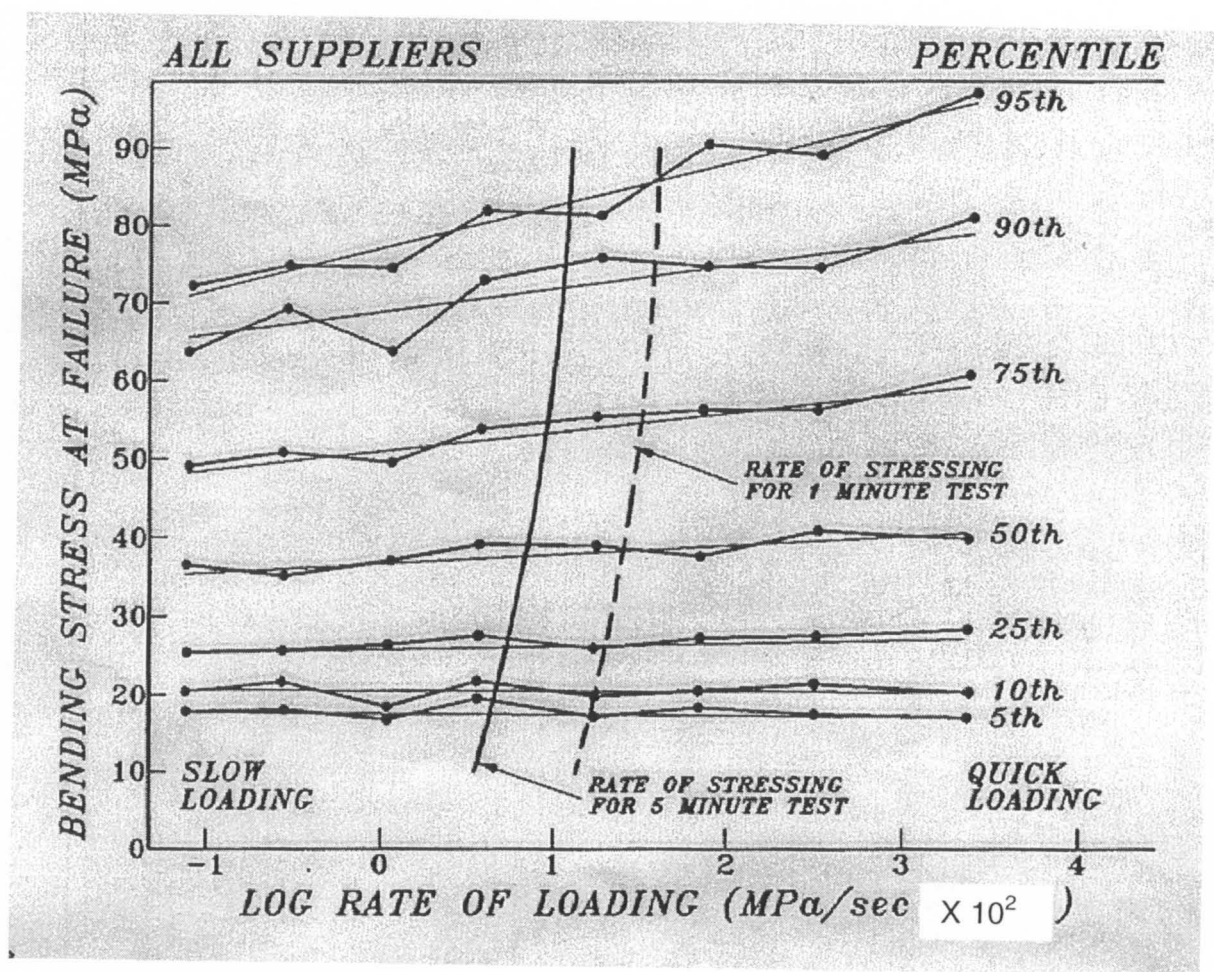
Figure 2-4: – Bending stress at failure vs. logarithm of ROL

Bending stress at failure is plotted against log rate of loading for the quantiles of 5th, 10th, 25th, 50th 75th, 90th and 95th calculated using three parameter Weibull distribution (Equation 2-6) for each rate of loading indicated in the Table 2-1. A straight line is fitted through each quantile plot and it shows very low deviation from this regression in each case. The test result is compared with two lines of standard time to failure levels (5 minutes for ASTM test and 1 minute for In-Grade testing) to assess the difference.

$$f(x_i, \theta, p, \beta) = \frac{p}{\theta} \left(\frac{x_i - \beta}{\theta} \right)^{p-1} e^{\left[-\left(\frac{x_i - \beta}{\theta} \right)^p \right]} \quad , \qquad x_I > \beta \qquad [\,2.6\,]$$

14

where θ - scale parameter (>0)

p – shape parameter (> 0)

β - location parameter (any real number)

Table 2-1 indicates the average times to failure for the specimens of 5th , 50th (mean), and 95th percentiles of the graphs plotted in Figure 2-4.

Table 2-1: Times to failure under different rate of loading

	Rate of Loading kN s^{-1}	Rate of Stressing MPa s^{-1}	Average Times to Failure		
			5th Percentile	Mean	95th percentile
1	222	750	0.22 - s	0.061 – s	0.13 -s
2	11.0	38	0.45 – s	1.2 – s	2.3 -s
3	1.10	3.8	4.9 - s	12 - s	23 -s
4	0.15	0.23	3.5 min	1.4 min	2.7 - min
5	0.015	0.023	6.5 min	14.1 min	27 min
6	0.0025	0.0083	34 min	1.3 hr	2.5 hr
7	0.00030	0.00046	5.0 hr	11 hr	21 hr
8	0.000050	0.000015	33 hr	72.2 hr	130 hr

The above results clearly demonstrate the effect of rate of loading as shown in the Figures 2-5. This plot consists of two parts high stress numbered from 1 through to 4 and low stress numbered from 5 through to 8 in Table 2.1. We plotted the average times to failure as the ordinate and the reciprocal of the rate of stress as the abscissa since straight rate of stress did not give a clear pattern. Notice that at the very high rate of loading, average times to failure in the cases of1, 2 and 3 behave in different a way as we think and in cases 4 through to 8. This could be due to turbulent behaviour displayed at high rates of loading as discussed under 5.7 of Chapter 5.

15
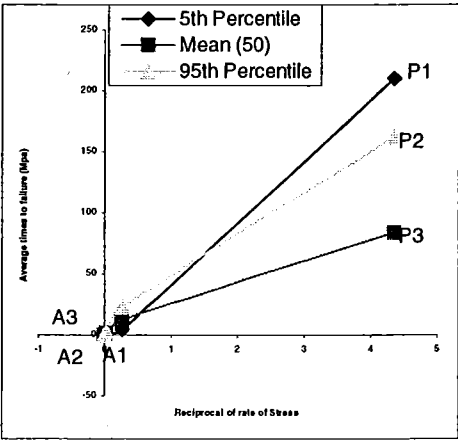
(a) (High stress rates – 1 through 4 in Table 2.1) The pattern of decrement has got changed from (b) below ; ie: low strength member tries to fail rapidly
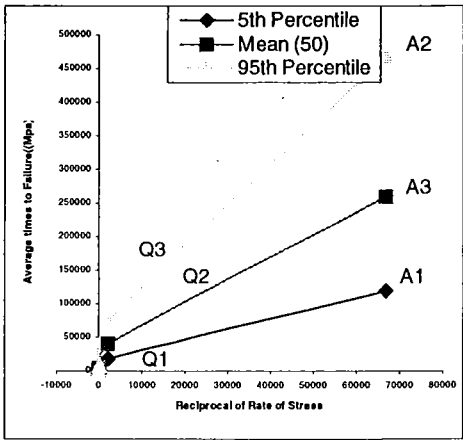
(b)- (Low stress rates – 5 through 8 in Table 2.1) Average Time to failure is rapidly decreased as the rate of stress is increased in high strength member

Figure 2-5: Plot of Average Time to Failure versus Reciprocal of rate of Stress (a) Low Stress (numbered 1-4) (b) High Stress (numbered 5-8)

Figure 2.5 (a) represents the data numbered 5-8 and Figure 2.5 (b) represents the data numbered 1-4 in Table 2-1. A_1P_1, A_2P_2 and A_3P_3 of Figure 2-5 (a) are plot lines, which continue from P_1, P_2 and P3 in Figure 2-5 (a). In other words, $P_1A_1Q_1$, $P_2A_2Q_2$ and $P_3A_3Q_3$ are the plot lines that represent average times to failure related to percentiles shown in Table 2-1. At high rate of loading weaker materials show fast failure and when the rate is low {Figure (b)}, it fails slowly. In case of stronger material the behaviour is vise-versa that is, it fails fast or slow depending on high or low rate.

Maximising the above formula for Weibull distribution (Equation 2-6) using the partial derivatives, estimate of the parameters θ,p,β -, ie: hat values can be obtained (Maximum Likelihood Estimation) as follows.

$$L(\theta, p, \beta) = \prod_{i=1}^{n} \frac{p}{\theta}\left(\frac{x_i - \beta}{\theta}\right)^{p-1} e^{\left[-\left(\frac{x_i-\beta}{\theta}\right)^p\right]} ,$$

[2.7]

The Figure 2.4 shows the regressions of different percentiles of bending strength for the tested specimens. Each data set fitted with relevant regression has shown similar trend indicating very little deviations between regression lines. Increase in rate of loading means decrease in time to failure. Bending strength of commercial timber is normally about 35 MPa and the plots have shown a decisive boundary line of about 25 MPa. This line separates effectiveness of rate of loading on weaker member and the stronger member.

Therefore Spencer (1979) concluded the following.

- Time to failure is strength dependent and rate of loading affects bending strength.

- Strength of a material increases or decreases as rate of loading increases depending on whether its strength is above or below 35 MPa. Therefore he further indicated that establishing the bending stress purely based on rate of loading is trivial.

2.4 Crack propagation with time

A relationship between the velocity of cracks and stress intensity factor obtained from the experiments carried out by Mindness et al (1978) for Douglas-Fir, stressed in tension perpendicular to grain fits the following equation:

$$\ln u = n \ln K_I + \ln A \qquad\qquad [\,2.8]$$

where, u - crack velocity ; n, A - constants

K_I - critical stress intensity factor for opening mode

They found that the algorithm of failure strength versus logarithm of rate of loading followed a straight line with a slope of 1/(1+n) in the experiments of specimens loaded at a constant rate of strain. However, the experiments of Mindess, et al (1978) did not produce results that verified the above equation.

Barrett et al (1978) indicated the following equation for damage rate for creep-rupture (creep is considered as a long duration of load):

$$\frac{d\alpha}{dt} = a(\sigma - \sigma_0)^b + \lambda\alpha \qquad\qquad [\,2.9\,]$$

where

α - current damage; $0 \le \alpha \le 1$; 0 – no damage, 1 – failure state,

($\alpha = 0$ means the virgin state and $\alpha = 1$ is considered rupture)

σ - applied stress ratio,

σ_0 - threshold stress ratio,

a, b, λ - material constants,

$\dfrac{d\alpha}{dt}$ is the damage rate at time t and lower limit of α indicates no damage while upper limit where the fracture follows (Barrett , 1978).

In case of constant rate of loading where the stress is a first degree linear function of t, the stress can be expressed as

$$\sigma(t) = mt \qquad\qquad [\,2.10]$$

where, m – constant.

The Equation 2-9 may be interpolated for rate of loading.

2.5 Size Effect

Weibull's weakest link model computes the probability of failure p_f of the volume v which is given by a 3 parameter equation as follows [Barrett D, 1978]:

$$p_f = 1 - e^{-\int_v \left[\frac{(\tau - \tau_0)}{m}\right]^k dv} \qquad\qquad \textbf{[2.11]}$$

where m, k and τ_0 are material constants.

p_f is computed over the volume v where a local value of stress distribution is such that $\tau \geq \tau_0$ (ie: τ_0 is the local minimum strength).

Take an unrealistic zero value for τ_0 to simplify the model. Thus it becomes,

$$p_f = 1 - e^{-\int_v \left[\frac{\tau}{m}\right]^k dv} \qquad\qquad \textbf{[2.12]}$$

If we consider two volumes V_1 and V_2 and assumed that both have equal probability of failure based on uniformly distributed stresses τ_1 and τ_2 over local volumes of V_1 and V_2 respectively, it should satisfy the following equation:

$$\int_{V_1} \tau_1^k dV_1 = \int_{V_2} \tau_2^k dV_2 \qquad\qquad \textbf{[2.13]}$$

therefore there is a possible existence of a value of τ^* over a unit volume (V = 1) such that:

$$\int_{V_1} \tau_1^k dV_1 = \int_{V_2} \tau_2^k dV_2 = [\tau *]^k$$

or $\qquad\qquad\qquad\qquad\qquad\qquad\qquad\qquad\qquad$ **[2.14]**

$$\int_V \tau^k dV = [\tau *]^k$$

for a volume V.

When the distribution τ is normalized with the function $\Phi(x,y,z)$,

$$\tau = \tau_M \phi(x, y, z) \qquad\qquad \textbf{[2.15]}$$

where τ_M - stress parameter

(ie : τ_M may be maximum bending stress or maximum shear stress in case of elementary beam theory.).

19

By substituting (2-15) into (2-14)

$$\tau_M^k \int_V \phi^k(x,y,z)dV = \left[\tau^*\right]^k$$

[2.16]

The integral in Equation [2.16] can be expressed as follows using a numerical model such as the finite element method or using stress distribution:

$$\int_V \phi^k dV = I(k)V$$

[2.17]

Substituting Eq. 2.17 into 2.16,

$$\tau_M = \beta \frac{\tau^*}{V^{\frac{1}{k}}}$$

[2.18]

where $\beta = \left[I(k)\right]^{-\frac{1}{k}}$

which is dependent on stress distribution.

Therefore the normalized value of parameter τ_M is volume dependent under the prescribed assumptions (in spite of Bohannan's findings about length times depth) .

The maximum bending stress is highest in the bottom surface of a beam in three point bending configuration. If there is a crack in the middle plane of the span the highest tensile stress occurs in the lowest un-cracked line (see Figure 2.2).

The bending moment normally varies along the length of the beam; therefore, stress also varies accordingly. Moreover for a given section through the depth of the beam, stress varies in relation to the distance from the centre to the point of interest. Therefore the probability of coincidence of the weakest spot and the maximum bending stress of a beam is low compared to a tension member where tensile stress is uniform through the thickness (Madsen 1992). Therefore, the tension member in which, the whole volume is stressed is weaker than the bending member. It was incorrectly assumed earlier that the tension and bending strengths are equal. According to this, the length effect seems to be a considerable factor than width and the height. Although Madsen (1992) has indicated only the length effect, the weakest

20

spot may be found in the three dimensional location of the beam and therefore it may not be the position that experiences a very high stress.

Pederson et al (1999) suggests the height as the size effect instead of volume for tension perpendicular to grain. It has not been clearly indicated how the difference was identified. The paper explains how the strength perpendicular to grain is calculated using the weakest link theory as in the following formula. The strength x over the local volume V in a member is,

$$x = x_0 \left(\frac{V_0}{V} \right)^{\frac{1}{k}} .$$ [2.19]

where x_0 – known strength of a strength distribution of volume V_0

   k – shape parameter of 2 parameter Weibull distribution for weak spots and is calculated from the Equation 2.20 below..

Probability distribution function $F_v(x)$ of weak spots over the volume is defined such that

$$F_v(x) = 1 - e^{-v \left(\frac{x}{\delta} \right)^k} ,$$ [2.20]

where δ - scale factor.

   from which k is to be calculated for equation 2-19.

Nevertheless they have observed and argued against this weakest link theory and showed that the strength was influenced by height instead of volume for the planks they used under tension perpendicular to grain as shown in Table 2-2. The following chart shows the mean values extracted from the paper for four different heights in their study.

Table 2-2: Results of Pedersons et al (1999) – Shown mean strength against height for each set of planks they used.

Height (mm)	Mean Strength (MPa)	Standard Deviation
25	3.5	0.4
45	2.7	0.3
70	2.1	0.4
130	1.6	0.2

The paper shows that the double logarithmic plot [log(strength) vs log(height)] provides a good empirical fit to the raw data with good correlation R^2 of 0.86. It also shows that there is a large size effect for small clear specimens. The weakest link theory of strength-volume relationship has not been explained by the results of their experiments.

It indicates the failure occurs at the *event the maximum stress reaches the critical value of the material*, which is a material constant, whereas *it is the mean stress to reach a critical value* that is described by the *Weibull's theory*.

The former (authors') $\sigma_{max} = f(\sigma_{mean}, \Gamma, \nabla)) \rightarrow \sigma_{cr}$ [2.21]

Where, σ_{mean} - applied mean stress

The latter (Weibull's) $\sigma_{mean} = f(\Psi, V) \rightarrow \sigma_{cr}$ [2.22]

Where Γ - stiffness orthotropy

∇ - geometry

Ψ - strength distribution

V – volume of the specimen

$\rightarrow$ - symbol indicates reaching

The paper argues if the failure occurs due to randomly distributed weak points, the location of the failure cannot be predetermined. Therefore the paper suggests

replacing the volume with a constant value and to use the deterministic maximum stress failure criterion. It concludes that the strength decreases as the height increases using its maximum stress failure criterion (equation 2.21) and cylindrical orthotropy.

But the authors say in the paper that they have kept all parameters constant except the height of the specimen. Therefore their findings are not reasonable enough to argue for them to make suggestions to replace the stochastic volume dependent strength with a constant and also there is no basis to argue that the strength is height dependent rather than volume.

2.6   Standard barrier

ASTM standard on fracture mechanics indicates the span to depth ratio as well as pre-crack length. Madsen (1982) says that very few researchers have deviated from the standard test methods in order to research on size effect and used a constant ratio of length to depth so that the size effect was not highlighted.

Reference:

2.1 Madsen, B., 1992, Structural Behaviour of Timber, pp 128,129,153, 177, 241.

2.2 Foschi, RO, Folz, BR, and Yao FZ, 1989, "Readability based design of wood structures", Structural Research Series Report 34, Department of Civil Engineering, University of British Columbia, Vancouver, Canada, P.282.

2.3 Spencer RA, July 1979, "Rate of Loading Effect of Bending for Douglas Fir "First International Conference on Wood Fracture:, Proceedings Forinteck Canada Corp., Vancouver, Canada pp. 282.

2.4 Pederson, MU, Clorius, CO, Damkidle, P, Hoffmeyer, P & Traberg, S., 1999, "Size Effect in Tension Perpendicular to the Grain", Department of Structural Engineering and Materials, Technical University of Denmark, DK 2800 Lyngby, pp. 207 – 214.

2.5 Bandara, DMD, Samarasinghe, S & Mackenzie, D, 1999, "High Speed Video Imaging to Study effect of Volume and Speed of Testing on Fracture Dynamics of Wood", Proceedings of Pacific Timber Engineering Conference Rotorua, New Zealand, pp 300 - 307.

2.6 Barrett, D. and Foschi, R.O., 1978, On the application of brittle fracture theory, fracture mechanics and creep-rupture models for the prediction of the reliability of wood structural elements, First International conference on Wood Fracture, pp 1 - 37.

2.7 Mindess, S., Madison, B., and Barrett, J.D., 1978, Rate of loading and duration of load tests on Douglas-Fir in tension perpendicular to the grain; First International conference on Wood Fracture, pp. 143 - 157.

2.8 Nielsen, L.F.,1978, Crack Failure of dead-, ramp- and combined-loaded viscoelastic materials, First International conference on Wood Fracture, pp. 187 - 200.

2.9 Irnov; Y.M., 1978, Evaluation of long term bearing capacity of wood structures by their performance under short term loading, First International conference on Wood Fracture pp. 63 - 71.

2.10 Abraham, FE, 1997, "Portrait of a crack; Rapid Fracture Mechanics Using Parallel Molecular Dynamics", Journal of IEEE Computational Science and Engineering, IBM Almaden Research Centre, pp. 66 - 77.

Bibliography:

2.11 Pilkey, W.D., 1994, "Linear Elastic Fracture Mechanics and Applications", Chapter 7, Formulas for stress , strain and structural matrices.

2.12 Kerchof, F, 1978, "Wave Fractographic Investigations of Brittle Fracture Dynamics", Institut fir Festkorper Mechanik der Fraunhoper-Gesellschaft e. V. D, pp. 3 – 35.

2.13 Bassani JL, 1988, "Mechanics of Damage, Crack Growth and Life Prediction Under Creep Conditions", Journal of Material Science and Engineering, Elsevier Sequoia Science Ltd., pp. 115 – 123.

2.14 Tay, TE, Yap, CM,Jay CJ, 1995, "Crack Tip Notch Plastic Zone Size Measurement by the Laser Speckle Technique", Engineering Fracture Mechanics, Vol 52, No. 5, Elsevier Science Ltd., pp. 879 – 893.

2.15 Zhimming YE, and Ayali, ML, 1994, "Prediction of Crack Propagation in Anisotrophic Solids", Journal of Engineering Fracture Mechamics vol 49, No. 6, pp 797 – 808.

2.16 Borjen, Y, and Schniewind, AP, 1992, "Elasto-Plastic Fracture Mechanics of Wood Using J-Integral Method", The Society of Wood Science and Technology, Wood and Fibre Science, 24(3) pp 364 - 376.

2.17 Madsen, B., Structural Behaviour of Timber, 1992.

Chapter 3 Methodology

3.1 Introduction

The preparation of specimens including crack length, equipment and technical requirements needed for experimentation and the procedure are explained in this chapter. Further the data captured by the experiments is categorised into three groups in order to ease the process of data handling.

3.2 Specimen selection and equipment used

Test methods were developed in order to

- Record the process of crack propagation and extract distance and velocities in crack propagation process.
- Study the effect of rate of loading, specimen size, crack length and moisture content on fracture dynamics and toughness.

Specimens were prepared from kiln dried wood from a log of a NZ Pinus Radiata tree aged 29 to 30 years, grown on Lynton Downs of Kaikoura in the southern soil of New Zealand. Tests were carried out on a sophisticated testing machine SINTECH 30/D controlled by computer software, which is the major testing equipment used in these experiments. The supporting experimental resources are as follows.

- A high-speed frame capturing camera HSC 250x2 of JC Labs. Inc. and high speed recording device (SVHS Panasonic AG 5700 video cassette recorder) and a monitor.
- A camcorder (Ikegami HC240 camera) mounted with MSF758 lens that captured near crack tip images, and a video monitor.
- Image capturing and digitizing hardware and software installed on a computer
- Two light sources to focus on length-height faces of specimens.
- a wrist watch and a stop watch which read up to 0.01 s.
- Supporting beds and rollers
- Load applicators, and
- Sharp edged knives specially made in order to make proper crack tips in order to maintain high accuracy of experimental data.

3.3   Preparation of Specimens and loading configuration

As the size effect is a major variation that has to be looked into, four sizes were selected as tabulated below. Dressed beam specimens were pre-cracked with a band saw (Figure 3.1), and crack tips were sharpened by knife-edges. The following tables indicate the entire organisation of specimens used for experiments. Table 3.1 describes the size (length * height * width), span length, number of batches and number of specimens in each batch, crack length and the ratio of the crack length to height.

Table 3.2 shows the allocated rates of loading (ROL) configuration over each batch i (i = 1,2,3). ie: The specimens in each batch, labelled from 1 through to 8, 9 through to 13 and 14 through to 17 were categorised into three groups of rates of loading 2.5, 10.0, and 0.625 mm s^{-1}, respectively.

Table 3-1: Sample Sizes and Crack Lengths

Sample Type	Sizes (mm) (L - 40) x H x W	Span (mm) L	No. of Samples			Crack Length a (mm)	a/H
			Bch 1	Bch 2	Bch 3		
A	1040 x 90 x45	1000	17	17	17	41	0.46
B	640 x54 x27	600	17	17	17	25	0.46
C	340 x 27 x13.5	300	17	17	17	13	0.48
D	190 x 13.5 x6.75	150	17	17	17	6	0.45

Table 3-2: Distribution of specimens of each batch over rate of loading

ROL (mm/s)	2.5	10.0	0.625	Total
Sample Type				
A	(1 - 8)	(9 - 13)	(14 - 17)	17
B	(1 - 8)	(9 - 13)	(14 - 17)	17
C	(1 - 8)	(9 - 13)	(14 - 17)	17
D	(1 - 8)	(9 - 13)	(14 - 17)	17
No of specimens	32	20	16	68

A,B,C and D represent size category of the specimens. An excess 40 mm from the span length of each specimen was allocated for the provision for supports. There were 17 number of specimens organised in each of the 3 batches, totalling 51 for each size. The intended ratio of crack length/height averaged to be just above 0.45 for all specimens.

L - Span, H - Height, W - Width, a - Crack length
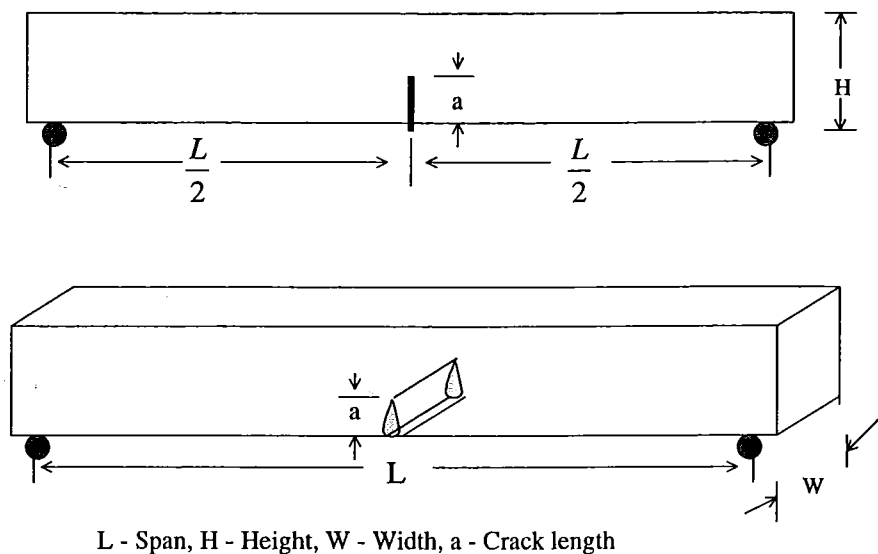
Figure 3-1 Sample and Crack Configuration

It can be noticed that ratio of H/W was maintained to be 2 in all specimens. ALL specimens were stacked in the laboratory environment for several months before making cracks. All specimens were uniquely coded for ease of identification.

3.4 Crack length

After the initial free drying, cracks were made at the centre of the bottom surface as shown in Figures 3.1 and 3.2. A machine saw blade was used to make a pre crack and a sharp knife-edge made the crack tip conform to ASTM standards $0.45H \leq a \leq 0.55H$ (ASTM standards, 1995).

The final crack length was as in the Table 3.1 for each specimen size and the maximum knife-edge cut was about 2 mm. The a/H was selected to be 0.46 in this study, in order to avoid practical difficulties with the smallest specimen size.

Knife edge cut ⟶

Saw blade cut ⟶

$$0.45 \le \frac{a}{H} \le 0.55$$
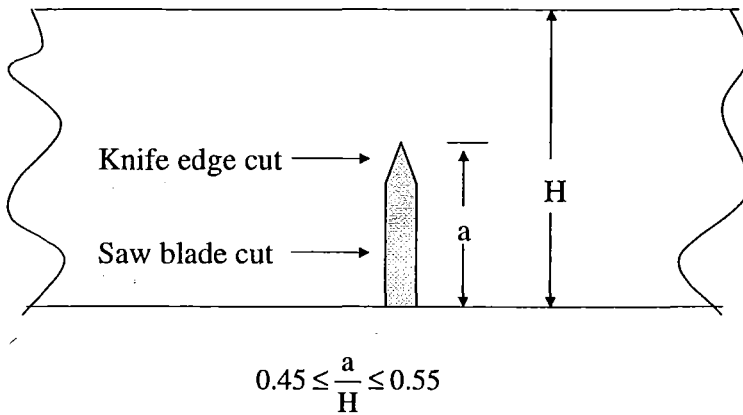
Figure 3-2: Crack dimension: 0.45 H ≤ a ≤ 0.55 H

3.5 Moisture contents and conditioning

Moisture content of the specimens was intended to reflect interior normal conditions of a building. One batch from every size category (17 specimens from each size totalling 68 pieces) was placed in an environmental chamber conditioned to 20°C at 8.2% moisture content for about 3 months. The conditions in the chamber were monitored using a wet and dry bulb thermometer and found to be in proper order. The other two batches were placed in the normal interior laboratory conditions but care was taken to prevent over drying (wrapped in plastic) in order to avoid possible damage to the specimens.

3.6 Supports

Two smooth rollers on a test bed provided the simply supported test apparatus that can be adjusted to provide 1000, 600, 300 and 150 mm spans. The rollers that rotate freely were axially fixed on to the roller supports and no marks were found at any

support locations of specimens after each test. The bed was made to provide a full view of the deformation of the specimen. Similarly the roller supports can be moved and fixed along the bed to provide other span lengths using bolts and nuts and relevant holes as in Figure 3.3. Four load applicators in cylindrical form were made one for each size, according to the ASTM standard (1995) specifications for wood so that radius of curvature of the applicator is one and a half times the depth (height) of the specimen.
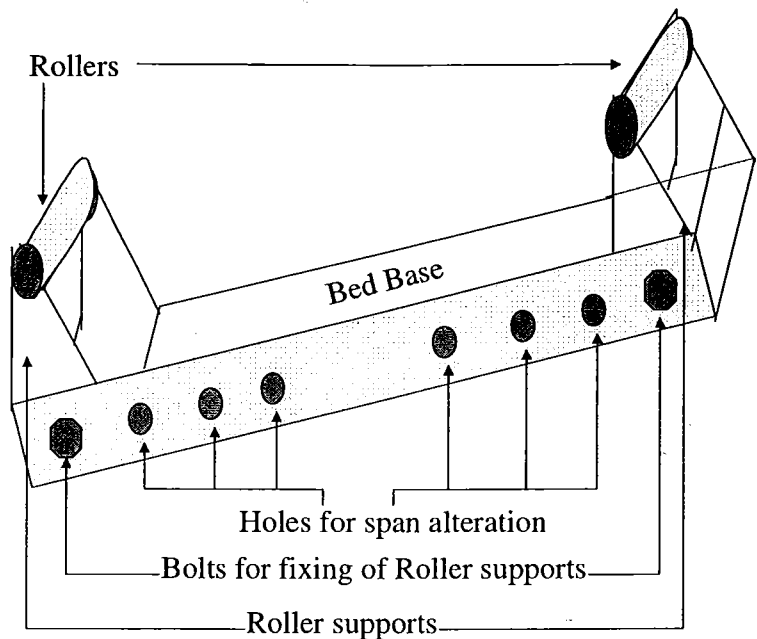
Figure 3-3 Bed, roller supports and rollers to simply support beam specimens

3.7   Experimentation

Experimental data were categorized into three major groups as follows:

- **CTDIM**: Crack Tip Displacement Image Data,
- **NISD**: Non-Image Static Data, and
- **CDID**: Crack Dynamic Image Data

We simply call them data objects and detail them as below.

CTDIM: Information about images of the near crack tip deformation under loading, ie: Data captured by the camcorder video camera.

NISD: Static data such as crack initiation load, catastrophic fracture load, Young's modulus,. ie: Data captured manually and by testing machine.

CDID: Fracture dynamics data, ie: information such as crack length, crack speed etc. extracted from the recorded fracture processes captured by the high speed video camera (These data were collected from batch 1 only).
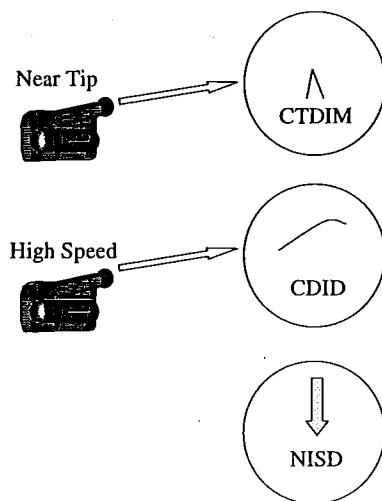
Figure 3-4: Categories of data obtained from experiments (definition of data objects)

3.7.1. Data capturing procedure

Figure 3.5 shows the schematic diagram of the experimental set up and Figure 3.6 shows a photograph of the physical test set up. The bending tests were carried out on the material testing workstation controlled by computer software and provided a part of NISD data. Simultaneously the above noted high speed camera, that coupled with SVHS video cassette recorder and was set at the speed of 200 frames per second, recorded the entire fracture process (CDID) while the other CCD camera captured near tip large still images (CTDIM). This particular high-speed camera has got a capability of recording up to 400 frames per second.
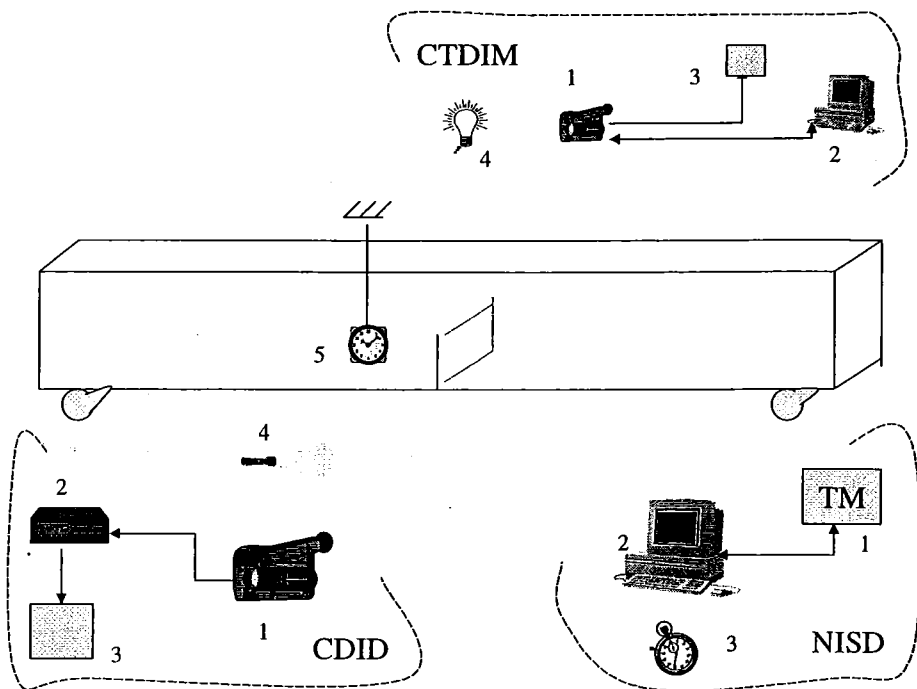
Figure 3-5: Experimental Set-up

The equipment set up in Figure 3.5 shows the three data capturing categories explained earlier and highlights equipment in each of these categorised objects.

Table 3-3: Resources used for capturing data under the specified data object

Equi. No.	CTDIM	CDID	NISD
1	Camcorder Camera	High Speed Camera	Testing Machine (TM)
2	Computer with ICSH	SVHS Recording Device	Computer with MCSH
3	Display Unit	Display Unit	Timer (0.01 s units)
4	Light Source	Light Source	
5		Hanging Timer (0.01 s units)	

ICSH   – Image capturing software and hardware

MCSH – Machine Control Software and Hardware
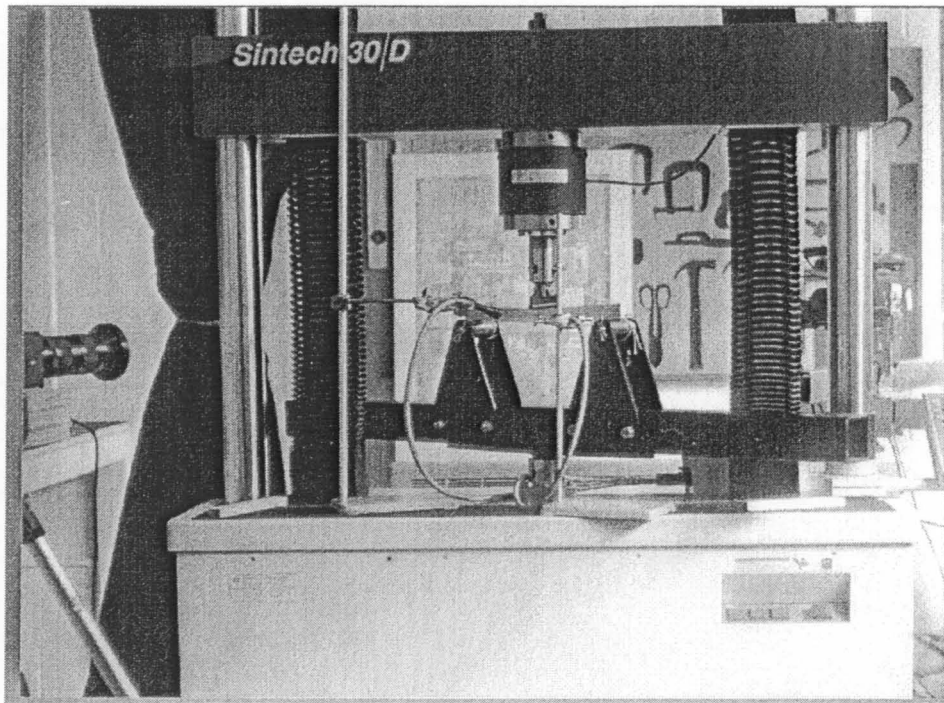
Figure 3-6: Pictorial View of the real experimentation. The high-speed camera focuses on the loaded sample from front while camcorder focuses from back; axis of both cameras and the crack plane of the sample are aligned with each other.

Figure 3.5 shows a specimen placed on the rollers and the cameras placed in line through the crack plane and focusing on crack surfaces of the specimen. Crack tip area was speckled with black spray paint to obtain a random light intensity pattern required by processing still images. Two light sources illuminated both sides of the crack surfaces to support image capture. As the load was applied the L1 (CDID 1) camera recorded the entire process of the fracture of every sample while L2 (CTDIM 1) camera was capturing near tip still images. A 0.01s accurate electronic watch (CDID 5) presented fracturing time as part of the recorded image. The testing machine software captured the real time graphical presentations of the load versus time/extension with relevant stress and strain data (NISD). The following classical flow chart represents the experimental procedure taken.
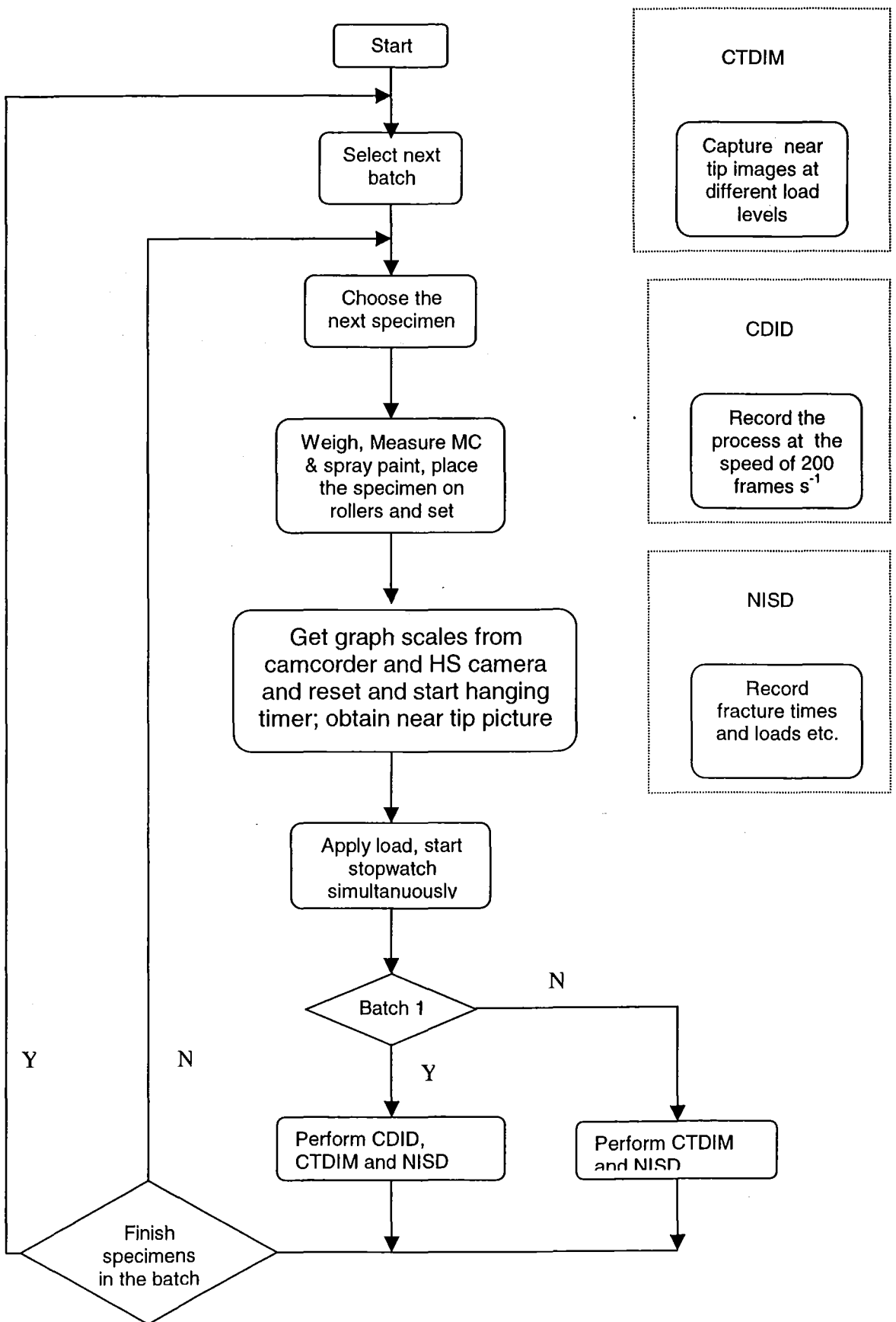
Figure 3 - 7: Procedure chart for experimentation

34

3.8 Practical problems and solutions

3.8.1. Time confusion

SVHS videotapes were used to record fracture processes. There was a total of 68 processes to be recorded for 68 specimens and we faced some practical problems while recording. The picture capturing speed of high-speed camera was set to 200 frames s^{-1} (f s^{-1}). And the accuracy of time display was 0.01 s, which means that the camera can capture 2 frames during the smallest displayable time interval. For this reason there were two consecutive frames that indicated the same time.

3.8.2. Determination of light intensity

Since the camera speed used for fast image capture was much higher than the frequency (50 Hz) of the power supply, the online process of fracture was not visible through the monitor. Hence setting up of light intensity for the intended frame capturing speed was hard and it resulted in capturing of blurred pictures. The following action was taken to minimise this technical problem.

- Set the camera speed to 60 f s^{-1} which is the highest available visible state and set the light intensity.
- Reset the speed to 200 f s^{-1} and continue experiments.

Still the light intensity set for the speed of 60 f s^{-1} was not suitable for 200 f s^{-1}. After all there was no alternative other than gaining experience and guessing the intensity that helped this setting. In some cases the light intensity, was either too bright or too dark to read the time digits although the picture was very clear. Hence some recordings were discarded due to the invisibility of time. Setting of lighting was not a problem for still image capture.

3.9 Summary

The chapter provided description of the experimentation covering the preparation of specimens, crack lengths, equipment and procedure. The organisation of data started at this experimentation level. Finally practical problems faced were described briefly.

Reference:

1. ASTM standards, 1995, E 1290 – section 7.1.2 - page 869.
2. ASTM standards, 1995, Loading block for wood D 3043, page 410

Chapter 4 Data Capture and organisation

4.1 Introduction

We discussed in detail the development of the following three data categories in the previous chapter.

- **CTDIM**: Crack Tip Displacement Image Data,
- **NISD**: Non-Image Static Data, and
- **CDID**: Crack Dynamic Image Data

In addition to these data categories, an additional data object is defined here in order to include the other relevant data because only the experimental data was categorised in Chapter 3.

Definition of new data object GEN

GEN = {data specific to specimen exclusive of NISD, CTDIM and CDID}

GEN has been incorporated of measurements such as density, moisture content, crack length, grain orientation and weight etc. of specimens.

This chapter basically explains the data extraction procedures for the GEN, NISD and CDID objects. The CTDIM data is not intended to be used in this thesis but will be used in a separate study. Extraction of the data related to GEN and NISD is not difficult but CDID is a long and complicated process. In addition to the methodology described in Chapter 3, this extraction falls into post-experimentation especially in extraction of CDID data. Technical information pertaining to computing this data is explained under the following CDID data extraction.

4.2 CDID extraction

Tapes containing images captured by high-speed camera were played-back and important still images (between 20 - 100 images and one graph scale image per specimen) at required events were captured using a multimedia imaging software. Subsequently, measuring the length of cracks appearing in these still images at

37

appropriate time events, was performed using MS Paint imaging software, followed by the author developed C++ programs to handle the database for verification and calculation purposes.

4.2.1. Resources used

- A computer installed Vedium Movie clip multimedia software and relevant hardware (Videum Capture 1998: video capture of Winnov multimedia program)
- SVHS video player
- MS Paint
- MS Excel
- Borland C++
- Dbase IV database

4.2.2. Procedure

01. Study tapes carefully until it reaches near crack initiation.
02. Capture still images before initiation and continue capturing through to the end of selected fracture process.
03. Use recorded graph scale to calculate conversion factors f_x and f_y for rows and columns, respectively. Suppose y_s mm is represented by p_y pixels vertically and the x_s mm is represented by p_x pixels horizontally on the graph recorded, then scale parameters are,

$$f_x = \frac{x_s}{p_x} \text{mm pixel}^{-1}$$

[4.1]

$$f_y = \frac{y_s}{p_y} \text{mm pixel}^{-1} \qquad .$$

[4.2]

04. Analyse each still image using MS Paint and obtain the readings according to the following format. (Readings are presented in Appendix A)

Table 4-1: Format of the data sheet used for crack dynamics (CDID)

Sample No	Pict. No	Time (Hanging) M	S	D	Crack No	Side1 Col	Side1 Row	Side2 Col	Side2 Row	Manual Time	Tip Col	Tip Row
*	*	*	*	*	*	*	*	*	*	*	*	*

The columns of the data sheet are as described below.

* Sample No. – Unique Specimen code given ie: AA9999

        AA   – Size code / two alpha characters

        First 99   – batch number (08,12,20 represented 1,2,3)

        Second 99 – running number (01 – 17) in the batch

* Picture No. – Identification number of the still image, which is a running code, tagged to the Sample No.

* Time (MSD) – Display of hanging timer: M-minutes, S-seconds, D–decimals.

   •   *The following text explains information about the newly generated crack due to load application*

* Crack No – A99; ie: A – **Left/Right** (Boolean), 99 – crack number under L/R.
* Side 1 Col and Row – (side1 co-ordinates of a crack) – (x1,y1) (see Figure 4.1)
* Side 2 Col and Row – (side2 co-ordinates of a crack) – (x2,y2)

(x2,y2)

(x1,y1)
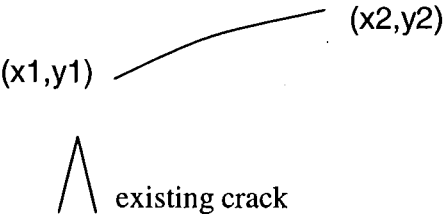
existing crack

Figure 4-1: Crack co-ordinates in pixels and this particular crack has been generated on the Right of the existing crack

* Manual Time – Time indicated by the stopwatch. (00:00 is the absolute load starting time therefore it calibrates the hanging timer which indicated the relative time.

For example,

Hanging timer	Manual timer	Load
02:50:25 (170.25 s)	00:00:00 (0 s)	Start
03:11.88 (191.88 s)	00:21:63 (21.63 s)	at a certain point

(Notice that both time differences between two events are the same. This means that load starting point of the hanging timer is 170.25 s. This is useful for calculation of time to reach fracture states.)

* Tip Col and Row —co-ordinates of the tip of the pre-crack.

4.2.3. Measuring crack length over time and crack speed

There can be several cracks developed in the member until it fails but the first crack $A_1{}^1B_1{}^1$ (see Figure 4.2) starts at time t_1. Suppose j^{th} crack A_i^j B_i^j at time t_i extended to A_{i+1}^j B_{i+1}^j at time t_{i+1} and the jth crack has started at the time t_k ($k \leq i$). Therefore the crack length of this j^{th} crack for $t < t_k$ is 0. The event diagram Figure 4-3 illustrates the crack development of the jth crack between times t_i and t_{i+1}. Co-ordinates of pre-crack tip at the two instances are $(x_{i,0}^j, y_{i,0}^j)$ and $(x_{i+1,0}^j, y_{i+1,0}^j)$, respectively.

$\underline{i^{th}\ event\ at\ time\ t_i}$

A_i^j $\qquad$ B_i^j

$(x_{i,0}^j, y_{i,0}^j)$

$A_i^j = (x_{i,1}^j, y_{i,1}^j)$
$B_i^j = (x_{i,2}^j, y_{i,2}^j)$

$\underline{(i+1)^{st}\ event\ at\ time\ t_{i+1}}$

B_{i+1}^j

A_{i+1}^j

$(x_{i+1,0}^j, y_{i+1,0}^j)$

$A_{i+1}^j = (x_{i+1,1}^j, y_{i+1,1}^j)$
$B_{i+1}^j = (x_{i+1,2}^j, y_{i+1,2}^j)$
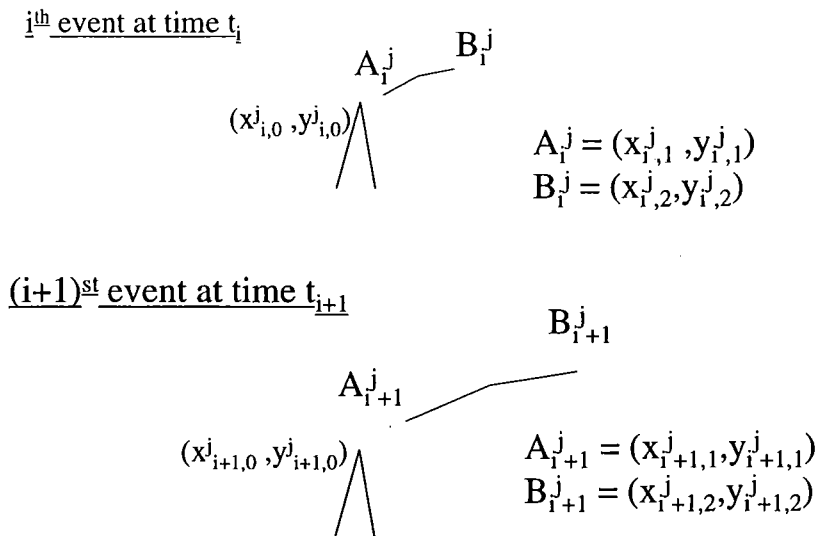
Figure 4-2: Event Diagram - illustrates crack development with time

$$l_i^j = \sqrt{f_x^2 \left(x_{i,2}^j - x_{i,1}^j\right)^2 + f_y^2 \left(y_{i,2}^j - y_{i,1}^j\right)^2} \qquad \textbf{[4.3]}$$

$$l_{i+1}^j = \sqrt{f_x^2 \left(x_{i+1,2}^j - x_{i+1,1}^j\right)^2 + f_y^2 \left(y_{i+1,2}^j - y_{i+1,1}^j\right)^2} \qquad \textbf{[4.4]}$$

where f_x and f_y are scale convertion factors.

If c = crack development from time t_i to time t_{i+1},

$$c = l_{i+1}^j - l_i^j . \qquad \textbf{[4.5]}$$

Note: if there was a reasonable bend in the crack between any AB stage, it was considered as two cracks separating at the bent.

4.2.3.1 Time to crack initiation

Two time events i = i_{int} - 1 and i+1 = i_{int} can exist that satisfy the following equations for crack lengths.

ℓ_i^j = 0 and $\forall$ j for a certain i $\in$ { {0} $\cup, \angle^+$ }

at least one value for single j exists such that $\ell_{i+1}^j \neq$ 0.

and the event $t_{i_{int}}$ is crack initiation time. Therefore the time to crack initiation t_{ci} is given by the following (consider k = 0)

$$t_{ci} = t_{i_{int}} - t_0 . \qquad \textbf{[4.6]}$$

where t_0 is the time at the start of load application.

The value t_0 was extracted from the graph drawn by the testing machine computer software and compared with the manually measured t_0 (using stopwatch) to obtain the proper t_0 value. The manual time is helpful only for the cases where many breaking points (failure) appear in the graph. The most suitable graphical time was taken as t_0 by comparing the manually measured time. Typical examples are shown in the Figures 4-4, 4-5, 4-6 for the three rates of loading studied.

4.2.3.2 Crack length and the speed

Net crack length has been calculated as the total lengths of the cracks at time t. This calculation started at the time of crack initiation and the net crack length is zero at the time just before crack initiation.

This means

$$\sum_j l_i^j = 0 \text{, at } t < t_{i_{int}} \qquad\qquad [\,4.7]$$

$$\sum_j l_{i+1}^j \neq 0 \text{, at } t \geq t_{i_{int}} \qquad\qquad [\,4.8]$$

The developed crack is calculated as in Equation 4.5. Then the net crack length developed during time interval [t_i,t_{i+1}] becomes,

$$c_i = \sum_j l_{i+1}^j - \sum_j l_i^j \qquad\qquad [\,4.9]$$

Therefore the net crack speed during the same time interval $\Delta t = t_{i+1} - t_i$ is calculated by

$$s_i = \frac{c_i}{\Delta t} = \frac{\sum_j l_{i+1}^j - \sum_j l_i^j}{t_{i+1} - t_i} \qquad\qquad [\,4.10]$$

These equations have been utilised to create a module in C++ programming environment to manipulate the data arranged in Dbase IV for calculating the net crack length and the net crack speed at time t_i. The measurements of individual crack development as in these equations are not presented here which can be extensively used for a simulation of fracture propagation. (Therefore the equations and calculation methods required only for the information presented in this thesis are furnished).

42

Assumption made: All cracks were connected at a given time t according to the weakest link concept so that any crack development with more than one crack is also inter-related.

4.2.3.3 Distance between the initial crack and the available pre-crack tip

Consider the crack tip co-ordinate (x_0, y_0) and the crack initiation. There is low probability of generating more than one new crack simultaneously at the event of crack initiation. Therefore the following procedure was used to calculate the distance between the original crack tip and the ends of the new crack and thereby to find close end of the new crack to the existing crack. Take the initial new crack end co-ordinates to be $(x^1_{1,1}, y^1_{1,1})$ and $(x^1_{1,2}, y^1_{1,2})$.

- Compare and find i (i =1,2) corresponding to the minimum $\min\left\{\left(x^1_{1,1} - x_0\right)\left(x^1_{1,2} - x_0\right)\right\}$.

- Calculate the distance using,

$$\sqrt{f_x^2\left(x_i - x_0\right)^2 + f_y^2\left(y_i - y_0\right)^2} \,. \qquad \qquad [\,4.11\,]$$

4.3 GEN data

GEN data contained weight of specimens, crack length, density moisture content and grain pattern. Weight and crack length were straight forward measurements. In the following sections, method used for measuring density, grain orientation and moisture content are explained. Immediately after each test, two pieces were cut off from every specimen and weighed on an electronic balance.

4.3.1. Density

One of the above pieces was dipped in melted paraffin to make a thin coat to make it waterproof. A beaker about half-filled with water was placed on the zeroed electronic scale. The paraffin coated wood piece was dipped into water and pushed carefully until it entirely got submerged in water and reading of the balance (u) was recorded. Ratio of raw weight (m_d) to u is the specific gravity of wood and it was multiplied by 1000 to calculate the density in SI units (kg m^{-3}).

4.3.2. Moisture content

4.3.2.1 Oven dry method

The other piece (weight m_w) was placed in the oven set at 110^0C for 24 hours and then weighed (weight m_o). The percentage of moisture content was calculated by

$$\left(\frac{m_w - m_o}{m_o} \right) x100 \qquad\qquad [\,4.12]$$

4.3.2.2 Direct measurement of moisture content (using hygrometer)

In addition to this method a hygrometer was used to measure the moisture content over the surface of the specimen volume just before placing the specimen on the test bed rollers. The advantage of this method is that it shows the moisture distribution over the volume when measured systematically. Sixteen readings were collected on one height-length surface of the largest specimen while four readings were collected from one side of the smallest one. Reading for other specimens were taken proportionately. But only the result based on the oven dry method was used in modelling fracture toughness.

4.3.3. Measurements of Grain pattern

It was observed that the fracture occurs along the grain. Therefore the *face angle*, *grain angle* and the curvature of the growth ring were used as a measurement of grain pattern. Consider the following grain orientation depicted in Figure 4.3.

XY   - section of a growth ring on the cross section ABCD

OX = OY = r - radius of the growth ring; (assumed grain is circular)

O   – Centre of the growth ring (pith)

XQR – tangent at X

YQP – tangent at Y

If 2γ = $\angle$ XQY and 2a = XY (chord length)

$$\Rightarrow \quad \text{curvature} \quad \frac{1}{r} \approx \frac{\cos \gamma}{a} \qquad\qquad [\,4.13]$$
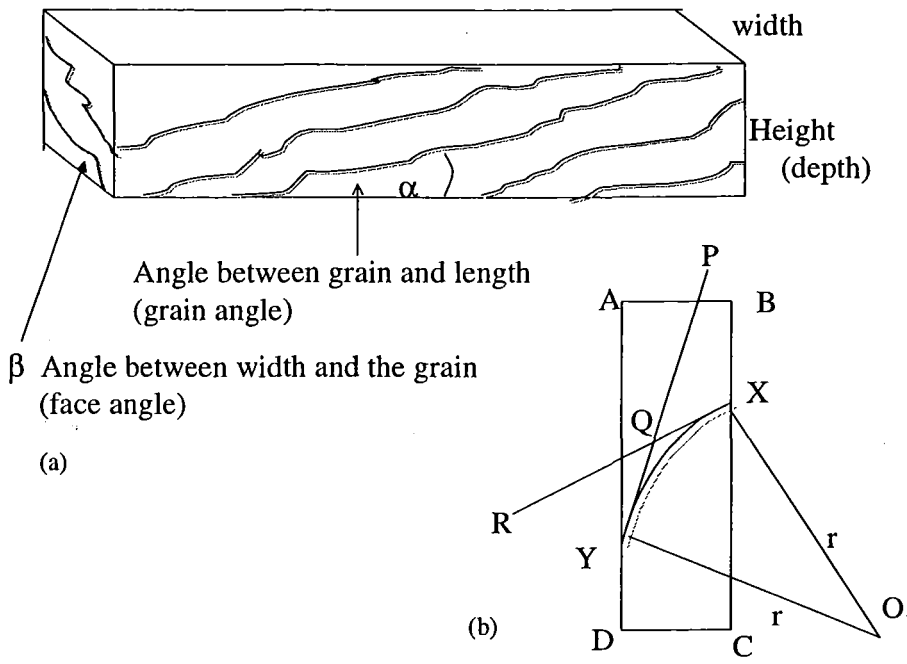
Figure 4-3: (a)Typical grain orientation of a beam, (b) tangents drawn at points X and Y of growth ring XY on cross section ABCD; O is the centre of the ring or pith.

4.4 NISD

Only the required data capture is explained here although there are more data that can be extracted from the results. The following are the variables required for every specimen.

- Time to crack initiation
- Time to catastrophic failure
- Load carried at the crack initiation
- Load carried at the catastrophic failure
- Peak load carried
- Young's modulus

The computer connected to the testing machine drew a graph of load versus time or extension for each specimen. Most important graph was load versus time, which showed the time to failure states accurately. This was better than the time recorded manually using a stopwatch. Therefore manually recorded times were only used to verify the graphically obtained time data. Time to crack initiation read from the graph was especially used to determine the load starting time of the hanging timer so that the time of load application on this hanging timer was calibrated (see Figures 4-4, 4-5, 4-6).

As the load is applied on the beam it demonstrates certain uniformity with the extension. But at crack initiation the load drops and deflection increases. For these reasons a bend is found on the chart at this event of Failure State. The time was noted down as the time to crack initiation and corresponding load was read as the load carried at this event. Similarly, the catastrophic failure event was noted down manually as well as from the machine generated plot at the point at which there is no load on the beam. Practically there is a huge load drop at this event. In some cases, there were more than one such event but most suitable one was selected. Similar to the case of crack initiation, catastrophic fracture load and time to fracture were noted down.

Peak load was taken down from the graph as well. When two suitable points are marked within the elasticity range in the plot and made it default, computer software calculates Young's modulus for every specimen.

4.5   Rate of loading

This variable can be set using the testing machine software to obtain the rates shown in Table 3.2. The Figures 4-4, 4-5, 4-6 show plots from three specimens tested at the rates of loading of (ROL) 2.5, 10.0 and 0.625 mm s^{-1}, respectively. Notice that the time to reach failure states under slow rate of loading is longer than that under high ROL.

4.6 Time to crack initiation

The exact crack initiation point was located by zooming out the area around the initiation point, so that the load drop and the bend is clearly visible. For example, if the crack initiation was at the point (100,1000) on the load-time plot, it was viewed by narrowing the time scale to the range of [95,100] and load scale to the range of [900,1100]. (If required, this range is further reduced to enlarge the appropriate portion of the graph.) Then only a portion of the graph within the scale limits was visible and therefore the most appropriate initiation point was found. However, viewing the whole graph didn'tenable the exact crack initiation point.
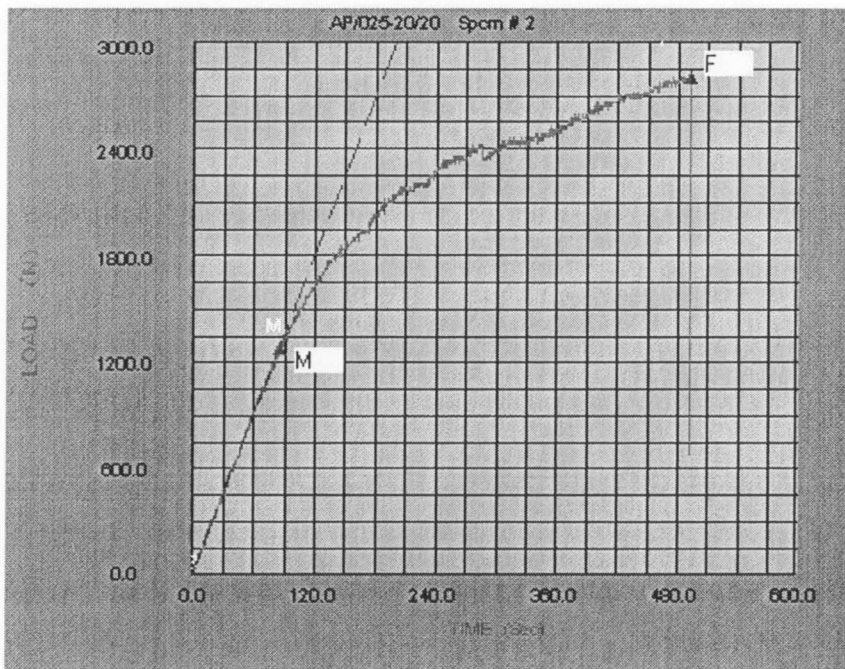
Figure 4-4: A typical plot showing a clear catastrophic failure state at point F, and crack initiation point M. Crack initiation can be accurately observed and reading can be taken by enlarging the plot around M. Reducing the scale to enlarge the plot around M shows the crack initiation point of the graph. ROL = 2.5 mm s^{-1}.
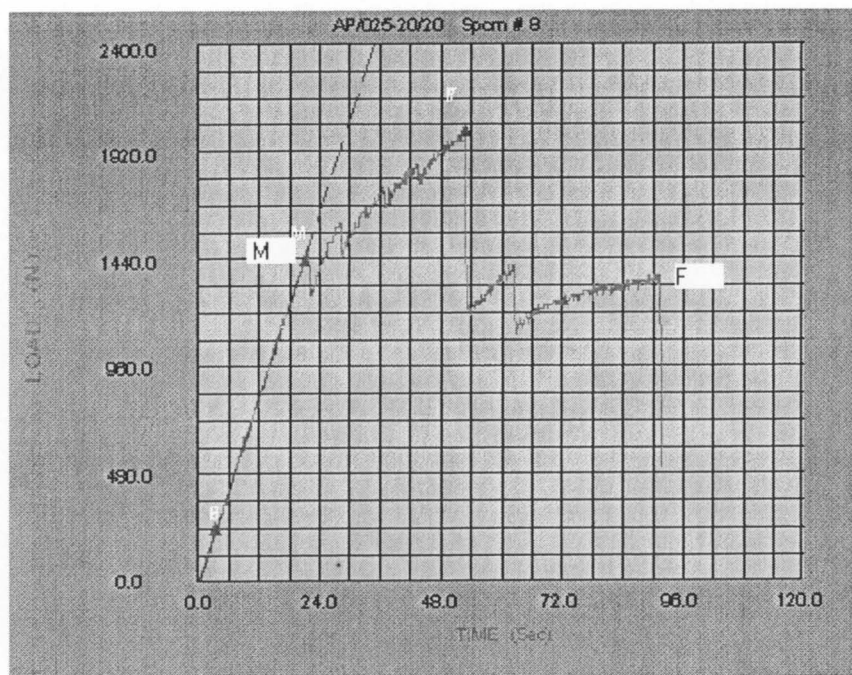
Figure 4-5: Load-Time plot showing a two breaking points. (Observed information is used to get the Catastrophic failure state at around 90 s. ROL used is 10.0 mm s^{-1}.)
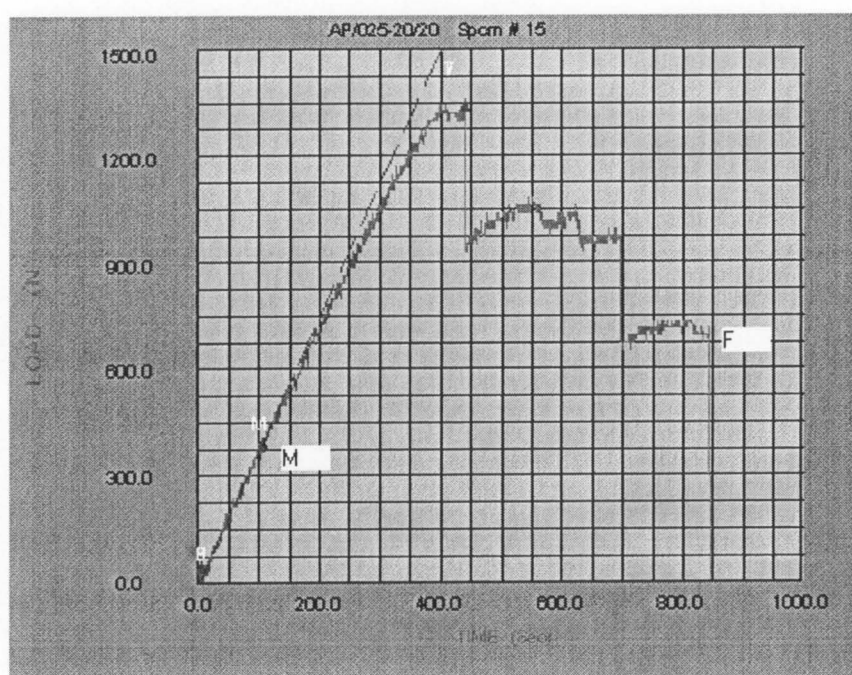
Figure 4-6: Load-Time plot showing the longer time taken to reach failure states than that taken in the above two cases since the ROL is 0.625 mm s^{-1}.

48

4.7 Summary

This chapter discussed the data extraction procedures for the following data objects.

- **GEN**: General data such as measurements of specimen geometry, density, whole weight, crack length and moisture content. These were straight forward and easy to record.

- **NISD**: The plots drawn by the computer were used to obtain data under this category. Especially, the time to crack initiation and catastrophic failure as well as the corresponding loads were recorded.

- **CDID**: Crack dynamic data such as crack length over time, speed and other fracture behavioural information were extracted from the recorded fracture processes using post-experimental procedures.

- **CTDIM**: Data has not been extracted from the images captured under this data object but has been left for future use.

Extracted data were used in the following chapters for analysis.

Chapter 5: HIGH SPEED VIDEO IMAGING TO STUDY EFFECT OF SIZE AND RATE OF LOADING ON FRACTURE DYNAMICS OF WOOD

Part 1: Analysis, Results and Conclusion

5.1 Introduction

Crack propagation in wood was studied using high-speed imaging to investigate the crack velocities and the effect of size and rates of loading on time to failure. High-speed crack extension and closure indicated that fracture is not solely a forward propagating process. Farid Abhraham (1997) of IBM Almaden Research Centre says "Continuum fracture theory typically assumes that cracks are smooth. For dynamic cracks, it predicts that, as they propagate, they accelerate to a limiting velocity equal to the Rayileigh speed of the material. In contrast, experiments tell us that, in a common fracture sequence in some polymers, glasses, and ceramics, an initially smooth and mirrorlike fracture surface begins to appear misty and then evolves into a rough hackled region with a limiting velocity of about six tenths the Rayleigh speed. In some brittle materials, the crack pattern can also exhibit a wiggle with a characteristic wavelength. Recent experiments have clearly shown that violent crack velocity oscillations occur beyond a speed of about one-third the Rayleigh speed and are correlated with the roughness of the crack surface". He indicates further that continuum fracture theory cannot explain some of the features of crack dynamics and there cannot be a limiting factor of crack speed. Recording this process is hence very useful for studying fracture dynamics. Our study clearly indicated a wave pattern of fracture when the recorded video-tapes were viewed and further confirmation is given by calculations.

One can study the recorded videotapes to see the oscillations of grain patterns and generated cracks, before the catastrophic failure. Rates of such oscillations were found to be much higher near catastrophic Failure State than prior to reaching that point. Careful viewing of tapes revealed a process of crack closures in addition to extension. The crack closure means that lips of crack ends touch each other instantly reducing the crack length, which cannot be seen while testing. Since playback is repeatable it is observable

50

conveniently. It was clearly observed that the point of crack initiation was the crack tip in some cases while in other cases cracks initiated from a point close to the crack tip. Fracture process for all the specimens were recorded on 3-hour SVHS videotapes and each played back 9 hours. Extracting information from tapes were strained and strenuous on the eyes but not only they provided wealth of information but also revealed highly interesting details of fracture and stimulated the curiosity to understand this complex process of fracture dynamics. Therefore one doesn't have to do more experiments to investigate crack propagation if these tapes are available. Once copied into the hard disk, more computer facilities can be utilized but video frames of 2 to 3 minutes duration occupy about 100MB HD space. Since wood properties and loading configuration affect the fracture and post fracture behaviour, mapping these multiple inputs onto the results mathematically and statistically would be a very useful model. This thesis has not gone into modeling due to time limitations. However it has analyzed and highlighted the effects of size and rate of loading on fracture behaviour. The following paragraph highlights the important findings and a summary of the study, which is given in section 5.3. The considered size effect is the volume effect that is to be focused in this chapter.

The volume effect is insignificant at highest (10 mm s^{-1}) rate of loading but significant at lower rates (2.5 mm s^{-1} and 0.625 mm s^{-1}) used in the experiments. Crack speed is the highest near the catastrophic failure and speed profiles varies with the rate of loading. The analysis confirms that the determination of crack speed is a reliable method to ascertain the events of crack initiation and catastrophic failure states. Furthermore, the point of crack initiation was not necessarily the existing crack tip for almost half of the total number of specimens. Fracture propagation invokes an irregular wave pattern.

Part I of this chapter covers crack dynamics data that analyzed using C++ programming and database techniques. Part II presents the relationships that can be formulated among variables and the strength of the relationship using SPSS statistical package. At the end, a summary and a brief discussion is presented.

5.2 Definition of failure: State of Failure and time to failure

Failure is the state where (Neilsen 1978),

> *material damage starts or crack propagation is initiated; and*

> *the damage level has reached a point where there is no load carrying capacity left or the rate of crack propagation increases rapidly (catastrophically).*

The time to reach any of these failure states is said to be time to failure. The first case is the lower limit of failure (safe mode) and the second case is the upper limit of failure which is complicated to handle as mentioned Nielsen (1978).

Wood is a material that can endure higher (ultimate) stresses for short duration than those for long time periods. The weak bonds are referred to as tiny cracks in wood and a very high number of such tiny cracks are distributed over the volume of a member. There should be certain duration of load required to invoke these natural cracks in order for them to support crack propagation (Mindess, 1978). Therefore the rate of loading and the duration of loads are important factors in wood testing in general, and in fracture studies, in particular.

5.3 Results

It is hard to discuss the size effect without indicating loading configuration. Therefore the size effect discussed here is always incorporated with the rate of loading.

5.3.1. Size effect and rate of loading on time to Failure

Mean times to failure at both states (crack initiation and catastrophic failure), are tabulated in Table 5.1 and plotted against volume in Figures 5.3 through to 5.5. Since the camera speed was set up to capture 200 frames per second, times of some important events could not be indicated by the timer which could only capture in a minimum of 1/100 s intervals. As a result the timer indicated the same time digits for two consecutive frames (events) at some high-speed fracture instances. The time difference between two such events was approximated to be 0.005 s.

52

The 4 sections of the Table 5-1 indicate the volumetric effect on, mean time to crack initiation, mean time to catastrophic failure and mean time duration of fracture (ie : duration between time to crack initiation and time to catastrophic failure) and the catastrophic failure loads, respectively. The instant of the catastrophic failure was determined to be associated with event of highest speed of crack propagation. The Figures 5-3, 5-4, 5-5 and 5-6 provide the graphical presentation of the above data in Table 5-1.

Table 5-1: Time to failure and failure loads

	Vol x 1000 - mm^3	13.66875	109.35	874.8	4050
Section 1	ROL - mm/s	D	C	B	A
Mean Time	0.625	95.00	93.75	305.00	341.67
to Crack	2.5	24.00	57.36	78.33	125.00
Initiation - s	10.0	39.25	8.50	35.00	24.00
Section 2					
Mean Time	0.625	271.01	186.19	458.26	424.62
to Catastrophic	2.5	60.45	107.49	157.25	133.65
Failure - s	10.0	41.56	21.31	46.35	46.20
Section 3					
Mean time	0.625	176.01	92.44	153.26	82.95
Duration of	2.5	36.45	50.13	78.92	33.65
Fracture	10.0	2.31	12.81	11.35	22.20
Section 4					
Mean	0.625	115.0	206.8	875.0	2012.5
Catastrophic	2.5	137.5	346.3	1223.3	2178.6
Failure Load-N	10.0	116.0	368.0	1046.0	2320.0

The discussion under the following sections from 5.3.2.1 through to 5.3.2.4 is an elaboration of size and rate of loading effects on times to fracture states, duration of fracture and fracture load which is extensively discussed in the overview section 5.4.

5.3.1.1 Time to Crack Initiation

As shown in Section 1 of Table 5-1 and the relevant Figure 5-1, the volume effect on mean time to crack initiation is diminished significantly as the rate of loading increases to 10.0 mm s^{-1}. This time gradually increases as volume increases for constant rates of loading of 2.5 mm s^{-1} and 0.625 mm s^{-1} but not for 10 mm s^{-1}. In other words there is almost an insignificant effect of volume at the highest rate of loading but this effect becomes significant as volume increases for decreasing rate of loading. Results for the two smallest volumes are close to each other and therefore cannot be differentiated properly.
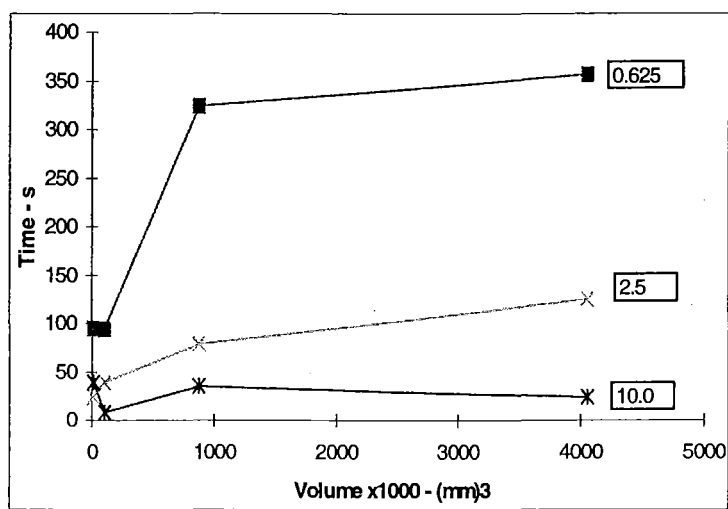
Figure 5-1: Relationship between Time to crack initiation and volume for different rates of loading

5.3.1.2 Time to Catastrophic Failure

Section 2 of Table 5-1 and the relevant Figure 5-2 show the mean time to catastrophic failure which slightly differs in pattern from the mean time to initiation but exhibits a similar trend. It shows a slight decrease in time to failure for the high volume studied. As was the case for the time to crack initiation, time to catastrophic failure decreases significantly as the rate of loading increases. Once again effect of volume seems insignificant at the highest rate of loading.
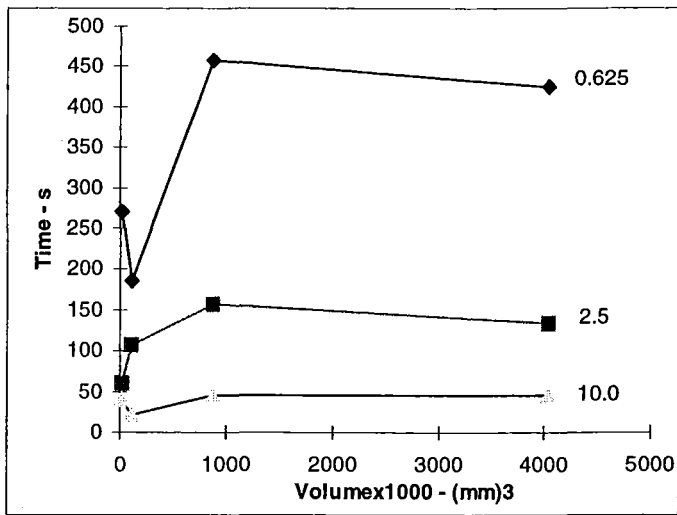
Figure 5-2: Relationship between Time to catastrophic Failure Initiation and volume for different rates of loading

5.3.1.3 Duration of Fracture

Section 3 of Table 5-1 and the relevant Figure 5-3 show the mean time duration of fracture. For higher rate of loading conditions it shows almost no volumetric effect on this time duration. Nevertheless this duration effectively decreases as the volume increases under lower loading rates and also shows further decrease as this rate increases.
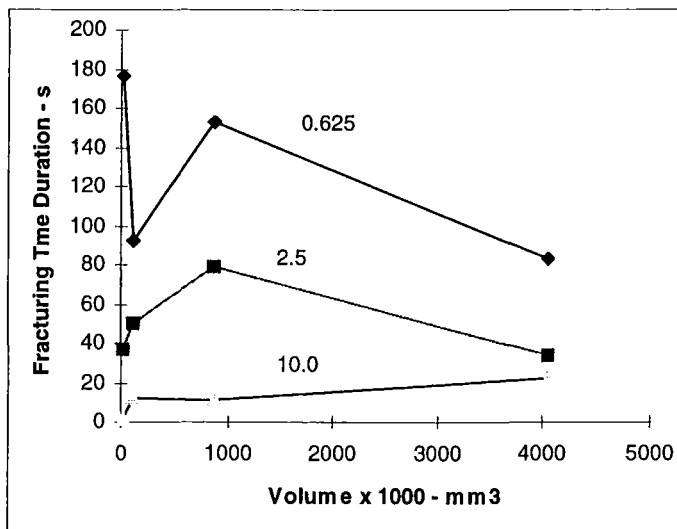
Figure 5-3: Duration of fracture as a function of volume for various rates of loading

Therefore, it appears that once crack propagation starts, large volumes have less resistance to propagation than smaller volumes. Also, as rate of loading increases to a certain level, volume effect disappears.

5.3.1.4 Fracture load at catastrophic failure

Section 4 of Table 5-1 and the relevant Figure 5-4 show the mean fracture load at catastrophic failure events. The relationship between the volume and the fracture load is not linear but looks like a hyperbolic pattern. For the defect free specimens tested, load increases with the volume and rate of loading. It appears that the rate of loading does not have a very significant influence on the fracture load for a particular volume. It was also found that loading rate had no effect on failure stress of cracked wood beams for the range tested.
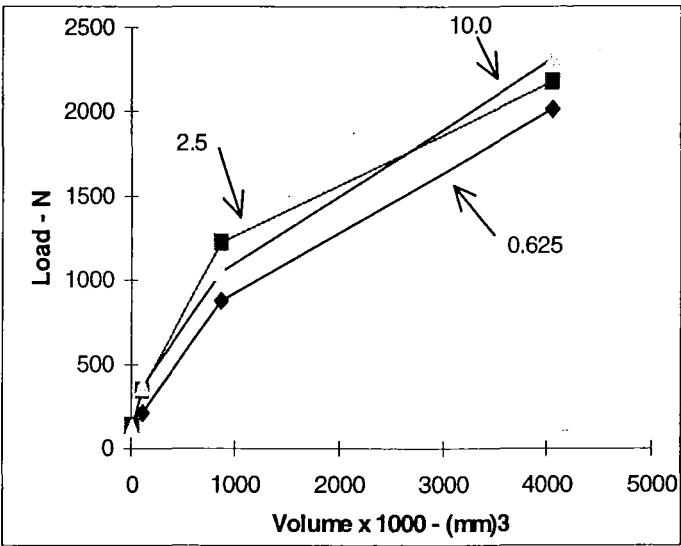
Figure 5-4: Variation of catastrophic failure load with volume for different rates of loading

5.3.2. Crack Speed

The total net crack length and total net crack speed were calculated at different events of the crack growth process as discussed in Chapter 4. The line graphs of Figures 5.5, 5.6 and 5.7 illustrates these variations in turbulent patterns of crack speed over time for selected three specimens of the same volume of 1000mm x 90mm x 45mm under different rates of loading (0.625 mm s-1, 2.5 mm s-1and 10.0 mm s-1). Fluctuation of crack speed at the lowest rate (0.625) of loading is very low within the duration of fracture and sudden spikes (one here) show the

catastrophic failure. At the highest rate (10.0mm s-1) it fluctuates more than that at the lowest and fluctuation is average at the middle rate. But the highest crack speed shows under the mid-rate condition. A simulation may provide better explanation to this observation but this is discussed in the conclusion. The rate of change of crack speed is different at different events in the same fracture process. Propagating crack looked like an irregular (non-uniform) wave pattern and the highest speed indicated the catastrophic failure. At this event the highest frequency (variability) of the speed pattern was found. This means that the highest crack speed and the highest frequency of the speed pattern occur at the catastrophic failure stage (Figures 5-5, 5-6, 5-7). Minus values indicate the crack closure while plus values obviously stand for extension. (These fluctuations were also visible in the playback process of the recorded tape.)
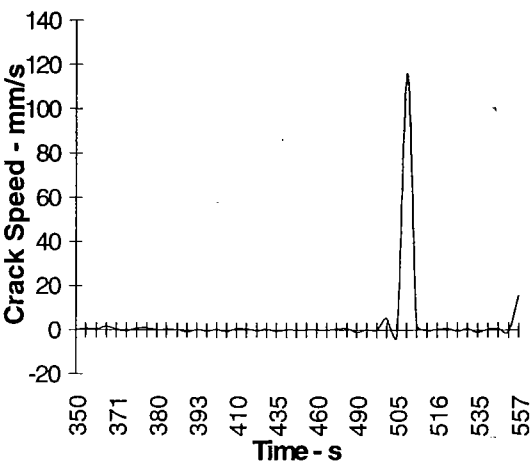
Figure 5-5: Variation of crack speed with time (ROL 0.625 mm s^{-1})
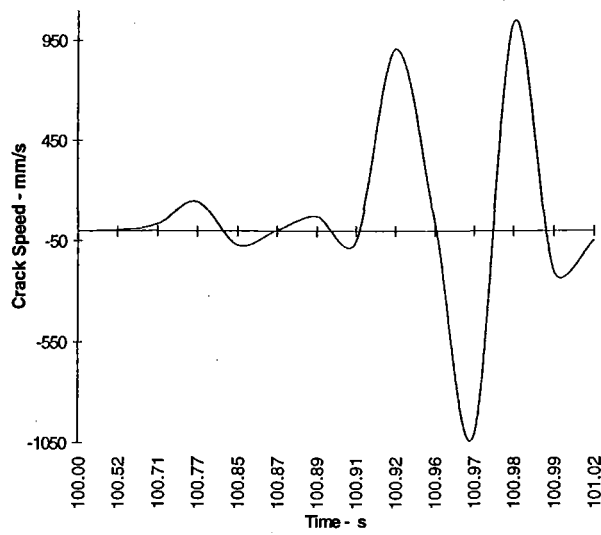
Figure 5-6: Variation of crack speed with time (ROL 2.5 mm s^{-1})
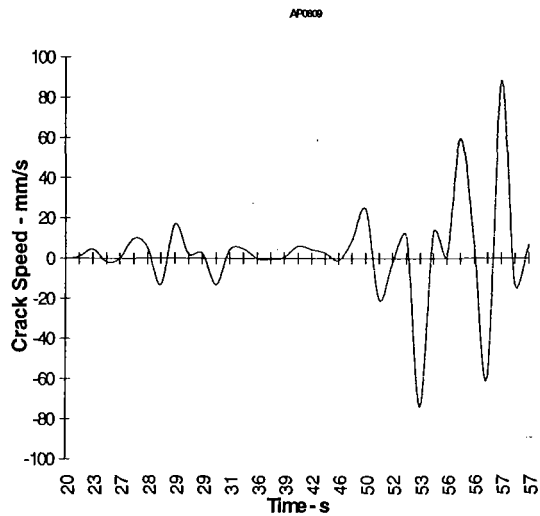
Figure 5-7: Variation of crack speed with time (ROL 10.0 mm s^{-1})

Similarly very high crack speeds and accelerations are common for all the specimens at the stage of failure. For further illustration, these spiky speed and acceleration values at catastrophic failure stage of every specimen (except specimens in the smallest volume) tested are tabulated in Table 5.2.

58

Table 5-2: Highest speed and the highest speed variation at catastrophic failure stage

Specimen ID	Crack Speed - mm s^{-1}	Crack Acceleration - mm $^{-2}$
AP0801	1040.94	206204.70
AP0804	3493.78	378427.63
AP0805	54.38	256.93
AP0807	27.05	693.32
AP0808	12.80	18.23
AP0809	87.76	1051.40
AP0812	205.21	1293.28
AP0813	-429.17	-4903.10
AP0814	311.69	62331.56
AP0815	4025.72	1582553.82
AR0801	116.21	1326.18
BP0810	-2275.74	-239899.53
BP0811	-26.44	-90.28
BP0812	-132.35	-3285.84
BP0812	33.26	331.22
BP0813	15.37	163.84
BP0814	318.28	63496.53
BR0801	3205.46	320583.72
BR0802	18.36	206.09
CP0801	41.22	213.64
CP0802	17.83	166.02
CP0803	-308.67	-46354.30
CP0804	-69.38	-631.41
CP0805	253.55	14248.32
CP0807	65.18	13048.26
CP0808	229.44	22881.98
CP0810	-60.76	-3751.87
CP0811	17.63	-106.38
CP0812	414.23	4071.70
CP0814	8.45	37.78
CP0815	-5.62	-12.16
CR0801	146.11	2067.82
CR0802	90.82	205.50

5.3.3. Auxiliary observations

The point of crack initiation was not necessarily the crack tip. In some cases one or more crack(s) originated at point(s) close to the tip. Propagation in twenty-one out of forty-one specimens, did not start right from the existing crack tip. All those cracks not originated from the tip subsequently joined the crack tip and Figure 5.9 demonstrates the development of such a crack. Most of the specimens showed crack propagation along the grain. In few cases, a multitude of small cracks developed in different layers of the grain as shown in Figure 5.8 followed by fracture in staggered condition along these small cracks.

Grain direction
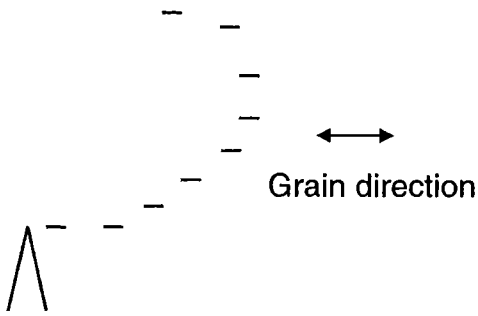
Figure 5-8: A multitude of small cracks in different layers demonstrates a special fracture path

Further, there was a clear observation of crack extension and closure especially in the events closer to the catastrophic failure instant, which was subsequently confirmed by calculations performed using C++ program modules.
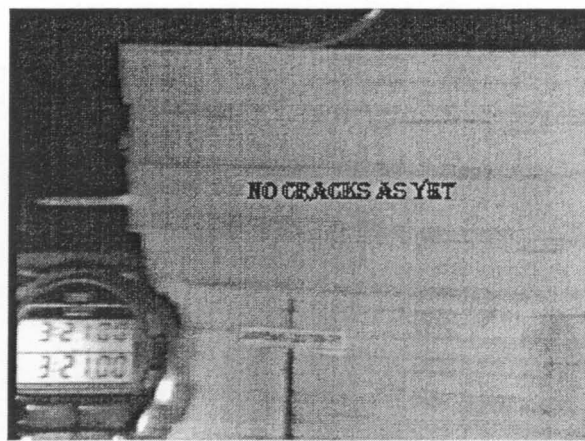
(a)
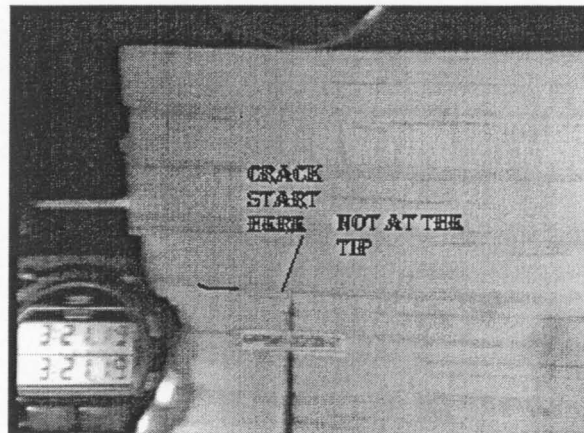
(b)

©
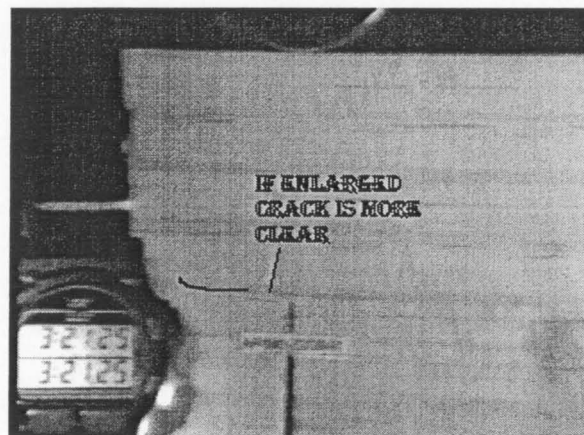
Figure 5-9: Stages of crack propagation: (a). before initiation, (b). Crack Initiated at a point above and to the left of the tip, (c). Crack propagated but not yet joined the tip.

5.4 Overview of Results

5.4.1. Time to crack initiation (Figure 5.1)

- The volume effect increases as ROL decreases. Therefore the volume could be highly effective on fracture in cases such as creep.

- The volume effect is not significant on time to crack initiation at the highest rate of loading (10.0 mm s^{-1}) tested. This indicates that volume effect can be generally insignificant at very high rates of loading.

5.4.2. Time to catastrophic failure (Figure 5.2).

- The volume effect increases as ROL decreases, nevertheless the volume effect slightly decreases for the largest size tested, indicating that larger volumes offer low resistance to fracture once propagation has started at low ROLs.

- The volume effect is not significant on time to catastrophic failure at the highest rate of loading (10.0 mm s^{-1}) tested.

5.4.3. Duration of fracture (Figure 5.3)

- It seems to be that the average fracture duration is the highest for the medium size category tested.

- The volume effect is again insignificant at the highest rate (10.0 mm s^{-1}) tested, but exhibits a slight increase only in this case.

- This is a good demonstration of the weakest link theory because as the volume increases, the member decreases the load holding capacity after a crack initiation beyond a certain volume. This means there can be a maximum volume with the highest capacity in a group of beams of different volumes. However it seems that the weakest link effect is valid only after crack initiation.

5.4.4. Fracture load at catastrophic cailure (Figure 5.4)

- Fracture load is increased as the volume increases, but does *not* show a linear relationship and it shows a parabolic pattern of increment.

- The load carrying capacity at low and high rates of loading is lower than that at the mid range of rate of loading (2.5 mm s^{-1}) for the middle size specimens. Nevertheless, when the size increases this capacity increases with rate of loading which was the case for the two smallest volumes.

5.4.5. Speed patterns (Figure 5.5, 5.6 and 5.7)

As the rate of loading increases the crack speed exhibits an increasingly turbulent pattern. At the lowest rate tested, crack speed is more visible only near the catastrophic failure point producing a spike like speed change. All specimens in each category showed similar speed patterns and therefore, the sample speed patterns indicated in the figures are good examples of behaviour at different rates of loading. Hence,

at lowest ROL used ,

- it showed a uniformity in speed pattern most of the time except at catastrophic failure,

- and catastrophic failure occurs instantly

and at highest ROL used ,

- it showed more frequent variable (turbulent) speed pattern most of the time than that at lower rates,

- and the catastrophic failure state is reached gradually.

5.5 Discussion and conclusion

- Catastrophic failure is associated with the highest crack speed and the region of the largest oscillation of speed.

- Size effect is significant in fracture and it is effectively controlled by rate of loading as discussed above. However the volume effect is not significant in both fracture states at the highest rate of loading. Therefore it confirms a requirement of a possible threshold time to invoke natural tiny cracks in the fracturing member. Hence the volume effect is significant only after this criteria is satisfied. There should be a separate model to determine this criteria because it requires additional experiments to do so.

- Crack propagation can be considered as a vibrational process. As a load is applied perpendicular to the beam the points in the beam undergo tension, compression and shear stresses involving fibre elongation, contraction and sliding with respect to each other. The process appears to propagate a wave front incorporating the elasticity in the fibres of the member. Points in a virtual

63

(instantaneous) plane may be considered to invoke the propagation. If the resultant stress at a point at time t is σ_t, it experiences a stress of $\sigma_{t+\delta t}$ at time $t+\delta t$. This agrees with the Equation 2.8 due to a significant change in crack velocity during the fracture process. Any minus value of the velocity indicates crack closure at this instant probably indicating a stress reversal.

- Neilsen (1978) used an assumption of non-negative crack speeds in the time intervals between crack initiation and catastrophic failure to derive expressions for crack propagation in his paper. According to these studies, this assumption is questionable due to alternate negative and positive speeds (Figures 5.7,8,9) and cannot be neglected since the negative speeds are reasonably high in many cases. However this alternate speed is highly variable at high rates of loading than at low rates. This fact ignored by him affects his mathematical integration in the equations for time to catastrophic failure. Due to the alternative speed patterns, there could be a stage d_1 sandwiched between d and e of crack propagation as shown in Figure 5.10 replication of Figure 2.1of chapter 2 for which crack length is less than that for the previous stage d.

Time: $t_1 \geq t_s$ $t_3 > t_2$ t_{cat}

               $t_2 > t_1$

     d d_1 f   e
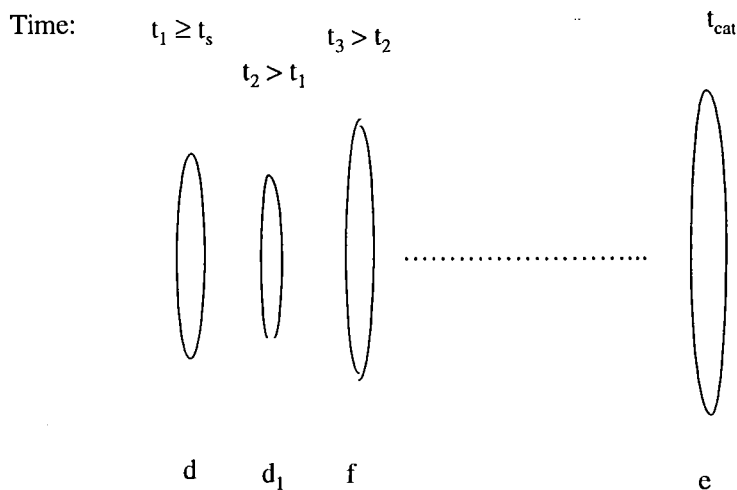
Figure 5-10: Stages between crack initiation and catastrophic failure abstracted from Neilsen's concept indicated in Figure 2.1.

- The starting point of crack propagation for almost 50% of the tested samples was not exactly the existing crack tip. Another criterion has been satisfied to initiate a crack close to the existing crack thus violating the Linear Elastic Fracture Mechanics concept, which predicts crack propagation from the existing crack tip.

- Size effect is significant in fracture. Time to failure and failure (ultimate) load values showed it clearly. These studies confirm a requirement for a possible threshold time to invoke natural tiny cracks in the member and it is interesting to see that volume doesn't affect much on the time to failures until this criteria is satisfied. This fact has been evidenced by the insignificant volume effect in the case of 10.0 mm s^{-1} rate of loading. These results may be interpolated to larger sizes and different rates of loading conditions to estimate failure conditions.

- The size is immaterial for time to failure at high rates of loading conditions as this study showed. Therefore in an environmentally disastrous situation where load can be applied rapidly on beams, they do not wait to obey the Weibulls weakest link concept and can fail simultaneously and quickly, before the tiny cracks in the member come into action.

- Recording of fracture process with high speed imaging is a successful method for obtaining information about fracture dynamics though it is a very costly, time consuming and resource hungry process.

Chapter 5 : Part II - Crack Dynamics– Modelling

5.6   Model development using Statistical Package for Social Science (SPSS)

The following Table 5-2 shows the results of statistical analysis of the fracture dynamics data obtained from SPSS. The first set of rows indicates the coefficients of the input variables relevant to each output. The input variables used are crack length (C_L), ROL, volume (V) and fracture toughness. The abbreviation ln indicates the natural logarithm. The sets of second, third and fourth rows provide statistical analysis results regression relations, F-test and Durbin-Watson score. The columns under "Values/Coefficients for output" are individual output variables used in the model.

Table 5-2: Regression results for models for Time to Fracture states and Failure Load.

		Output variables		
		ln (Time to Crack Initiation)	ln (Time to Cat Failure)	ln (Catastrophic Failure Load)
Inputs and their coefficients	Crack Length(C_L)	0.08549	0.023526	0.13148
	ROL	-0.216779	-0.201831	0.008517
	Volume (V)	-0.0000003387	-0.0000001013	-0.0000004298
	Constant	3.438966	5.548345	-2.926249
Regression Relation	Multiple R	0.86594	0.74459	0.963
	R Square	0.74985	0.55442	0.928
	Adjusted R Sq.	0.73734	0.53214	0.925
	Std. Error	0.60822	0.72422	0.3145
Hypothesis test	F	59.95212	24.88503	258.82659
	Significane F	0.0000	0.0000	0.0000
Serial co-relation	Durbin-Watson	1.48039	1.75756	1.92826
All variables used, were in SI units				

Number of cases used = 65

5.6.1. Time to crack initiation

Raw time to crack initiation values did not provide good statistical results but natural logarithm of time to crack initiation did better. The analysis gave an R^2 value of 0.75 and Durbin-Watson score of 1.48 for the following regression model. The Durbin-Watson score is a measure of serial correlation that gives a value of 2 for the maximum correlation.

$$\ln(t_{Int}) = 0.0855C_L - 0.2168R_{OL} - 3.3873x10^{-7}V + 3.4390 \qquad \textbf{[5.1]}$$

The Durbin-Watson score closer to 2 is a high value and should yield good results. The scatter plot of Figure 5.11 and normalised cumulative predicted versus empirical probability plot of time to crack initiation (Figure 5-12) confirm this result.

5.6.2. Time to catastrophic failure

Similarly time to catastrophic failure was modelled with R^2 of 0.55 and Durbin-Watson score of 1.75 resulting in the following regression equation.

$$\ln(t_{cat}) = 0.0235C_L - 0.2018R_{OL} - 1.0127x10^{-7}V + 5.5484 \qquad \textbf{[5.2]}$$

Since the Durbin-Watson score is closer to 2 than that for time to crack initiation, it has given a better model, which was confirmed by the normalised cumulative predicted versus empirical probability plot of Figure 5-13 and the scatter plot of Figure 5-14.
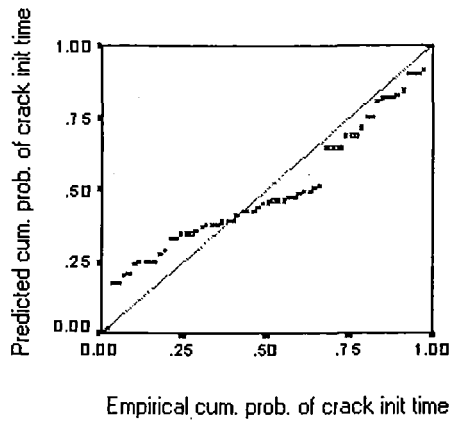
Figure 5-11: Cumulative probability of logarithms of empirical and predicted time to crack initiation
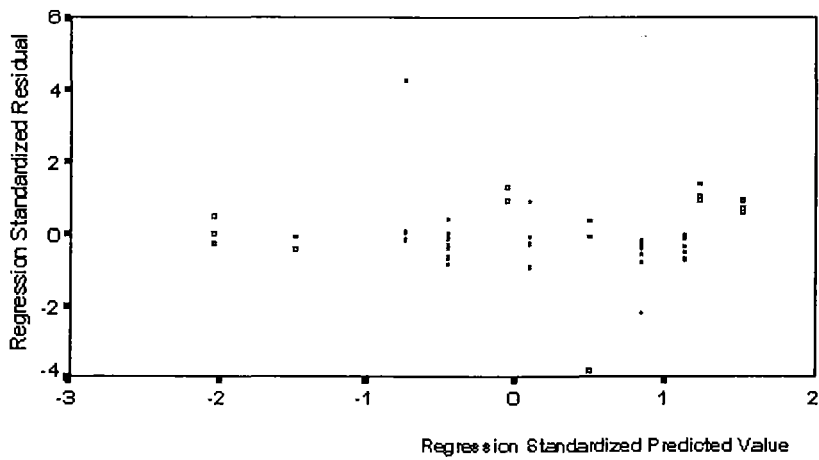
Figure 5-12-Standardised Scatter plot of predicted logarithm of time to crack initiation

68
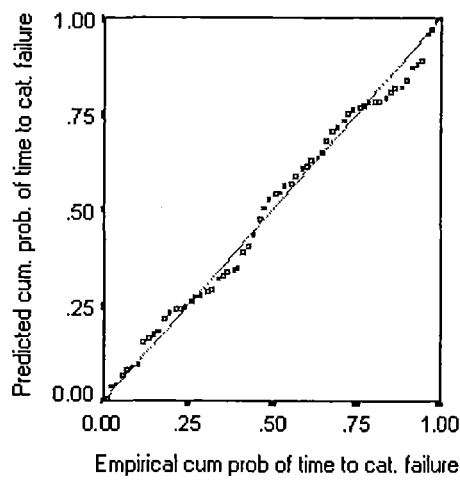
Figure 5-13: Logarithms of empirical and predicted cumulative probability of time to catastrophic failure
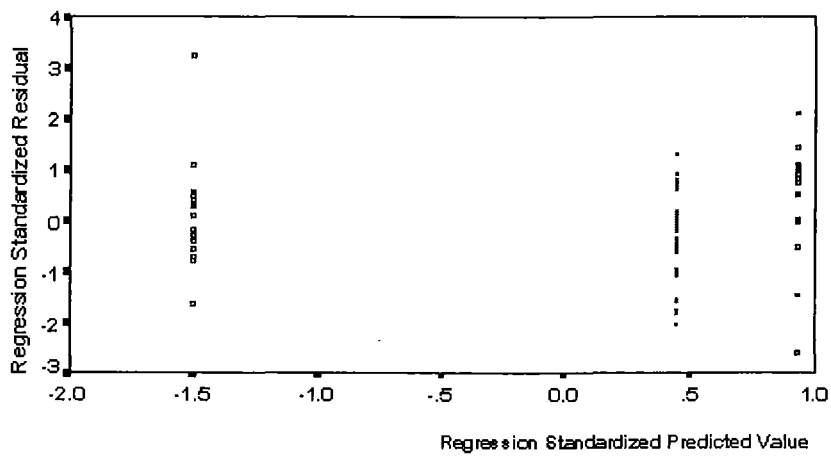
Figure 5-14: Standardised Scatter plot of predicted logarithm of time to catastrophic failure

5.6.3. Catastrophic failure Load

Similarly catastrophic failure load was modelled with R^2 of 0.93% and Durbin-Watson score of 1.92 regression giving the following equation.

$$\ln(P_{cat}) = 0.1315C_L + 0.0085R_{OL} - 4.2978 \times 10^7 V - 2.9263 \qquad \text{[5.3]}$$

The Durbin-Watson score is much closer to 2 than that found for time to initiate fracture and time to catastrophic failure states. This model is better than the above two as can be seen from the normalised cumulative forecasted versus empirical probability plot of Figure 5-15 and the scatter plot of Figure 5-16. And also notice that all the regression relation values are higher than the above two cases.

70
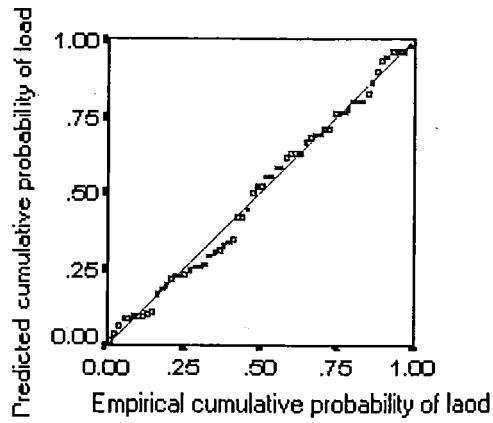
Figure 5-15: Cumulative probability of logarithm of predicted and empirical catastrophic failure load
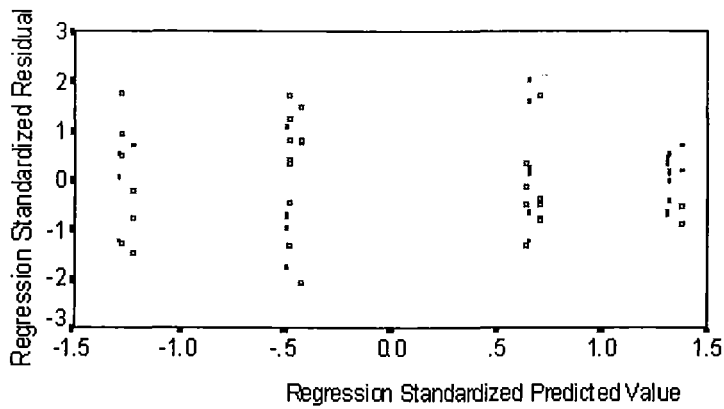
Figure 5-16: Standard scatter plot of logarithm of standardised predicted catastrophic failure load

5.7 Summary

In this section, fracture dynamics data were used to develop models using the statistical package SPSS. Natural logarithm of time to crack initiation and time to catastrophic failure were highly correlated to crack length, rate of loading and volume. The logarithm of catastrophic failure load was also highly correlated to these same input variables. However, time to crack initiation and catastrophic failure load are highly correlated to the indicated input variables with R^2 of 0.75 and 0.93 and serial correlation values of 1.5 and 1.9 respectively.

Further analysis on crack propagation is required in order to discuss the insensitive volume effect of time to failure of both states at the highest rate loading tested. This analysis tends to be another massive project, as it is beyond the expectation of this thesis. However the statistical models indicated in Equations 5.1 and 5.2 cannot predict this sophisticated property. The idea of deriving these equations is to show that these simple models cannot describe the diminishing volume effects on time lengths to crack initiation and catastrophic failure states when the loading rates are extremely high. Recorded videotapes displayed the brutal and turbulent behaviours occurred at catastrophic failure instances that none could imagine and see with naked eyes.

5.8 References :

5.1. Barrett, D. and Foschi, R.O., 1978, On the application of brittle fracture theory, fracture mechanics and creep-rupture models for the prediction of the reliability of wood structural elements, First International conference on Wood Fracture, pp. 1 - 37.

5.2. Mindess, S., Madison, B., and Barrett, J.D., 1978, Rate of loading and duration of load tests on Douglas-Fir in tension perpendicular to the grain; First International conference on Wood Fracture, pp. 145.

5.3. Nielsen, L.J., 1978, Crack Failure of dead-, ramp- and combined-loaded viscoelastic materials, First International conference on Wood Fracture, pp. 187 - 200.

5.4. Irnov; Y.M., 1978, Evaluation of long term bearing capacity of wood structures by their performance under short term loading, First International conference on Wood Fracture, pp. 63 - 71 .

5.5. Pilkey, W.D., 1994, Formulas for stress, strain and structural matrices, pp. 298-299.

5.6. Madsen, B., Structural Behaviour of Timber, 1992.

5.7. Abraham, FE, 1997, "Portrait of a crack; Rapid Fracture Mechanics Using Parallel Molecular Dynamics", IBM Almaden Research Centre, IEEE Computational Science and Engineering, April – June 1997, pp 66 - 77.

Chapter 6: Application of Artificial Neural Network towards fracture mechanics

6.1 Artificial Neural network in Fracture Dynamics

Fracture dynamics in wood is a complicated process, which does not always comply with usual Linear Elastic Fracture Mechanics (LEFM) theories. Many non-linear factors related to wood structure complicate its fracture mechanics. Wood is considered as an orthotrophic material in its engineering use whereas in the natural form wood is anisotropic and heterogeneous.

Past experiments on fracture have provided inconclusive results as discussed in Chapter 2. Some arguments for volumetric effect of the Weibull's weakest link theory were presented in section 2.2. It was explained that the opinion about the size effect on fracture differs among scientists. Different researchers have seen the size effect differently as volume, height, or height*length and so on. It seems implementing a suitable model for fracture behaviour of wood is a difficult task. It is true that wood behaves differently in the three different orthotropic directions. Furthermore, the deviations from orthotropy, generally caused by interruptions to the uniformity of grain pattern, lead to certain local anisotropy. The fracture propagation falls on a path of the grain orientation, which enables one to assume that the grain affects the fracture strength. It is very hard for someone to work with many parameters simultaneously due to practical problems. In most cases, parameters are kept constant except for the ones that are tested. Certain dependent parameters might vary with the independent variables very significantly when other independent ones are kept constant, but when the ones held constant are allowed to vary the effect of the former may considerably differ.

For the following discussion, the approach taken to model fracture toughness is discussed in a general sense as it applies to processes that depend on the simultaneous or parallel action of multitude of variables.

All systems have to undergo certain process prior to generating outputs. Most of the inputs are organised in a relatively parallel manner in these processes. For example, the measure of performance of a vehicle can vary with its capacity weight, mileage, performance of fuel injectors, dirt level deposited on ignition plugs and even the way it is driven. A plant grows when all growing requirements are fulfilled and lack of certain nutrients affects the growth but it still grows. A product is not manufactured unless raw materials, spare parts, power and operational assistance are sequentially placed in the machine. No typical computer so far can identify a person by focusing at him/her like humans do because the processing in the human eye, which focuses on an object, is highly parallel. Researchers have enhanced some systems towards parallelism in order to increase the system performance. Techniques such as bus with CSMA/CD (Carrier Sense Multiple Access and Collision Detection) and token ring topologies, have improved the performance of data communication networks. All these evidence that those serial systems can be made to perform better if techniques are introduced towards parallelism. Therefore, propagation takes place in case of fracture when all necessary parameters fulfil certain requirements simultaneously. Beyond the closed surface that covers the minimum requirements of fracture as shown in Figure 6-1, it might give noisy results which may lead to unreliable conclusions.
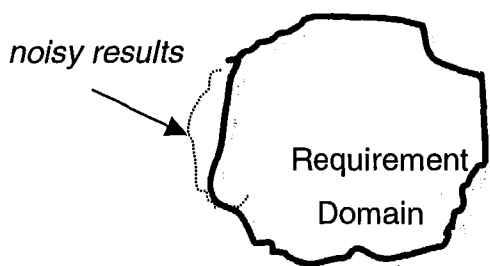
Figure 6-1 Requirement Domain and noisy results

The parallelism of artificial neural networks is capable of handling such simultaneous tasks. Also properly trained networks can perform prompt predictions. Hence artificial

neural network applied to fracture mechanics is expected to generate very good results.

"ANNs ability to generalize relationships from input patterns make them less sensitive to noisy data than other approaches. Their ability to represent non-linear relationships makes them well suited for a large variety of applications, such as some industrial control systems or financial forecasting, where linear relationships do not hold.

Although the original inspiration for ANNs come from neural behaviour in nature, current technology differs in having much simpler interconnections between processing cells and much faster processing within a cell than natural systems. The majority of ANN implementations are software simulations of parallel computations, with tens or hundreds of "neurons" being executed in rapid succession. The earliest neural chips are now appearing, and these are likely to find application in particularly demanding applications, such as image processing and real-time control" (Brunel University www.mbfys.kun.nl/SNN 1998/1999,). In deed, the human neural system performs much better in pattern recognition than current ANN technologies. However, faster processing ANN techniques are being continuously developed.

This chapter starts with an introduction to ANN and covers the required topologies and learning modes, different topological techniques and how the learning occurs under learning modes. Since the software package Neurosolutions version 3.02, which was used in this study, has captured the Neural Network theory it was not intended to design and develop a system or source code.
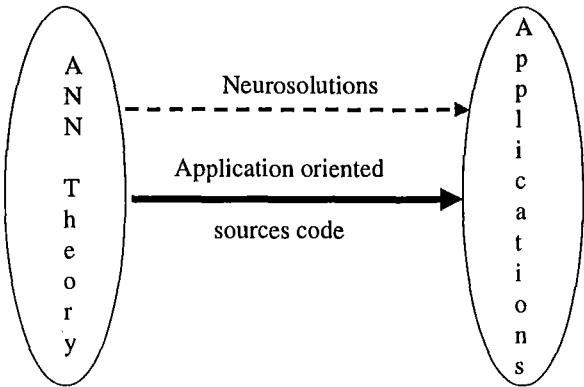
Figure 6-2: Bridge between theory and applications, Our bridge is Neurosolutions software package and application is Fracture Toughness

6.2 Use of Artificial Neural Networks

Bernard Widrow in 1950s introduced ADALINE to work perfectly in a noise cancelling process in telecommunication systems. In modem there is a tiny artificial neural network which carries out an adaptive filtering. Artificial Neural Networks have successfully worked in many more domains such as biological, business, environmental, financial, manufacturing, medical and even military applications. However neural networks are based on universal approximations.

- *What is an Artificial Neural network ?*

Neural nets can be thought of as consisting of distributed inter-connected neurones linked together by synapses as shown in Figure 6.3. When enough of the input synapses send a signal to a neurone, it 'fires', causing signals to be sent down its output synapses, which in turn cause other neurones to fire, and so on (Wu JK 1994, Brunel University www.mbfys.kun.nl/SNN 1998/1999). In an ANN, neurones are modelled by Processing Elements (PEs) possessing non-linear transfer functions and synapses, which are modelled by connection weights indicated by arrows (Figure 6.3) that constitute the most important parameters that get adjusted in a Neural Network.

Therefore an Artificial Neural Network (ANN) is a set of distributed interconnections of adaptive non-linear processing elements (PE^s), which is an intelligent technique that can be applied where the standard mathematical techniques cannot be. Reliability, high throughput, co-operative computing and fault tolerance are significant in distributed computing. A Neural Network gets adapted by changing its parameters according to certain learning rules in order to perform optimisation of the system by minimising an error function based on the difference between the network and desired outputs. Non-linearity is applied to produce powerful computation schemes. Referring to the last introductory section it is a fact that biological information

processing systems differ from other information processing systems in terms of distributed processing, adaptation and non-linearity. The non-linearity has been applied by mapping mathematical theories into hidden layers. The artificial Neural Networks are extremely simple biological brain models to which complex tasks can be assigned and solved. Being a simple abstract model of human neural learning system, ANN is applicable irrespective of the application area.

The input data is mapped on to the output of aforementioned interconnections in an ANN.
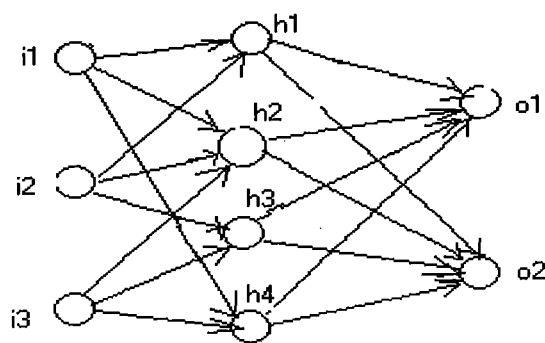
i – input, h – hidden, o - output

No of PEs in input, hidden and output layers: Input – 3, Hidden – 4, Output – 2

Figure 6-3 - Typical AN network with one hidden layer

As stated before, a simple network has input and output vectors linked through some connections called weight vectors (arrows in Figure 6.3). Figure 6.4 (a) is a single input single output- processing element, which relates input (x) to output (y) by multiplying by a weight m with added θ which is called a threshold or offset. The weight m is called a weight vector. Similarly the processing element in Figure 6.4 (b) has two inputs (x_1 and x_2) connected with two weight vectors (w_1 and w2) providing a single output.
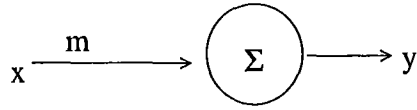
$$y = mx + \theta$$

(a)
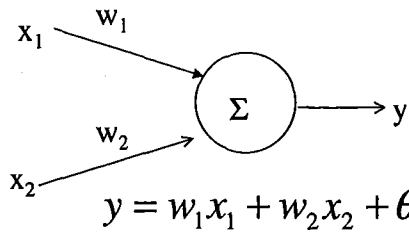
$$y = w_1 x_1 + w_2 x_2 + \theta$$

(b)

Figure 6-4: Processing Elements (PE) : (a) Single input and single output PE

(b) Two inputs and single output

As can be seen, the output is generated from the inputs by a processing element. In general, there are three functions called input, activation and output functions which carry out processes of a PE as shown in Figure 6.5. Input function may be simply a summation (say s) or dot product of input vectors (x_i) and weight vectors (w_i) associated with inputs vectors. The state of activation is a discrete or continuous function depending upon the situation and embedded in PEs. For example a linear threshold function is discrete while sigmoid function is continuous as shown below.

Linear threshold : F(s) = 1, $\forall$ s > 0;

$$= 0, \quad \forall \ s \leq 0;$$

Sigmoid : $F(s) = \dfrac{1}{1 + e^s}$ [6.1]

$$s = \Sigma\, w_i x_i + \theta$$

$$F(t+1) = F(s, F(t))$$
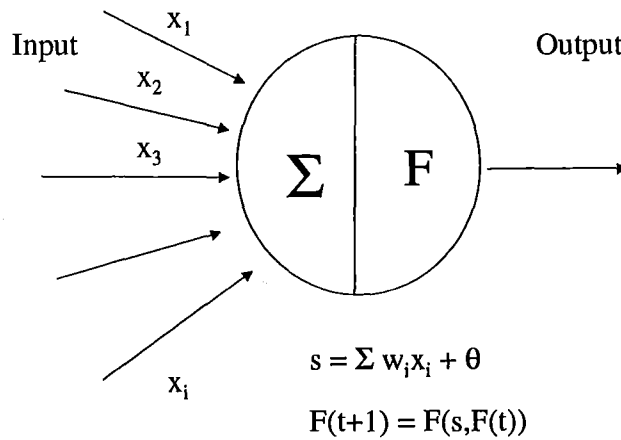
Figure 6-5– Configuration of a processing element

The output function can be another statistical function but in most cases the state of output is the state of activation (Wu, JK 1994, Chapters 1 and 4). Therefore in most cases this function is not used.

6.2.1. Learning in a network

According to Britannica Dictionary of Funk and Wagnall, learning is defined as "The modification of behaviour following upon and introduced by interaction with the environment and as a result of experiences leading to the establishment of new patterns of response to external stimuli".

Mathematical environment artificially created in an artificial neural network provides the framework for the desired pattern space, which provides a boundary for the output by means of the error space.

6.2.1.1 Learning as an Approximation

The learning in systems occurs interactively by means of a weight change that is computed in order to change the weight for the next iteration of the computational routine. Learning occurs when the new weight is adapted to the system through the iteration process. This learning or adaptation can be supervised or unsupervised like a child is taught by a teacher or learns by her/himself. A student may always solve a problem approximately to its perfect solution. If test marks of a student is closer to 100 his/her performance or quality measure (low deviations from 100) is high. We look at the mathematical approximation in learning as follows (Wu, JK 1994, pp.105 – 106).

Suppose a continuous function f exists such that

$$\mathbf{x} \in 3^n \text{ and } f(\mathbf{x}) \in 3^n, \quad \text{where } \mathbf{x} \text{ - input vector.}$$

Our problem is to find a best approximation to f(X).

∴ Define a topological approximation (mapping) function

$$F(\mathbf{w},\mathbf{x}) : 3^n \rightarrow 3, \quad \mathbf{w} \in P \ (\subseteq 3^n). \qquad [\ 6.2]$$

If w^b exists such that,

$$d[f(\mathbf{x}),F(w^b,\mathbf{x})] \leq d[f(\mathbf{x}),F(\mathbf{w},\mathbf{x})] , \quad \forall \ \mathbf{w} \in P; \qquad [\ 6.3]$$

where $d[f(\mathbf{x}),F(\mathbf{w},\mathbf{x})]$ – quality measure, then w^b provides the best solution.

A simple approximation function is the scalar product of **w** and **x** which is,

$$F(\mathbf{w},\mathbf{x}) = \mathbf{w}.\mathbf{x} \qquad [\ 6.4]$$

6.2.1.2 Learning Rules

Next problem is how to find w^b – the best solution for weight vectors, or in other words how to make the network learn. The famous α-LMS (Least Mean Square) or Widrow-Hoff algorithm for the new weight takes the following form (Widrow, B. 1992).

81

$$\Delta w_k = \frac{\alpha \delta_k x_k}{|x_k|^2} \qquad\qquad \textbf{[6.5]}$$

$$\delta_k \cong (d_k - y_k) \Rightarrow \Delta\delta_k \cong \Delta(d_k - y_k) = -X_k \Delta w_k \qquad \textbf{[6.6]}$$

where w_k - weight vector

x_k – input vector

$y_k = F(w_k . x_k)$– output of the network

d_k – desired output

δ_k – difference between output and desired vectors

Δ – difference operator

α - ratio explained in the following paragraph

Substitute $\Delta\omega_k$ of Eq. (6.5) into Eq. (6.6) to obtain

$$\Delta\delta_k = -\alpha\delta_k \qquad\qquad \textbf{[6.7]}$$

Eq. (6.7) for the ratio of error reduction shows that error is reduced by the factor α if there is a weight change on clamped input pattern. When the error reduction is chosen continuously in an iteration process the error will converge to a minimum value. Back propagation learning method feeds back the error through the network into the input in order to make it reflect on the next iteration of the learning process. The α is a controller that monitors the stability and the speed of convergence. A practical range for α is in (0.1,1.0). Required error correction rules and back propagation are further discussed under the section 6.2.2.1 of this chapter.

6.2.1.3 Learning modes

There are two Learning modes in ANN, which are called supervised and unsupervised. A brief description of each of these modes is given below.

6.2.1.3.1 Supervised learning

Considering that the quality measure d_i-y_i at all iterations is one way of supervising, the external `teacher' here is the desired signal d_i, which regulates the error reduction.

The L^2 criterion (sum of square differences) is a popular measure of the error E for a single training pattern.

$$E = \frac{1}{2}\sum_i (d_i - y_i)^2 \qquad\qquad \textbf{[6.8]}$$

where d_i is the desired or target response on the ith unit, and y_i is that actually produced on the same unit.

6.2.1.3.2 Unsupervised learning

As the name indicates the learning is non-vigilant. We look into the techniques used in this category.

6.2.1.3.2.1 Competitive learning

Input patterns are clustered into groups in such a way that output cluster centres or masses represent original data. There are various algorithms for competitive learning. In clustering, the level of similarity (say m) is taken into consideration. Input patterns are organised into classes of similarities in such a way that a set of input vectors belonging to [m$_+$,m$_-$] is a cluster of similarity around m. The objective of clustering is to find an algorithm to maximize m among the patterns in the same cluster while minimizing same in different clusters. If m of a pattern is below the expected for the cluster, it means that the noted pattern may not belong to this cluster.
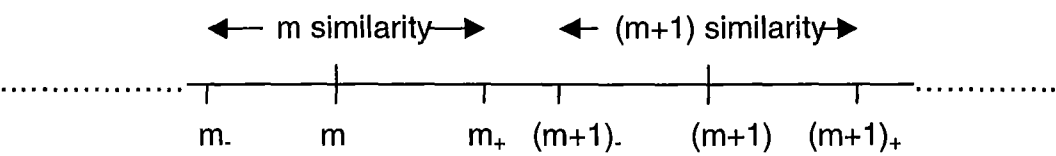
Figure 6-6: Similarity measures – m and (m+1) similarity areas. [m$_+$,m$_-$] shows the range for m similarity.

The following sections (6.2.1.3.2.1.1 – 3) explain different competitive learning methods.

6.2.1.3.2.1.1 Clustering - Dot product

The weighted sum of inputs is

$$s = \sum_{i=1}^{n} w_i x_i \qquad [\,6.9\,]$$

Norm of a vector is

$$\| X \| = \sum_i x_i^2 \quad \Rightarrow \quad \frac{\sum x_i^2}{\| X \|} = 1 \qquad [\,6.10\,]$$

Suppose $P^2 = \dfrac{\sum_i x_i^2}{\| X \|}$ and each component of the vector x_i is rearranged to calculate

the vector p, which also has the same number of components.

Then if the vector is expressed in normalised form and taken in such a way as to express,

$$p = \sum_i x_i = 1 \qquad [\,6.11\,]$$

where x_i is a component of the rearranged vector.

This means all the vector nodes lie on a hypersphere of unit radius.
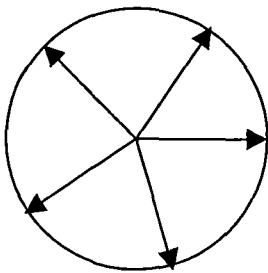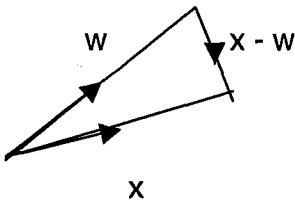
Figure 6-7: Hypersphere

If the weight vectors of these competitive vectors are also normalised, nodes of both types of vectors lie on the same hypershere.

As inputs are preserved the weights are made to rotate gradually and efficiently on the sphere at each iteration. If a node k is found with the highest excitation it is taken

84

as the centre of the winning node. When input and weight vectors are parallel to each other the dot product calculates the highest value. In order to rotate the nodes of the weight vector on the sphere, weight is changed according to,

$$\Delta w = \gamma \left(x - w \right).$$

[6.12]

Where, $0 < \gamma < 1$ is a parameter.

Then the output becomes,

$$y_0 \leq y_k \quad : \qquad \forall o \neq k.$$

[6.13]

where k is the winning neuron and o indicates another neuron while y indicates the output related to a neuron.

Input vector
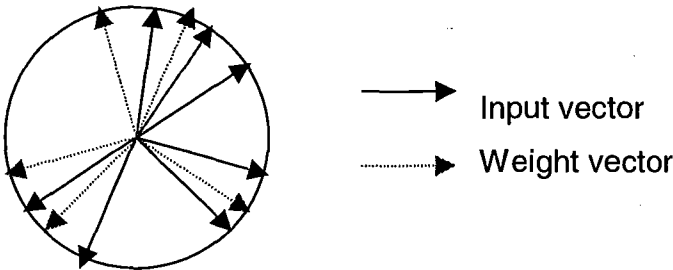
Weight vector

Figure 6-8-Rotating weight vector towards input vector

The following rule is imposed after the winner-take-all node is found so that the activation of the winning node is $y_k = 1$, making all other outputs $y_o = 0$, which satisfy the following.

$$\Delta w = \gamma \left(x - w \right) y_k$$

[6.14]

This implies zero weight change ($\Delta w = 0$) $\forall$ o $\neq$ k.

85

But,

$$\Delta w = \gamma x y_k - \gamma w y_k.$$ [6.15]

First term of this is similar to Hebb learning rule and 2nd is a weight decay. Total weight change over all the nodes is zero since $\sum_i x_i = \sum_i w_i = 1$ due to normalization.

$$\sum_i \Delta w_i = \gamma y_k \sum_i (x_i - w_i)$$ [6.16]

It implies that there is no total weight change over the nodes and therefore the winning node represents the input pattern vector x.

While one weight vector is closer to certain group of inputs another might facilitate the highest excitation of a winning node for another set of inputs. This is one way of labelling the cluster centres.

6.2.1.3.2.1.2 Clustering – Euclidean distance

In this case both weight and input vectors are not normalised. For raw inputs, winning neurone k is found such that (Efloft T, 1988, P 408-412),

$$k : \| w_k - x \| \leq \| w_o - x \| \quad \forall \, \mathbf{o}.$$ [6.17]

> where w_k – weight of the winner-take-all k to the pattern x (closest weight to the pattern x out of all other weights w_o),

When the winner is selected, weight of the winner is updated according to the following.

$$w_k(t+1) = w_k(t) + \gamma (x(t) - w_k(t))$$ [6.18]

There are more different clustering techniques such as self organizing neural network for clustering and labelling introduced by T. Eltoft and J.P. deFigueiredo in 1998 (Eltoft T et al, 1998), and k-mean and Isodata are some more examples (Wu JK, 1994).

Figure 6-9 shows clustered vectors that represent input vectors.
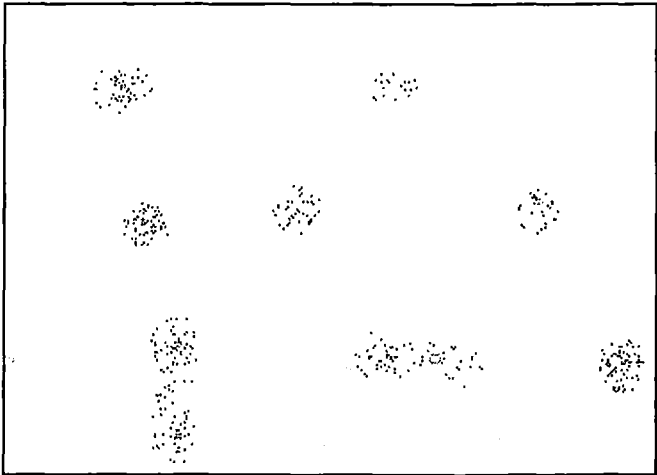
Figure 6-9-Clustering of vectors

6.2.1.3.2.1.3 Learning vector Quantisation (LVQ)

Vector Quantisation is a classical method that produces an approximation to a continuous probability function $p(\mathbf{x})$ of the input vector $\mathbf{x} \in 3^n$ using a finite number of codebook vectors $\mathbf{m}_i \in 3^n$, i = 1,2,3, ,k (Kohonnen T,1992). Once the code book is chosen approximation of $\mathbf{x}$ involves finding the reference vector m_c (codebook vector) closest to $\mathbf{x}$. The $\mathbf{m}_c$ may be based on minimized E which is the expected r^{th} power of error (when r = 2 it becomes L^2 criterion or square error.)

$$E = \int \| x - m_c \|^r \, p(x) dx$$
[6.19]

where dx is the volume differential in the $\mathbf{x}$ space, and the index c = c($\mathbf{x}$) of the best-matching codebook vector (winner) is a function of the input vector $\mathbf{x}$ which satisfies:

$$\| x - m_c \| < \| x - m_i \| \quad \forall \ i \ \{1,2,3, \ldots,k\};$$
[6.20]

ie:$\| x - m_c \| = \min_i \{ \| x - m_i \| \}$.

As Kohonen says there are no specific rules or closed algorithm domains in accomplishing this task that leads to **m**$_c$.

The classical vector quantisation method is similar to the above in that it approximates the input patterns or their probability density functions. The input space is categorised into subsets and the near-optimal boundaries between subsets are defined in Learning Vector quantisation (LVQ) method. The procedure is as follows.

- *use the above vector quantization method to classify the classes and find a reference or calibration vector of each class.*

- *Pull the codebook vectors away form the decision boundaries so that decision surfaces are clearly marked. This is done by the following algorithm*

$m_c(t+1) = m_c(t) + \alpha(t)[x(t) - m_c(t)]$,   if **x** is classified correctly.

$m_c(t+1) = m_c(t) - \alpha(t)[x(t) - m_c(t)]$,   if **x** is not classified correctly.

$m_i(t+1) = m_i(t)$,   for i $\neq$ c   **[6.21]**

Where 0 < α(t) <1, α(0) may be 0.01 or 0.02; t is the step size.

This algorithm, which starts with small α values, is used to train the network to decrease the error to zero in finite number of steps, which reduces the point density of decision boarder or Baysian decision surface. If two neighbouring classes are considered, the difference between the density functions of these two tends to zero, as the intersection of them becomes a null set. Figure 6.10 illustrates the concept of decision boundaries. The left figure shows scattering of the input vector nodes of probability density function of two dimensional vector **x** = $[x_1, x_2]^T$ (^{T} denotes the transpose) and the curve which separates this space into two classes. Two Gaussian

density functions are introduced into both classes and therefore it interpolates two centroids in both classes C_1 and C_2. The right chart of Figure 6.10 is based on codebook vectors and represents the results of Learning Vector Quantsation with enhanced decision surface shown by a continuous line. The broken line indicates the original separation which is shown on the left chart (Bayes decision surface). This is the basic LVQ1 method and the further enhancements of LVQ (LVQ2, LVQ3 etc.) are versions of this method.
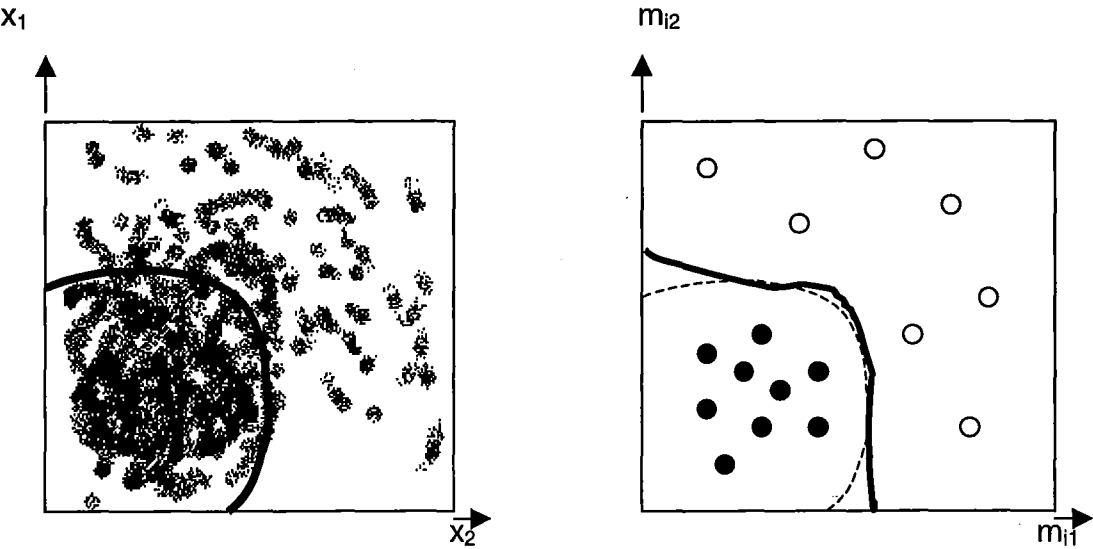
Figure 6-10 LVQ – Left: Raw input, Right: Code book Vectors & Bayesian surface

6.2.2. Network Topologies

Few network topologies are explained here that were used to train and predict fracture toughness. The illustration is based on j^{th} input vector on i^{th} PE, which generates l^{th} output.

6.2.2.1 Multilayer Perceptron (MLP)

MLPs are normally trained with the backpropagation algorithm. In fact the renewed interest in ANNs was in part triggered by the existence of backpropagation. The LMS learning algorithm proposed by Widrow (1992), cannot be extended to hidden PEs, since the desired signal for hidden PEs are not known. But the backpropagation rule propagates the errors (which contain the desired signal) through the network and allows adaptation of the hidden PEs.

Two important characteristics of the multilayer perceptron are:
- It has processing elements (PEs) with continuous nonlinear functions of which logistic function and the hyperbolic tangent are the most widely used;
- and their massive interconnectivity (i.e. any element of a given layer feeds all the elements of the next layer).

The multilayer perceptron is trained with error correction learning, which means that the network learns by looking at the desired signal. From the system response at i^{th} PE at iteration t, $y_i(t)$, and the desired response $d_i(t)$ for a given input pattern, an instantaneous error $E_i(t)$ is defined by

$$E_i(t) = d_i(t) - y_i(t) \qquad\qquad [6.22]$$

The theory of gradient descent learning is used to minimize error and weights are changed proportional to the present input and error for that weight. The following procedure is used in backpropagation learning rule (Neurosolutions Verson 3.02, 1997).

$$\Delta w_{ij}(t) = \eta \delta_i(t) x_j(t) \qquad\qquad [6.23]$$

where $\Delta w_{ij}(t) = w_{ji}(t+1) - w_{ij}(t)$, the weight change for j^{th} input on i^{th} output at the next iteration.

η = step size or learning rate - a constant

Since it calculates the weight change using the current information it can converge into a local minima. Therefore weight change can be updated with past information in order to speed up and stabilise convergence.

$$\Delta w_{ij}(t) = \eta \delta_i(t) x_j(t) + \alpha \Delta w_{ij}(t-1)$$
[6.24]

Where $\Delta w_{ij}(t-1) = w_{ji}(t) - w_{ij}(t-1)$

α is the momentum. Normally $\alpha \in [0.1, 0.9]$

6.2.2.2 Radial Basis Function (RBF)

Ill-posed noisy data that is difficult to map onto output domain can be smoothed using RBF functions that have a very strong mathematical foundation based in regularisation theory (Neurosolutions Verson 3.02 1997). Therefore a multivariate Gaussian (Equation 6.25) function can be assigned to reduce the error between the desired output and network output.

$$G(x; x_i) = \exp\left[\frac{-1}{2\sigma_i^2} \sum_k (x_k - x_i)^2 \right]$$
[6.25]

Each radial basis function represents a node i in the hidden layer, which is a p multivariate Gaussian function of mean x_i (each data point), and variance σ_i. And gives the output according to

$$F(x) = \sum w_i (G(x; x_i))$$

x is input vector $(x_1, x_2, ..., x_p)$
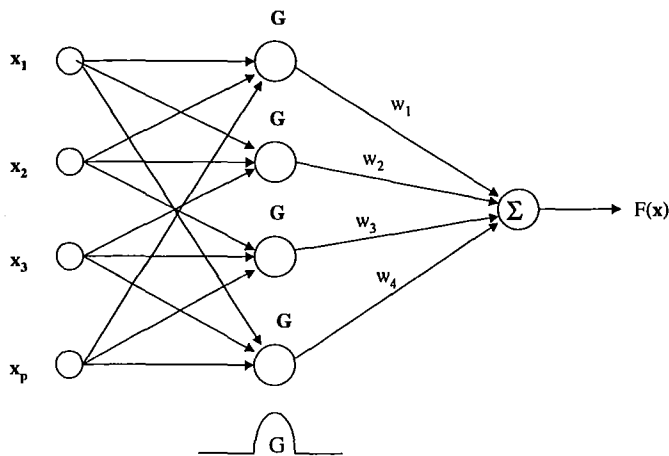
Figure 6-11 Radial Basis Function (RBF) network

91

6.2.2.3 Jordan Elman Network

The theory of neural networks with context units can be analyzed mathematically only for the case of linear PEs. In this case the context unit is nothing but a very simple lowpass filter. A lowpass filter creates an output that is a weighted (average) value of some of its more recent past inputs. In the case of the Jordan context unit, the output is obtained by summing the past values multiplied by the scalar (τ) as shown in the figure below (Neurosolutions Version 3.02 1997).

$$y(t) = \sum_{i=0}^{t} x(t) \tau^{t-i} \qquad\qquad\qquad [6.26]$$
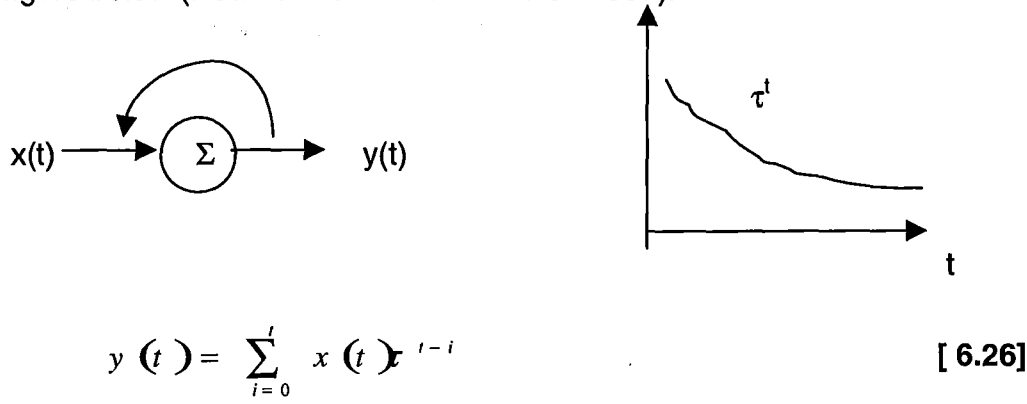
Figure 6-12: Context unit response

Notice that an impulse event x(t) (i.e. x(0)=1, x(t)=0 for t>0) that appears at time t=0, will disappear at t=1. However, the output of the context unit is τ_1 at t=1, τ_2 at t=2, etc. This is the reason these context units are called memory units, because they "remember" past events. The t should be less than 1, otherwise the context unit response gets progressively larger (unstable).

The Jordan network and the Elman network combine past values of the context units with the present inputs to obtain the present net output. The input to the context unit is copied from the network layer, but the outputs of the context unit are incorporated in the net through adaptive weights. NeuroSolutions uses straight backpropagation to adapt all the network weights. An option is given to pre-select the context unit time constant. One issue in these nets is that the weighting over time is inflexible since we can only control the time constant (i.e. the exponential decay). Moreover, a small change in t is reflected in a large change in the weighting (due to the exponential relationship between time constant and amplitude). In general, we do not know how

large the memory depth should be, so this makes the choice of t problematic, without a mechanism to adapt it. See time lagged recurrent nets for alternative neural models that have adaptive memory depth.

The Neural Wizard of Neurosolutions Verson 3.02 (1997) provides four choices for the source of the feedback to the context units (the input, the 1st hidden layer, the 2nd hidden layer, or the output). In linear systems the use of the past input signal creates what is called the moving average (MA) models. They represent well signals that have a spectrum with sharp valleys and broad peaks. The use of the past output creates what is called the autoregressive (AR) models. These models represent well signals that have broad valleys and sharp spectral peaks. In the case of nonlinear systems, such as neural nets, these two topologies become non-linear (NMA and NAR respectively). The Jordan net is a restricted case of an NAR model, while the configuration with context units fed by the input layer are a restricted case of NMA. Elman's net does not have a counterpart in linear system theory. As can be gathered from this simple discussion, the supported topologies have different processing power, but the question of which one performs the best for a given problem is left to experimentation.

6.2.2.4 Self Organising Feature Maps (SOFM)

One of the most important issues in pattern recognition is feature extraction. Self-organising feature map is a technique suited for such feature extraction.

SOFM nets are based on competitive learning networks, which consist of one layer of linear PEs. In these nets there is *one and only one* winning PE for every input pattern (i.e. the PE whose weights are closest to the input pattern).

Weights of neighbouring neurones also get updated with a smaller step size in SOFM as an additional feature to the competitive learning (LVQ) in which only the winning neurone is updated. The principal goal of self organizing feature maps is to transform patterns of arbitrary dimensionality into the responses of one or two dimensional arrays of neurones, and to perform this transform action adaptively in a topologicallly ordered and manageable fashion. The transformation makes the topological neighbourhood relationship geometrically explicit in low dimensional feature maps. Following are the essential constituents of SOFM.

- an array of neurones that computes simple output functions of incoming inputs of arbitrary dimensionality,
- A mechanism for selecting the neurone with the largest output,
- An adaptive mechanism that updates the weights of the selected neurone and its neighbours.

The SOFM algorithm is formulated as follows:

- *Initialization:* Initialise the weights with small different random values for symmetry breaking.
- *Winner-take-all:* Find the winning neurone j^* at time k using a minimum distance rule, ie:

$$j^*(x) = \arg_j \min \| x(k) - w_j \| . \quad j = 1,....,n \qquad \textbf{[6.27]}$$

where $\mathbf{x}(k) = [x_1(k),........,x_n(k)]^T$ is the kth input pattern

$\|.\|$ - Euclidean norm.

- *Weight Update:* For the winning PE and those in its neighbours $\Lambda(t)$, weights are then updated by

$$w_j(k+1) = w_j + \eta(k)[x(k) - w_j(k)] , \quad \forall j \in \Lambda_j^*(k) \qquad \textbf{[6.28]}$$

$$= w_j(k) \qquad \text{otherwise}$$

where $\eta(k)$ - positive constant (step size or learning rate)

$\Lambda_j^*(k)$ - topological neighbourhood set of winner PE at time k.

Success of the map formation is dependent on the selection of main parameters (such as $\eta(k)$ and $\Lambda_j^*(k)$), initial values weight vectors and the number of iterations.

Note that both the neighbourhood and the learning rate are dependent on the iteration, i.e. they are adaptive. Kohonen suggests the following Gaussian neighbourhood

$$\wedge_{j,j}(k) = \exp\left(\frac{|r_* - r_j|_j}{2\sigma^2(k)}\right)$$

[6.29]

$\left|r_j - r_{\hat{j}}\right|$ is the spatial distance from the winning node to the jth PE. The adaptive standard deviation controls the size of the neighbourhood through iterations. The neighbourhood starting as the total output space should decrease towards zero (only winner is zero) according to

$$\sigma(k) = \frac{1}{c_\sigma + d_\sigma(k)}$$

[6.30]

where c_σ and d_σ are constants. The step size $\eta(k)$ should also be made adaptive starting from a large value and decrease towards zero again.

$$\eta(k) = \frac{1}{a_\eta + b_\eta^k}$$

[6.31]

where a_η and b_η are also problem dependent constants which are capable of fine tuning the map by establishing local neighbourhoods..

The SOFM should be followed by an MLP to classify the neighbourhoods to complete any learning.

References:

6.1   www.mbfys.kun.nl/SNN, 1999, Brunel University Web Page.

6.2   Introduction to Neural Network, www.mbfys.kun.nl/SNN, Brunel University Web Page.

6.3   Wu, JK, 1994, Neural Networks and Simulation Methods, Chapter 1 and 4,pp 408 – 412

6.4   Vemuri, VR, , 1992   Artificial Neural Network and control applications, Chapter 1, IEEE Computer Society Press, pp. 1 - 9.

6.5   Widrow, B. and Lehr, A, 1992, 30 years of Adaptive Neural Networks, Perceptron, Madaline and Backpropagation, IEEE Computer Society Press; pp. 327-354.

6.6   Gurney, K, 1999, www.shef.ac.uk/pchycology/gurney/notes/17/section-3_2, Competitive Learning and Competitive Dynamics.

6.7   Eltoft, T, De Figueiredo, JP, 1998, "A Self Organising Neural Network for Clustering Detection and Labelling", IEEE International Joint Conference on Neural Networks, Anchorage Alaska, pp 408 - 412.

6.8   Kohonnen, T, 1992, "Self Organising Map", Senior Member, IEEE, Invited paper, Artificial Neural Network and control applications, IEEE Computer Society Press, pp. 419-435.

6.9   Neurosolutions Version 3.02, help Text, 1997.

6.10 Su, M.C, Chang, H.O.T., 1998, "Genetic Algorithm Based Approach to Self Organising Feature Map and its Applications in Clustering", IEEE International Joint Conference on Neural Networks, Anchorage, Alaska, pp 735 - 740.

6.11 Chang, M, Yu, H.J. and Heh, J.S., 1998, "Evolutionary Self Organising Map - IEEE International Joint Conference on Neural Networks, Anchorage, Alaska, pp. 680 - 685.

6.12 Seibi, A, and Al-Alwi, SM, – 1996 "Prediction of Fracture Toughness Using Artificial Neural Networks", Engineering Fracture Mechanics, Vol 56, No. 3, pp. 311 - 315.

Chapter 7 Implementation on Artificial Neural Network for predicting Fracture Toughness

7.1 Introduction:

The fracture toughness for crack initiation has been modelled in this chapter. Firstly it uses data derived under NISD and GEN objects and organised them into suitable formats that can be used randomly efficiently. The first section of this chapter describes the organisation and the second section presents preliminary training to select a topology suitable for this data. This is followed by further filtering processes of input variables which are not suitable or show negligible effect. Fixing up the data sets to determine suitability of input variables carried out this process. The randomisation was used at last in order to increase correlation and error minimisation between desired output and network output. At last a network was trained that has drawn nil weights for several inputs.

This explains the possibility of using such a model in real world situations, especially where rate of loading condition is normally ignored due to high cost. In this case the rate of loading is considered as a short duration of load which could be extrapolated to long duration.

In brief, this chapter

- discusses capabilities of the software package Neurosolutions,in training, validating and optimising results (ie: usage of the package),
- co-ordinates and organises the inputs and
- explains important results from different network configurations and facilitates the presentation of the best network in chapter 8.

7.2 Data Preparation

Data preparation is very important for obtaining good results from a neural network. Therefore input and output domains were organised before using them in networks. Further data organisation that is needed for consideration of topology is discussed under the section 7.3.2 of Topology Selection. Let us discuss output first followed by input.

97

7.2.1. Output Domain

Fracture toughness (K_c) was obtained from three point bending tests of 4 sample sizes tested at different rates of loading as discussed previously. It was computed from Equation 7-1 formed by substituting C of Equation 2.1 for fracture with the geometry correction factor ($C = F(\frac{a}{h})$) given in Equation 7-2 (Pilkey WD, 1994).

$$K = \sigma\sqrt{\pi a}\,F(\tfrac{a}{h}) \qquad\qquad [7.1]$$

$$F\left(\frac{a}{h}\right) = 1.106 - 1552\left(\frac{a}{h}\right) + 7.71\left(\frac{a}{h}\right)^2 - 13.53\left(\frac{a}{h}\right)^3 + 14.23\left(\frac{a}{h}\right)^4 \qquad [7.2]$$

$$\sigma = \frac{6PL}{4h^2} \qquad\qquad [7.3]$$

where

       a = crack length

       h = height (depth) of the specimen

       L = span of the bed rollers

       P = applied load

       σ = remote (from the crack tip line) stress

A C++ program was developed and assigned to calculate the fracture toughness of all 199 specimens. The critical load values were read at the time of crack initiation failure state. These loads are applied in Equation (7-1), to calculate the K values, which are the only output of the intended neural network.

Raw values and calculated normalised values of K were intended to use in networks.

P - Applied Load

h

a

L
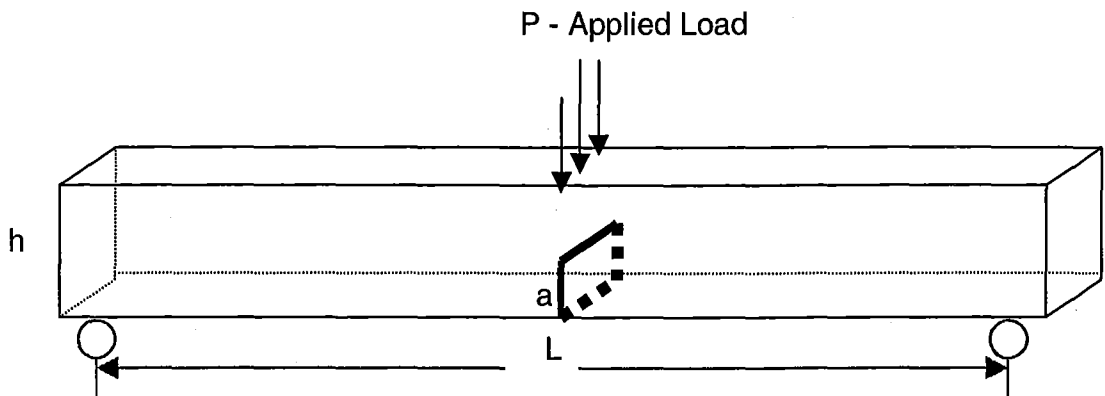
Figure 7-1: Bending configuration used for the above equations for fracture toughness.

7.2.2. Input Domain

Of the 204 specimens that were randomly arranged and tested in the laboratory, there were 199 successful records that could be organised at this stage of preparation of input data. The following variables have been used as input variables. The following categories 1, 2 and 3 have been used for easy handling.

♦ **Category 1 (basic dimensions)**
  - Rate of Loading (ROLMS)
  - Crack Length (Pre_Crack)
  - Length (LENGTHM)
  - Height (HEIGHTM)
  - Width (WIDTHM)
  - Weight (WEIGHTKG)
  - Moisture Content (MCPCT)
  - Length Angle (LENANGGRAD)
  - Face Angle (FACANGGRAD)
  - Curvature (CURVM)
  - Time to Crack Initiation (TTFINTS)
  - Load At Crack Initiation (FLINTN)
  - Density of the specimen (DNSTKGM3)

- Peak Load (PEAKLOADN)
- Young's Modulus (YNGMODPA)

♦ **Category 2 (effective dimensions)**
- Effective length
- Effective height
- Effective width

  Effective dimensions were defined after the training of S-1, S-2 and S3 networks (Figure 7-3). Effective length for example, is calculated by multiplying the original length with the contribution of the original length to the network output S-3.

♦ **Category 3 (areas)**
- Length * Height
- Height * Width (Hght * Wdth)
- Width * Length
- Crack Length * width (Cracked area)
- (Height - Crack Length) * width (Un-cracked Area)

♦ **Category 4 (volumes)**
- Volume
- Effective volume (Effective Vol)
- Length * Height * Effective width
- Length * Effective Height * width
- Effective Length * Height * width
- Cracked volume = Length * Crack Length * width
- Un-racked volume = Length (Height - Crack Length) * width

Note: Length = Specimen length; Height = Specimen height; Width = Specimen width

Raw and normalised values of input variables were prepared for use in the networks.

7.2.3. Organising data sets required for network

7.2.3.1 Data Sets

The data obtained for specimens are organised in row and columnar-wise matrix. For example all input attributes of a specimen are organised in an array or a row and when all rows for specimens are amalgamated it becomes a matrix.

Rows are tagged as "Training", "Cross Validation", or "Testing" data sets. Training process is run using training data set while cross validation is used as a tool for preventing over-training. The testing data rows, which can be tagged before or after the training process is run, are used for prediction or forecasting. And this data set is not involved in training process. The columns are tagged as input and output.

The following chart shows the number of data records pertaining to specimens in each size category of a batch of 17, distributed among training, cross validation and testing data sets. For example, the 8 specimens under the rate of loading of 2.5 mm s^{-1} were allocated as 5, 2, 1 data records to training, cross validation and test data sets, respectively.

Table 7-1: Distribution of specimens among training, cross validation and test data sets

Distribution of Number of Specimens				
Rate of Loading (mm/s)	Total No of Specimens	No of Specimens		
		Training	Cross Validation	Test
0.625	4	2	1	1
2.500	8	5	2	1
10.000	5	3	1	1

7.2.4. Selection of a suitable network topology

Neurosolutions 3.02, as it provides the facility for using different topologies discussed in Chapter 6, can be organised to select the best network topology. The following were considered in this study because it is a set of topologies that can incorporate supervised and unsupervised training techniques.

Multi layer Perceptron (MLP)

Generalised Feed Forward (GFF)

101

Jordan Elmann

Radial Basis Function (RBF)

Self Organising Feature Maps (SOFM)

7.2.5. Training

Select and open the required topology from the software package and change the network parameters as necessary. In this setting, preferable number of epochs also included for supervised or/and unsupervised training cases. Train the network randomising initial weights and the software automatically handles the training data set to train and cross validation data set to validate and monitor the process.

The learning curves for both the training and cross validation data sets are plotted in the same graph (see Figure 7-2, for example). The training is carried out until both training and (Boolean AND) cross validation mean-squared errors (MSEs) reach a minimum. The alternative option for terminating the training is minimum training MSE without using cross validation, but this was not selected here.

The training process automatically saves the best weights at the minimum cross validation error if cross validation is used or at the minimum training error if cross validation is not used (this option is not selected).
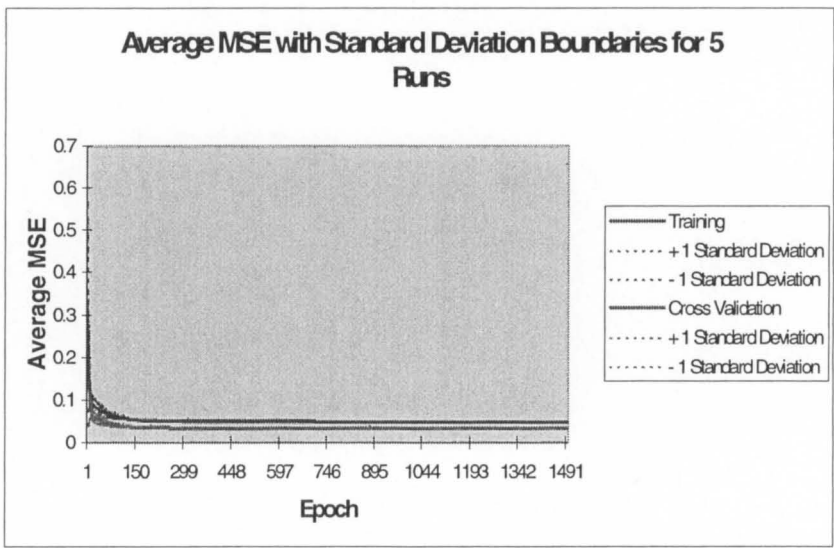
Figure 7-2: Average MSE for training and cross validation data sets for 5 training sessions. (All plots overlap each other.)

102

7.2.6. Testing, validation and enhancement

The testing option of the software generates the statistical data for the trained network. It provides MSE, NMSE (normalised MSE), minimum and maximum absolute errors and co-relation between desired and the network outputs. If required a plot between the desired and the network outputs is generated on selection. The option for sensitivity analysis about the mean generates a contribution and behaviour report of every variable in the training data set. This report is very useful for fact finding. The package is facilitated with the self changing options for the number of PEs in the hidden layer and for performing several runs. These options enhance accuracy of result.

As a strategy, the data rows were not randomised in order to make comparisons among different network configurations. Randomisation was included for the best network described in Chapter 8, which increased the co-relation by about 10-15%.

7.2.7. Detail discussion on training, validation and testing of the developed networks

7.2.7.1 Use of raw data and normalised data

Raw input data did not provide any difficulties or problems or reduction in performance compared to normalised data used in above topologies. Therefore it was intended to use raw input data for subsequent networks tested. Further checking was carried out from time to time in order to test whether normalised data would increase performance. Since the use of raw fracture toughness (FT) as network's desired output, resulted in abnormally high error value in the training output, it was decided to use normalised data. Normalisation of this FT was considered in two ways. One was dividing by the norm (|| . ||) of FT (vector) and the other was dividing by the average. Since both methods generated the same results with same performance measures, the latter (dividing by average) method was used for further analysis. As discussed in Chapter 6, normalisation of data (in unsupervised training) is not compulsory but can be used whenever needed. For example, the Euclidean distance measure used in a clustering technique (section 6.2.1.3.2.1.2 of Chapter 6) uses raw data instead of normalised data.

7.2.7.2 Topology

The basic data set in the category 1 (section 7.2.2) was used as input variables in order to select the highest performing topology.

The topologies RBF and SOFM trained data very well, but the other supervised training topologies mentioned above did not train so well, and found training difficulties. The RBF was found better than SOFM based on the comparison of statistical results of the outcomes. Therefore finally, it was decided to enhance the results RBF topology, using supervised and unsupervised training techniques. Specifically, scattered vector variables were clustered using unsupervised training, around manageable number of cluster centres (output of unsupervised training). These clusters became the input to the supervised portion of the network.

7.2.7.3 Optimisation of output

The following Table 7-2 shows the best found network configuration for the input variables described in Category 1. The table indicates the important parameters of unsupervised and supervised portions of the network. Unsupervised clustering required 500 epochs to generate the best results and best number of cluster centres was 20 (PE^s).
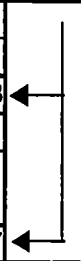
As discussed in section 6.2.3, Euclidean distance measure was assigned in clustering and the multivariate Gaussian function was used as the error reduction function. The best step size was 0.001 (γ value in Equation 6-18) and β parameter was 0.01.

In the supervised portion, best-configured network parameters were as follows.

- Number of epochs is above 2000
- One hidden layer and number of PE^s in the hidden layer is 25
- β value for both hidden and output axons is 1
- Important back propagation step size and the momentum (η and α of Equation 6.24 respectively in section 6.2.2.1) parameters are 0.02 and 0.7 for the hidden layer and 0.003 and 0.7 for the output layer
- The activation or transfer is with Tanh function in both hidden and output layers

This configuration is tabulated in Table 7-2.

Table 7-2: RBF configuration chart

	Unsupervised		Supervised Hidden		Supervised Output		Back Propa gation
	Synapse	Axon	Synapse	Axon	Synapse	Axon	
No. of epochs	500		>2000				
No. of PEs	20		25				
Rate (Step Size)	0.001		0.02	0.02	0.003	0.003	←
Consciencefull (Beta)	0.01			1		1	
Winner (Competitive) / Transfer Function	Euclidean	Gausian		Tanh		Tanh	
Momentum			0.7	0.7	0.7	0.7	←

7.2.7.4 Validation

Running the sensitivity analysis feature of Neurosolutions is carried out in validation. It gives the relative contribution of each input variable on output at training. The best-saved network weights are used for testing the network using test data. A plot of the network output versus the desired output is given simultaneously with the corresponding statistical information. Ten RBF networks (S-1 – S-10) were trained with different combinations of inputs and Table 7-3 and 7-4 summarises the results from ALL these networks and an appropriate discussion is given in section 7-3. The S-1, S-2 and S-3 are primary networks that indicate only basic input variables. (ie: They do not have multiple terms of two or more inputs such as width, height etc.). The columns labelled Parameter, FT Contribution and Con % of Table 7-3 show input variables used in the network, raw values of the contribution of each input variable on fracture toughness (FT) and the percentage of this contribution respectively. Table 7.4 is the performance of each network in tabulated form that described S-1 through to S-10 of Table 7-3. The correlation indicated in the table is between the desired output and the network output and it is above 60%, which indicates a good relationship. The S–1 network, showed the highest performance where the crack length is not included. Figure 7-3 shows comparison charts between the desired output and the network output for S-1 networks. Note that all of these networks were run without randomising input variables in order to keep uniqueness of them for easy comparison. Randomising and further analysis of data, which is discussed in Chapter 8, enhanced the final network.

Table 7-3: Sensitivity Analysis reports for networks using different sets of input variables (a) S-1 through to S-6 (b) S-7 through to S-10.

S - 1		
Parameter	FT Cont	Con. %
ROLMS	16.0085	77.81
WIDTHM	2.3382	11.37
HEIGHTM	1.7410	8.46
LENGTHM	0.1642	0.80
MCPCT	0.1141	0.55
LENANGRAD	0.0828	0.40
WEIGHTKG	0.0779	0.38
FACANGRAD	0.0427	0.21
CURVM	0.0025	0.01
TTFINTS	0.0003	0.00
DNSTKGM3	0.0002	0.00
PEAKLOADN	0.0001	0.00
FLINTN	0.0001	0.00
YNGMODPA	0.0000	0.00
Total	20.57	100.00

S - 2		
Parameter	FT Cont	Con. %
WIDTHM	6.5384	36.48
ROLMS	6.1706	34.43
HEIGHTM	3.7407	20.87
PRE_CRACK	0.9766	5.45
LENGTHM	0.2938	1.64
WEIGHTKG	0.0779	0.43
FACANGRAD	0.0598	0.33
MCPCT	0.0407	0.23
LENANGRAD	0.0254	0.14
CURVM	0.0006	0.00
DNSTKGM3	0.0001	0.00
YNGMODPA	0.0000	0.00
Total	17.92	100.00

S -3		
Parameter	FT Cont	Con. %
ROLMS	12.8203	57.55
WIDTHM	3.7764	16.95
PRE_CRACK	3.5122	15.77
HEIGHTM	1.7746	7.97
LENGTHM	0.1757	0.79
LENANGRAD	0.0893	0.40
WEIGHTKG	0.0480	0.22
FACANGRAD	0.0445	0.20
MCPCT	0.0367	0.16
CURVM	0.0007	0.00
DNSTKGM3	0.0001	0.00
YNGMODPA	0.0000	0.00
Total	22.28	100.00

S - 4		
Parameter	FT Cont	Con. %
Volume	85.5224	60.21
Hght*Wdth	43.6876	30.76
ROLMS	10.9552	7.71
PRE_CRACK	1.3624	0.96
WEIGHTKG	0.1320	0.09
LENANGRAD	0.1840	0.13
FACANGRAD	0.1179	0.08
MCPCT	0.0754	0.05
CURVM	0.0015	0.00
DNSTKGM3	0.0004	0.00
YNGMODPA	0.0000	0.00
Total	142.04	100.00

S - 5		
Parameter	FT Cont	Con. %
Volume	46.7019	51.15
Hght*Wdth	30.2280	33.10
ROLMS	9.8847	10.83
Wdth*Lngth	2.5797	2.83
Lngth*Hght	1.1573	1.27
PRE_CRACK	0.4895	0.54
WEIGHTKG	0.0551	0.06
FACANGRAD	0.0964	0.11
MCPCT	0.0608	0.07
LENANGRAD	0.0580	0.06
CURVM	0.0002	0.00
DNSTKGM3	0.0000	0.00
YNGMODPA	0.0000	0.00
Total	91.31	100.00

S - 6		
Parameter	FT Cont	Con. %
Volume	85.4509	77.18
ROLMS	13.2497	11.97
Effective Height*Width	9.4905	8.57
PRE_CRACK	2.0543	1.86
FACANGRAD	0.2092	0.19
WEIGHTKG	0.1602	0.14
MCPCT	0.0558	0.05
LENANGRAD	0.0455	0.04
CURVM	0.0038	0.00
DNSTKGM3	0.0001	0.00
YNGMODPA	0.0000	0.00
Total	110.72	100.00

(a)

106

S - 7		
Parameter	*FT Cont*	*Con. %*
Hght*Wdth	78.5770	71.07
ROLMS	21.6076	19.54
Effective Vol	7.8976	7.14
PRE_CRACK	1.8483	1.67
LENANGRAD	0.2802	0.25
WEIGHTKG	0.1096	0.10
FACANGRAD	0.1643	0.15
MCPCT	0.0761	0.07
CURVM	0.0015	0.00
DNSTKGM3	0.0002	0.00
YNGMODPA	0.0000	0.00
Total	110.56	100.00

S - 8		
Parameter	*FT Cont*	*Con. %*
(Hght-Crack Len) *Wdth	56.8273	41.31
Volume	38.4619	27.96
Hght*Wdth	35.1554	25.56
ROLMS	3.5766	2.60
PRE_CRACK	3.3308	2.42
MCPCT	0.0619	0.04
WEIGHTKG	0.0634	0.05
LENANGRAD	0.0377	0.03
FACANGRAD	0.0327	0.02
CURVM	0.0011	0.00
DNSTKGM3	0.0000	0.00
YNGMODPA	0.0000	0.00
Total	137.55	100.00

S - 9		
Parameter	*FT Cont*	*Con. %*
Hght*Wdth*Effctive length	106.9016	42.31
Crack Len *Wdth	49.1121	19.44
(Hght-Crack Len) *Wdth	42.9529	17.00
Hght*Wdth	24.3386	9.63
Volume	16.7592	6.63
ROLMS	10.6853	4.23
PRE_CRACK	1.5281	0.60
LENANGRAD	0.2125	0.08
FACANGRAD	0.0900	0.04
WEIGHTKG	0.0569	0.02
MCPCT	0.0435	0.02
CURVM	0.0022	0.00
DNSTKGM3	0.0001	0.00
YNGMODPA	0.0000	0.00
Total	252.68	100.00

S - 10		
Parameter	*FT Cont*	*Con. %*
Volume	83.3869	57.95
Hght*Wdth	47.5069	33.02
ROLMS	11.1636	7.76
PRE_CRACK	1.5279	1.06
LENANGRAD	0.1401	0.10
WEIGHTKG	0.0894	0.06
FACANGRAD	0.0539	0.04
MCPCT	0.0185	0.01
CURVM	0.0010	0.00
DNSTKGM3	0.0001	0.00
YNGMODPA	0.0000	0.00
Total	143.89	100.00

(b)

Table 7-4: Relevant   Performance   Measures   for   the   10   networks   shown in Table 7-3

Test/Predicted Data		Performance Measures						
Reference	NoR EUFP	MSE	NMSE	MAE	Min Abs Error	Max Abs Error	Correlation	Correct %
S - 1	48	0.2214	0.3855	0.3809	0.0069	1.4755	0.8158	100
S - 2	48	0.4582	0.7976	0.5042	0.0112	1.7969	0.6410	100
S - 3	48	0.4187	0.7288	0.5001	0.0011	1.6599	0.6453	100
S - 4	48	0.4441	0.7730	0.5131	0.0066	1.7840	0.6394	100
S - 5	48	0.4531	0.7888	0.5152	0.0132	1.8432	0.6387	100
S - 6	48	0.4084	0.7109	0.4805	0.0105	1.8215	0.6776	100
S - 7	48	0.4412	0.7680	0.5132	0.0079	1.8070	0.6294	100
S - 8	48	0.4512	0.7854	0.5104	0.0046	1.8418	0.6461	100
S - 9	48	0.4692	0.8168	0.5226	0.0015	1.9110	0.6158	100
S - 10	48	0.4668	0.8126	0.5304	0.0050	1.7386	0.5983	100

NoR EUFP - Number of Records Effectively Used For Prediction

MSE   – Mean Square Error

NMSE – Normalised Mean Square Error

MAE – Mean Absolute Error
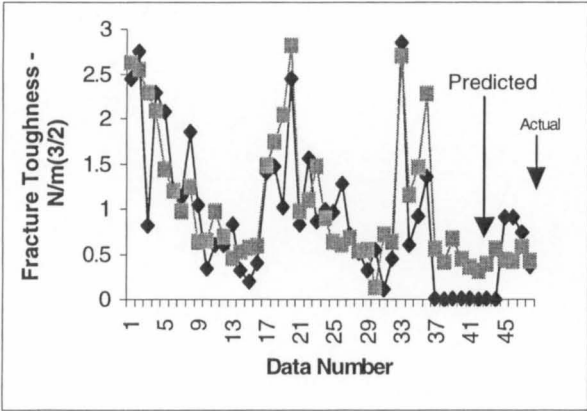
Test Data (Predicted)   Training Data
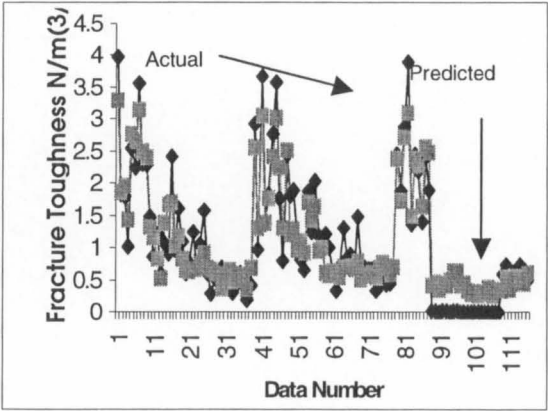
Figure 7-3 : Predicted Fracture toughness for training and test data using (S–1) network ◆ - Actual data plot   ■ - Predicted data plot

7.3 Discussion and primary conclusions

- According to the networks trained with very basic input information, the rate of loading (ROL/ROLMS) shows the highest contribution to the fracture toughness (FT) as cited in S-1, S-2 and S-3 of Figure 7-3. Of all basic variables, only ROL, crack length and height are significant for FT. Length and moisture content (MC) have shown low influence and time to crack initiation (TTFINTS), density, peak load, failure load and Young's modulus are insignificant within the context of the variability of the selected wood specimens tested. If the crack length is removed from the network and trained (see S-1), the contribution of ROL increases while width and height contributions remain unchanged (compare S-1 and S-3). Although the moisture content, grain-angle (LENANGRAD), face angle (FACANGRAD), peak load, failure load and time to failure show low effect on FT, they have influenced to change the network contributions for width and ROL (compare S-1, S-2, S3). Therefore it can be concluded that even though some variables that don't show a reasonable contribution to the output, may indirectly affect the influence of other input variables thereby changing their levels of contribution.

- In S-2 and S-3 sensitivity analysis shows that parameters can contribute differently at different instances. And also once a network got trained to give better results with minimum MSE and maximum correlation out of all 10 results shown (Table 7-4). With the same parameters and same network topology and the constant this performance was obtained only once. These two cases warn us to take care that not to confirm the trained network for prediction at the first successful instant of training. Further, the effect of width shows even higher than ROL in S-2, but ROL contribution is higher than that of width in S-1 and S-3. Hence it is very important to assign all possible basic input variables to be present in a network rather than removing less effective variables. These variables are given certain values in parallel processing, although they do not directly exhibit high contributions. This has been hypothezised as in Figure 7-5 where the effect of removing a variable with low influence is displayed. Therefore in all networks tested, basic input variables were included. Based on this parallelism, analysing individual input variable against the output was not included in this thesis. . We label these S-1, S-2 and S-3 as primary networks 1,

2 and 3 for easy understanding in subsequent discussion. The following sections show the changes occurred in contribution when the inputs are changed.

Level of contribution

(a)   (b)
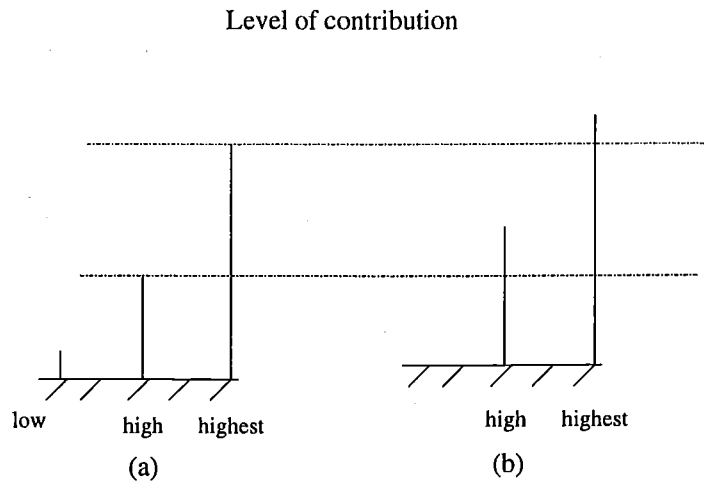
Figure 7-4: Different levels of hypothesized contribution at two stages. (a). All variables are presents (b). slightly influenced variables are removed

- The volume, length*height, height*width and width*length are included in S-5 replacing length, height and width. The variables multiplied by length has provided a reduced contribution due to low contribution of length as shown in S -1 through to S-3. Notice that the previous contributions of ROL and pre-crack length have gone down in the presence of the new ones. The contributions of volume and height*width have increased in S-4, since length*weight and width*length were removed from the network (notice that related contribution percentage of height*width has gone down). The volume is the most contributive variable so far, agreeing with the Weibull's theory.

- The contributions of (fundamental) input variables of a primary network (we used S-3), were used to find the effective values (For example, if the length contribution is x and the length is ℓ mm, then the effective length is xℓ). However effective (Height*Width) in S-6 and effective volume in S-7 have not made better contributions.

110

- Uncracked area [(Height-Crack length)*width] of the cracked plane is the highest contributor among inputs in S-8 which is effectively higher than the volume. In contrast a portion of the volume (Height*Width* effective Length) calculated using the effective length provided a very high contribution more effective than that for cracked area (Crack Length*Width) and uncraked area as shown in S-9. Therefore the whole volume effect has reasonably gone down in the presence of the other basic variables in these networks. Therefore we can argue that only a part of the volume is more effective on fracture than the entire volume. Also the next immediate contributors are cracked and uncracked areas. Therefore we can further conclude that a part of the volume around the crack plane contributes to fracture rather than the entire volume. It means the contribution of a local volume considered in Weibull's theory on fracture reduces as the distance from the crack plane increases. This has been hypothesized as in Figure 7-5 to give a clue for future investigations. Further the cracked and uncraked areas are also highly influential parameters.

Distance to local volume from crack plane in Weibull's concept
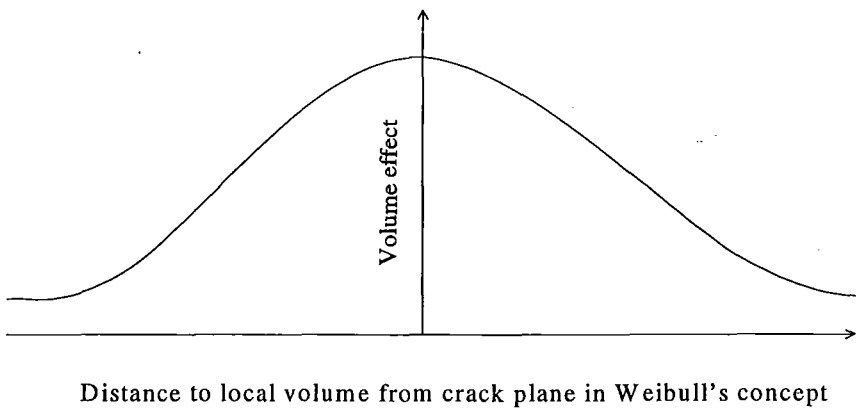
Figure 7-5: Hypothesised volume effect over the unit local volume

- A set of fixed input variables provides the same pattern at different training instances providing almost the same results. For example, S-4 shows it as S-10 has given very similar outcomes because the two networks have the same inputs but trained at two different occasions. The best networks found in this chapter are further referred in the next chapter for predicting fracture toughness.

111

Chapter 8: ANN Model for Fracture Toughness for crack initiation

8.1. Introduction

This Chapter is strongly based on Chapter 7, which dealt with the implementation of ANN models for fracture toughness. We develop a more refined model and discuss the influence of more important variables filtered from the networks discussed in the last chapter. As we were able to conclude that there is an effective portion of the whole volume that influences the fracture toughness, it can be utilised to find a better solution. We start the discussion with the three basic requirements of the desired neural network in section 8.2.

8.2. Configuration of best model

The configuration consists of the following factors that needed to be always considered in neural network modelling.

- *Network Topology*
- *Network parameters*
- *Set of input variables*

8.2.1. Network Topology

The best topology found was the RBF for an ANN model for fracture toughness as discussed in the last chapter.

8.2.2. Network Parameters

The important network parameters found so far are tabulated in the Table 8-1.

The distance measure under unsupervised portion indicates the clustering technique used. The dot product provided poorer results than Euclidean distance measure.

Table 8-1: Best parameter configuration for RBF network for fracture toughness

Unsupervised #500	Synapse	Beta	0.01
		Gamma	0.3
		Step Size	0.001
		Distance Measure	Euclidean
	Axon	No. of cluster centres (PEs)	20

Supervised > #2000	Synapse	PEs (Input)	20	
		PEs (Hiden)	25	
	Axon	PEs (out)	1	
	Error Criterion		L-2	
	Back propagation gradient	Hidden	Synapse	0.02
			Axon	0.003
			Momentum	0.7
		Output	Synapse	0.02
			Axon	0.003
			Momentum	0.7

8.2.3. Set of input variables

The following Table 8-2 tabulates the inputs used for the final stage of training. The set of input variables consists of those that are highly correlated with fracture toughness selected from the networks tested in the last chapter. It consists of four versions of the volume of specimen and two versions of area and the specimen geometry. After selecting the most influential versions of volume and area, other versions were removed from the list. [Following this, we removed all multiple termed variables but did not remove the fundamental variables.]

Table 8-2: Final stage input variables

1　ROL
2　Crack Length
3　Width
4　Height
5　Length
6　Volume
7　Uncracked Volume
8　Height*width*effective Length
9　Cracked Volume
10　Height*width
11　Crack Length*Width - Cracked area
12　(Height - Crack Length)*Width - Uncracked area

8.3.　Training results and validation

The sensitivity analysis, performance matrix and the plots between desired and network output are shown in Tables 8-3,4 and 5 and Figures 8-1,2,3 for training, testing and cross validation data sets. The table of sensitivity analysis is the left chart while performance matrix of statistical analysis is the right chart in each table.

Table 8-3: Sensitivity analysis and Performance matrix for training data set

Training Results				Perform	Value
Parameter	Cont.	Cont.%		Perform	Value
Uncracked Volume	53.57	77.05		MSE	0.3412
ROLMS	6.18	8.89		NMSE	0.4916
(Hght-Crack Len) *Wdth	5.88	8.46		MAE	0.4422
WIDTHM	1.58	2.27		Min Abs Error	0.0019
PRE_CRACK	1.28	1.84		Max Abs Error	1.6836
HEIGHTM	0.99	1.43		r	0.7130
LENGTHM	0.05	0.07			
Volume	0.00	0.00			
Height*Width*Effctive length	0.00	0.00			
Cracked Volume	0.00	0.00			
Hght*Wdth	0.00	0.00			
Crack Len *Wdth	0.00	0.00			
Total	69.53	100.000			

114
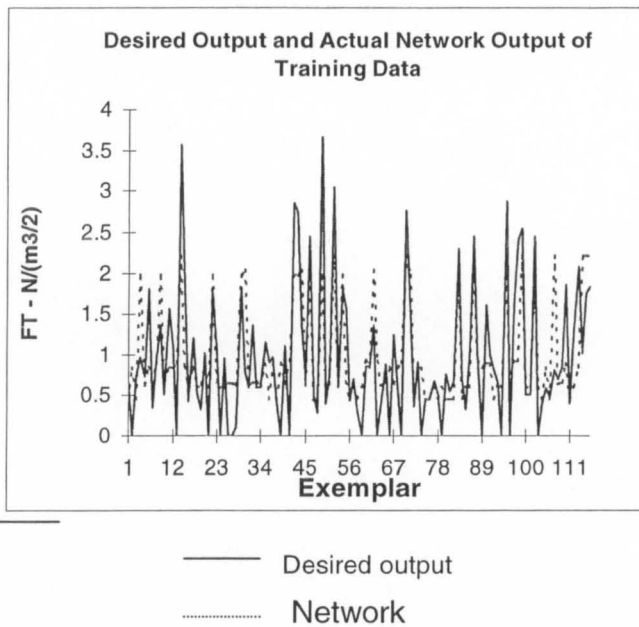
Figure 8-1: Comparison plot of desired versus network output for training data set.

Table 8-4: Sensitivity analysis and Performance matrix for testing data set

Testing Results				
Parameter	*Cont.*	*Cont.%*	*Perform*	*Value*
Uncracked Volume	57.33	73.64	MSE	0.4265
(Hght-Crack Len) *Wdth	8.91	11.45	NMSE	0.4331
ROLMS	7.45	9.58	MAE	0.4629
WIDTHM	1.68	2.15	Min Abs Error	0.0014
PRE_CRACK	1.39	1.79	Max Abs Error	1.9891
HEIGHTM	1.03	1.33	r	0.7626
LENGTHM	0.05	0.06		
Volume	0.00	0.00		
Height*Width*Effctive length	0.00	0.00		
Cracked Volume	0.00	0.00		
Hght*Wdth	0.00	0.00		
Crack Len *Wdth	0.00	0.00		
	77.85	100.000		

115

Desired output
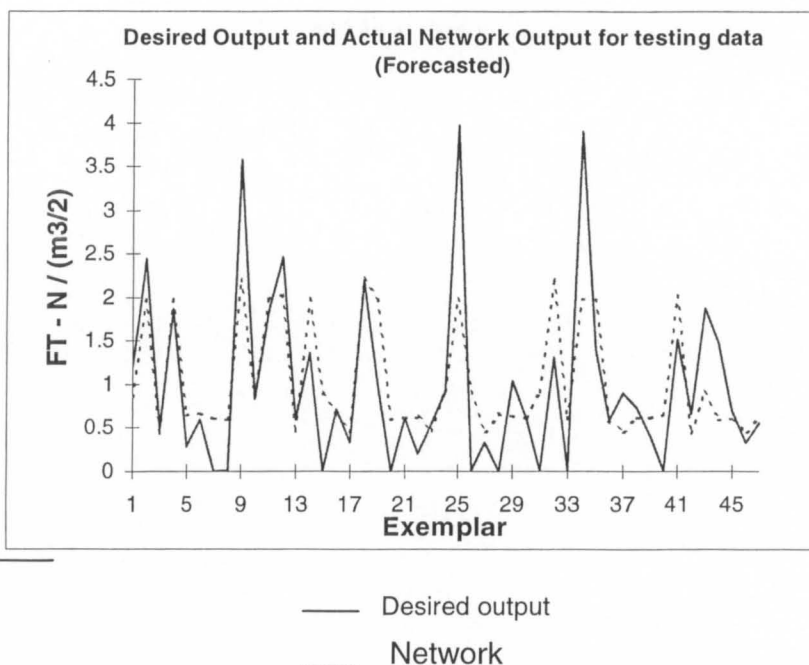
Network

Figure 8-2: Comparison plot of desired versus network output for testing data set.

Table 8-5: Sensitivity analysis and Performance matrix for cross validation data set

Cross Validation Report				
Parameter	*Cont.*	*Cont.%*	*Perform*	*Value*
Uncracked Volume	67.63	64.10	MSE	0.3956
(Hght-Crack Len) *Wdth	21.74	20.61	NMSE	0.5123
ROLMS	10.33	9.79	MAE	0.5077
WIDTHM	2.21	2.10	Min Abs Error	0.0082
PRE_CRACK	1.94	1.84	Max Abs Error	1.3713
HEIGHTM	1.54	1.46	r	0.7009
LENGTHM	0.10	0.10		
Volume	0.00	0.00		
Height*Width*Effctive length	0.00	0.00		
Cracked Volume	0.00	0.00		
Hght*Wdth	0.00	0.00		
Crack Len *Wdth	0.00	0.00		
	105.50	100.000		

116

Desired Output and Actual Network Output of Cross validation data

Legend:
— Desired output
.... Network
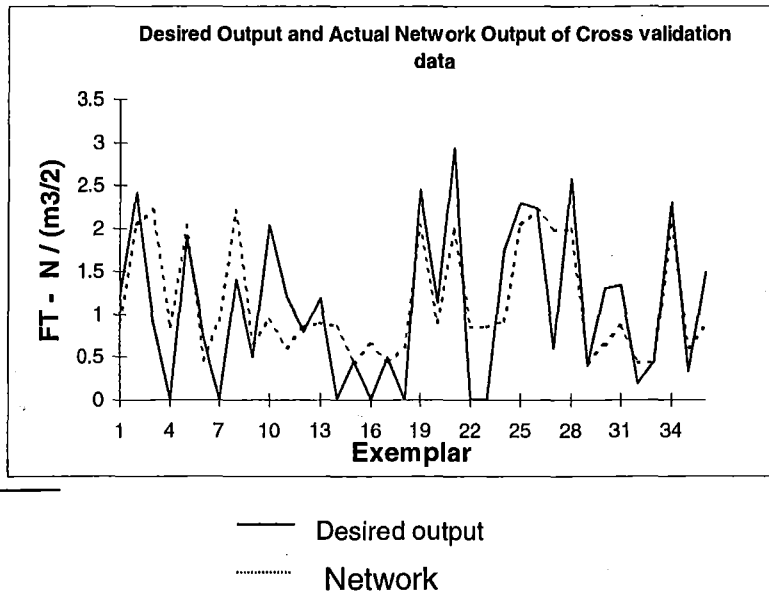
Figure 8-3: Comparison plot of desired versus network output for cross validation data set.

➢ Overview:

Tables 8-3,4 and 5 provide important information about the effects of input variables on FT. Whole volume, Height*Width*effective Length (a portion of the whole volume), cracked volume, area of the cross section and the cracked area have drawn zero contributions while uncracked volume, uncracked area, ROL, width, crack length and height are significant input variables. Length shows a very small contribution about 0.06%. Highest contribution, about 74% is from the uncracked volume which still confirms Weibull's theory as applicable to only this uncraked portion. This type of analysis may not be done using any other modelling methods. Co-relation coefficient for the predicted data (testing results) and for training and cross validation data sets shows 76%, 71% and 70%, respectively. The MSE, maximum and minimum errors displayed in all three cases are in a reasonably good range. The SPPS software has been used to compare the results with this model but it was not intended to proceed with detailed model development using this software.

8.4. Additional model validation using SPSS

The SPSS statistical package was used to derive an Ordinary Least Square (OLS) regression model of fracture toughness using seven selected input variables. The estimated results were successful with the input variables explaining 54% of the variation in fracture toughness. This model does not suffer from the presence of serial correlation to a large degree as indicated by the Durbin-Watson score of 1.36. Furthermore, the F-test is significant indicating that the multiple correlation coefficient in the population is not zero.

Table 8-6: Statistical analysis results for fracture toughness for crack initiation

Inputs and their coefficients	Crack Length	Uncracked Area	Uncracked Volume	ROL	Width	Constant	Height	Length
	57.203	2444.478	-731.407	9.571	-105	0.658	0.000	0.000

Regression Relation		Hypothesis test	
Multiple R	0.73427	F	45.16
R Square	0.53915	Significane F	0.0000
Adjusted R Sq.	0.52751	Durbin-Watson	1.359
Std. Error	0.60823		

Number of cases used
199

Uncracked volume = Length*(Height - Crack Length)*Width
Uncracked area = (Height - Crack Length)*Width

118

Therefore if the fracture toughness for crack initiation is T_{Fcint}, the developed model can be written as:

$$T_{Fc\text{int}} = 57.203a + 2444.478A_u - 731.407V_u + 9.571R_{ol} - 104.985W + 0.658$$

where   a - Crack Length

A_u – Area of the Uncracked plane

V_u – Uncracked Volume

R_{ol} – Rate of Loading

W – Width

The result shows the ineffectiveness of Length and Height in the equation. Similarly Height and Length had very little effect on same fracture toughness in the ANN model too.

Preliminary data analysis using a log-linear specification resulted in a low R^2 value than this.

The assumption of linearity is not violated as shown by the scatter diagram of standardised regression residuals obtained from OLS regression and plotted against standardised regression predicted value. The data points are randomly distributed around a horizontal line through zero. (Figure 8-4 and 8-5)

119
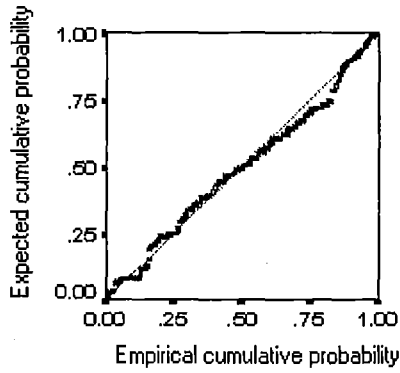
Figure 8-4: Cumulative Probability plot of normalised values of fracture toughness – It shows the tendency of empirical and expected values to coincide
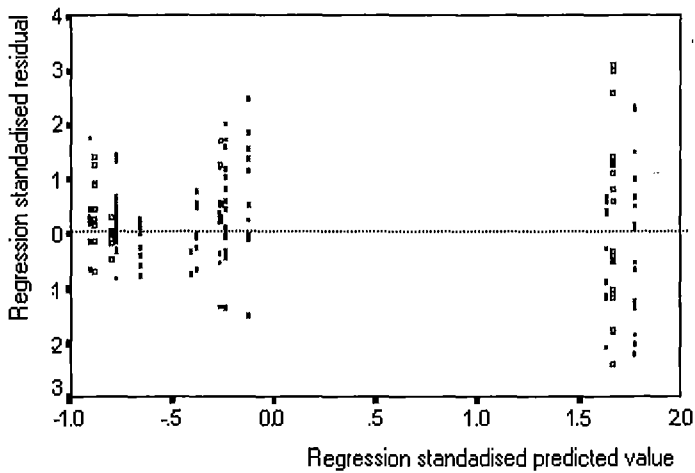
Figure 8-5: Standardised Scatter plot of normalised predicted fracture toughness

Figure 8-6 shows the comparison among empirical data, ANN and SPSS outputs. SPSS and ANN outputs show very similar patterns, following the empirical data

reasonably and closely. Some data points look like zero FT values which represents normalised FT data ranging from 0.0026 to 3.4.
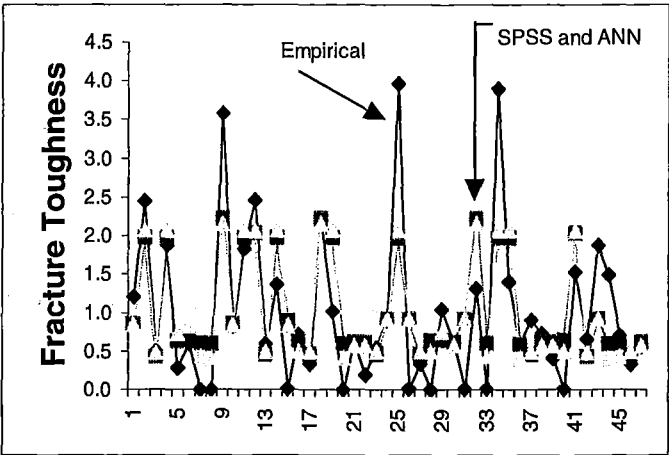
Figure 8-6: Comparison plot for empirical, ANN and SPSS data

Outputs: Blue – Empirical; Red – ANN; Yellow – SPSS

8.5. Usage of the model – automated Simulation and forecasting

Since the network requirements and best parameters have been already set user can use the network described above for forecasting fracture toughness for crack initiation. When the network is trained once, it can be used for prediction for any number of times in which case only 5,6 and 7 of the steps shown below are required to perform prediction (see figure 8-7). For the sake of completeness all the necessary steps for training, validation and prediction are given below for a network using Neurosolutions software.

1. Set the network parameters.
2. Tag the appropriate input vectors of the selected network.
3. Divide each fracture toughness value by the average (or by norm) of all values.
4. Train the network using training and cross validation data sets .
5. Input data rows for which the prediction required is marked as testing.
6. Test option for testing data will generate the predicted network output.

7. Multiply the each output by the *avg* to receive appropriate predicted fracture toughness.
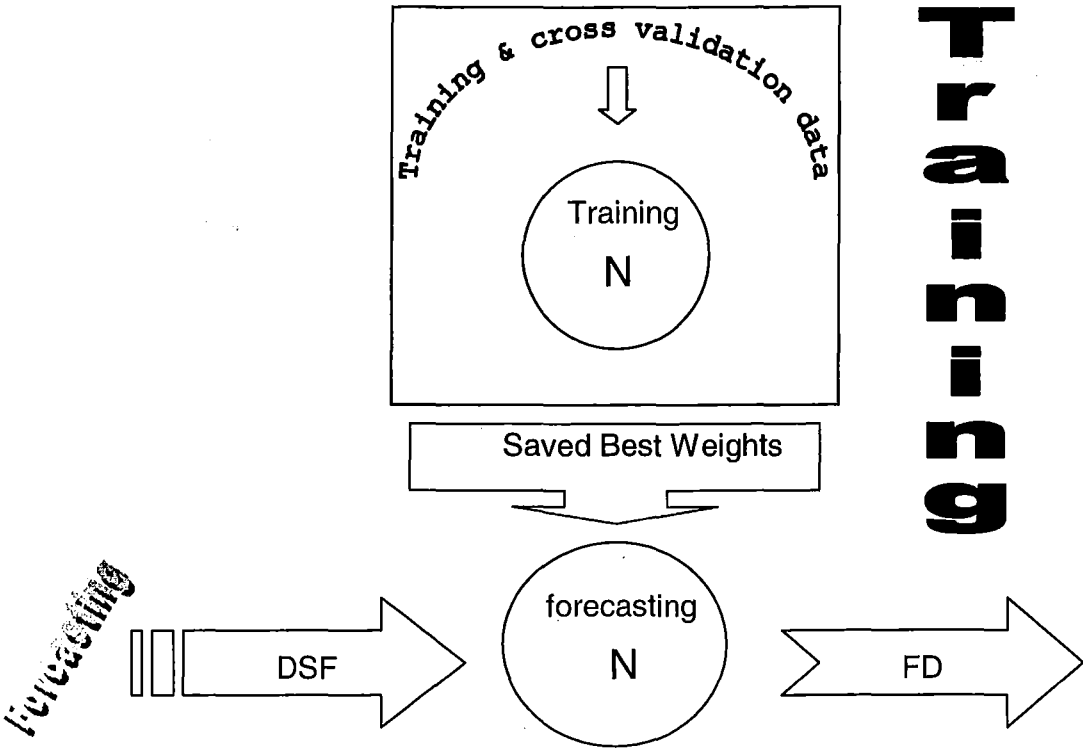
(N – RBF network)

DSF - Data Set (appearing as testing rows) for Forecasting

FD - Forecasted Data (network output)

Figure 8-7: Using the trained Network (RBF) for prediction of fracture toughness for crack initiation (Training portion is included for completeness).

8.6. Discussion and conclusion

8.6.1. Data and model validity

Time to crack initiation, time to catastrophic failure, peak load etc. included in the set of inputs as a trial, showed almost zero weight. Although density and Young's Modulus are fundamental properties of wood, they yielded almost zero weights indicating no influence. This may be due to the limited range of values for those parameters obtained for the specimens cut from the same tree. However Table 8.7, which shows the ranges for inputs, indicates that it is hard to substantiate the above reason pointing to a limited range of the above variables. The ranges of ROL, width, crack length, height which are the predominant input variables in the networks of S-1,S-2 and S-3 (Chapter – 7) are closer to that of Young's modulus, density and moisture content.

Table 8-7: Range of input data showing, lowest and highest are minimum and maximum values of a variable: (a) highly influencing variables (b) variables with very low influence

	Uncracked volume - m3	Uncracked area - m2	Rol - m/s	Width - m	Crack length - m	Height - m
Lowest	0.00000675	0.000027	0.000625	0.006	0.006	0.0135
Highest	0.002205	0.002205	0.01	0.045	0.041	0.09
Highest/Lowest	326.6666667	81.666667	16	7.5	6.833	6.667

(a)

	Young's Modulus GPa	Density - kg/m3	MC %
Lowest	1.36	198.57	4.13
Highest	6.11	930.26	22.89
Highest/Lowest	4.50	4.68	5.55

(b)

The validity of the data depends on the accuracy of measurement of the data. Therefore it is worth considering the accuracy of the input variables.

Geometrical measurements of the specimen and crack length were straightforward data while ROL was accurately set by the testing machine software when experiments were carried out. Moisture content, density, weight, and measurements of grain pattern were made carefully.

123

The fracture load was accurately observed using the real time graph plotted by the testing machine software. At the crack initiation the graph was interrupted and slightly bent and the load at this point was noted carefully as the fracture load.

- *Network*

The fracture toughness was calculated using Equations 7.1 and 7.2. These Equations are arguable when they are applied in these networks because they already contain geometrical measurements of specimens except for width in the geometry correction factor. All geometrical measurements were input to the neural network, which are obviously factors influencing fracture toughness. However, desired values used in a neural network are only used to calculate the suitable weights and do not directly involved in calculation of the network output. Further, the initial weight vectors at training are set randomly. Consider the generalised delta rule for weight changes. The expressions 7.21 or 7.22 for supervised training described the weight change at an iteration using the desired and network output of current iteration.

The components of the weight change at t^{th} iteration is the product of the amount of variation of the output from the desired output, first derivative of the output (activation function is differentiable), the input variable and the step size or the learning rate . In unsupervised training, for example clustering, weight change at clustering is never dependent on the desired value. Therefore the desired vector is not taken into account in the generated output. Therefore the network output does not depend on any component of the desired vector.

8.6.2. Conclusions

Volume, an effective volume (height * width * effective length), cracked volume, area (height * width) and cracked area (crack length * width) have shown *zero* weights in the input combinations shown in Tables 8.3, 8.4 and 8.5 which never occurred in any other training performed.

Further, Tables 8-3,4,5 indicate that the un-cracked volume is the mostly influenced input variable of all. The whole volume of the specimen shows null effect although it was effective on fracture toughness in the absence of uncracked volume in the input data set.

124

In summary the following can be concluded for fracture toughness for crack initiation for clear wood beams of NZ Pinus Radiata with grain almost parallel to the length.

- The fracture toughness can be successfully modelled using artificial neural network. The best network parameters are shown in Tables   8-1and 8-2 and the following inputs are given in Table 8-3 as being the most influential variables.

Uncracked Volume	Pre-crack length
Uncracked Area	Width
Rate of Loading	Height

  The length can be neglected.

- Uncracked volume was found to be the most influential variable for fracture toughness showing a 77% contribution.

  As the crack length tends to zero the uncracked volume reaches the whole volume. This implies the Weibull's volumetric effect on fracture which is more pronounced on the uncracked portion of the volume of a cracked member. Further research may be performed on different uncracked volume configurations due to different crack orientation.

- The second most influential variable is either un-cracked area or rate of loading which showed a similar contribution of about 8.5%.

- Grain orientation, density, weight, moisture content, times to failure states etc. did not affect the fracture toughness

- The variables can be collectively examined for investigations using ANN methods instead of treating them individually. Also ANNs are able to model non-linear relationships among variables.

- ANN is useful for analysing and sorting out the variables influencing fracture toughness as was clearly shown in this thesis.

- There were limitations and boundaries, which are common features of a general purpose (common) software package. Therefore training suffered

somewhat in timing and efficiency with the use of this ANN software package.

Chapter 9 Summary

9.1   Size effect and Loading Configurations

Most of the research works are based on single property factors or entities. For example, we can draw our intuitive attention to the section 2.5 of Chapter 2. As in Chapter 5 about the size effect, Pederson et al (1999) had highlighted the height effect over the volume effect. Nevertheless, one can argue that increase of height means increase of volume too, which increases the weak spots in the member that causes change in material properties influencing failure. But, the factors such as the position of the loading, member status whether stress or bending and the rate of loading etc, are the result of loading configuration as have discussed before (see Chapter 2 and the sections under the Discussion of Chapter 5). This means that there are two causes for the size effect in a bending member, one is related to the material properties and the other to the loading configuration. Therefore we can argue that the applicable criteria of size effect at fracture is to be determined as, whether the length, height, depth, height*length, length*depth, depth*height or any version of volume etc. of a member, when a particular loading configuration is incorporated. In other words, one cannot conclude the size effect of a failing member as an effect of volume, height, width or any other geometric factor without indicating its loading configuration. Hence further research on fracture need to consider the combined effect of the size and loading configuration without separating them. The results of past research indicate different size effects due to the separation of these two input factors. Therefore writer wishes to combine the effects of size and loading configuration as illustrated in Figure 9-1

Size

Loading Config.

Effect

Length Height Width Length* Height* Width* Volume
                 Height Width   Length

Unracked   Cacked
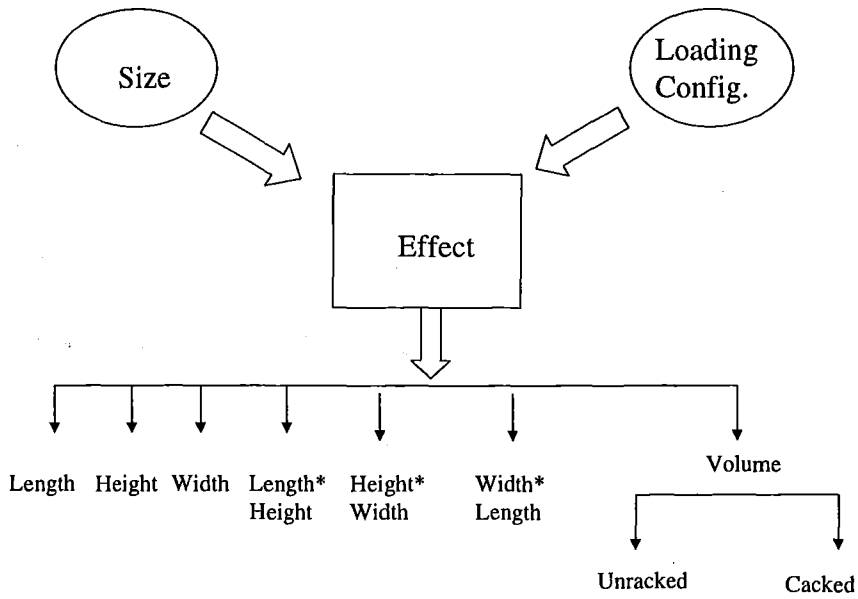
Figure 9-1: Hypothesis of the combined effect of size of a member and loading configuration. Size and loading configuration are sets of various size objects and loading configuration objects, respectively.

9.2 Research on uncracked volume in crack dynamics

It is convinced that if we consider the uncracked volume replacing the entire volume of a member to study times to failure, similar patterns as depicted by the entire volume (see failure graphs in Chapter 5), will be displayed. But ANN analysis on fracture toughness model clearly concluded that uncracked volume is more pronounced than the entire volume. Therefore further research is proposed to investigate the effect of uncracked volume on times to failure states. (For this, one can select different crack lengths for specimens of the same size.) The used analytical method and the available data are not suitable for studying uncracked volume on times to failure.

9.3 Volume effect on three point bending

It was proved that the volume effect of the used loading configuration (in the experiments carried out,) is insignificant on high rate of loading tested. But it is significant, for low rates.

9.4 Fracture toughness

Uncracked volume is the most effective parameter on fracture toughness and therefore it agrees with the Weibull's theory under the tested loading configuration. However uncracked area plays the second role in this regard and rate of loading (as an element of loading configuration object) is the third effective parameter that was followed by geometry factors and pre crack length.

Further, it is proposed to find a method for investigating the hypothesis appeared in Figure 7-5 of Chapter 7.

9.5 Training difficulties in ANN

There were limitations and boundaries when training was performed using neural network package used, which are common features of a general purpose (common) software package. Therefore training suffered somewhat in timing and efficiency due to the use of this ANN software package. A better solution is suggested by organising problem-oriented software as a computer science application since there are ways of enhancing the output by applying computer science and information technologies to a specific task. It could curtail the time, increase the efficiency and provide better results because it effectively handles the complexity of the problem. However, such a proposal is too huge to indicate in this thesis and it is beyond the scope of the current study.

Acknowledgements

And offers of millions of great thanks to Lakmini, our treasured daughter who had been waiting long for me to complete this thesis and to get freed for her innocent requirements. My little sweety, I highly regret for not accomplishing your wishes prior to your sudden departure that has been fracturing and tumbling down our hearts.

I forward this thesis in tribute to Lakmini with my great honour.

Appendix A

Crack speed of the fracturing specimens in the batch -1

SampleNo	Picture No.	HangTime	Net Tot. Crk Speed	Net Left Tot. Speed	Net right Tot. Speed	Manual Time
AP0801	00	199.25				0.00
AP0801	01	200.48	0.000000	0.000000	0.000000	100.00
AP0801	02	201.00	6.269737	6.269737	0.000000	100.52
AP0801	03	201.19	34.662626	34.662626	0.000000	100.71
AP0801	04	201.25	145.840152	145.840152	0.000000	100.77
AP0801	05	201.33	-69.045484	-69.045484	0.000000	100.85
AP0801	06	201.35	3.244256	3.244256	0.000000	100.87
AP0801	07	201.37	72.415489	72.415489	0.000000	100.89
AP0801	08	201.39	-52.828783	-52.828783	0.000000	100.91
AP0801	09	201.40	908.692707	908.692707	0.000000	100.92
AP0801	10	201.44	46.355690	46.355690	0.000000	100.96
AP0801	11	201.45	-1021.102983	-1021.103000	0.000000	100.97
AP0801	12	201.46	1040.944062	1040.944060	0.000000	100.98
AP0801	13	201.47	-199.018182	-199.018180	0.000000	100.99
AP0801	14	201.50	-47.244990	-47.244990	0.000000	101.02
AP0804	00	84.43				0.00
AP0804	01	86.43	0.000000	0.000000	0.000000	125.00
AP0804	02	86.48	26.045544	0.000000	26.045544	125.05
AP0804	03	86.52	58.539082	0.000000	58.539082	125.09
AP0804	04	87.07	3.034259	0.000000	3.034259	125.64
AP0804	05	87.10	-29.586340	0.000000	-29.586340	125.67
AP0804	06	87.13	416.049598	0.000000	416.049598	125.70
AP0804	07	87.15	22.113424	0.000000	22.113424	125.72
AP0804	08	87.20	36.290397	0.000000	36.290397	125.77
AP0804	09	87.25	71.575354	0.000000	71.575354	125.82
AP0804	10	87.30	171.861189	0.000000	171.861189	125.87
AP0804	11	87.35	17.493517	0.000000	17.493517	125.92
AP0804	12	87.40	44.102255	0.000000	44.102255	125.97
AP0804	13	87.45	46.393960	0.000000	46.393960	126.02
AP0804	14	87.50	26.777165	0.000000	26.777165	126.07
AP0804	15	87.55	36.755222	0.000000	36.755222	126.12
AP0804	16	88.00	1.923257	0.000000	1.923257	126.57
AP0804	17	88.05	0.221659	0.000000	0.221659	126.62
AP0804	18	88.10	25.420741	0.000000	25.420741	126.67
AP0804	19	88.15	56.378263	0.000000	56.378263	126.72
AP0804	20	88.20	27.090821	0.000000	27.090821	126.77
AP0804	21	88.25	1.138270	0.000000	1.138270	126.82
AP0804	22	88.28	268.899829	0.000000	90.343683	126.85
AP0804	23	88.29	-290.500179	2983.235220	-3273.735400	126.86
AP0804	24	88.30	3493.776132	43.778174	3449.997960	126.87
AP0804	25	88.32	-270.151289	-288.581130	18.429840	126.89
AP0804	26	88.32	-1451.418201	-99.030375	-1352.387800	126.89

Crack speed of the fracturing specimens in the batch -1

SampleNo	Pic	HangTime A	Net tot Crk Speed	Net Left Tot Speed	Net right Tot Speed	Manual Time
AP0805	00	0.00				0.00
AP0805	01	463.40	0.000000	0.000000	0.000000	0.00
AP0805	02	464.70	4.453437	4.453437	0.000000	1.30
AP0805	03	465.09	18.163010	18.163010	0.000000	1.69
AP0805	04	465.48	1.114996	1.114996	0.000000	2.08
AP0805	05	466.10	2.833817	2.833817	0.000000	2.70
AP0805	06	466.98	-12.424344	-12.424344	0.000000	3.58
AP0805	07	467.24	54.377508	54.377508	0.000000	3.84
AP0805	08	467.89	8.103768	8.103768	0.000000	4.49
AP0805	09	468.09	4.471025	4.471025	0.000000	4.69
AP0805	10	470.08	2.228715	2.228715	0.000000	6.68
AP0805	11	473.58	0.258912	0.258912	0.000000	10.18
AP0805	12	476.29	14.751787	14.751787	0.000000	12.89
AP0805	14	485.80	-4.439098	-4.439098	0.000000	22.40
AP0805	15	495.24	1.984691	1.984691	0.000000	31.84
AP0805	16	499.20	3.703411	3.703411	0.000000	35.80
AP0805	17	504.89	0.868863	0.868863	0.000000	41.49
AP0805	18	510.20	1.169434	1.169434	0.000000	46.80
AP0807	00	530.70				0.00
AP0807	02	654.38	0.000000	0.000000	0.000000	150.00
AP0807	03	654.90	11.041578	11.041578	0.000000	150.52
AP0807	05	664.04	1.300516	1.300516	0.000000	159.66
AP0807	06	668.10	0.988786	0.988786	0.000000	163.72
AP0807	07	680.49	-0.650006	-0.650006	0.000000	176.11
AP0807	08	685.20	1.021738	1.021738	0.000000	180.82
AP0807	09	690.61	-1.411511	-1.411511	0.000000	186.23
AP0807	10	697.01	1.398134	1.398134	0.000000	192.63
AP0807	11	700.90	1.701216	1.701216	0.000000	196.52
AP0807	12	701.01	-35.345498	-35.345498	0.000000	196.63
AP0807	13	701.10	27.053370	27.053370	0.000000	196.72
AP0807	14	701.17	18.346034	18.346034	0.000000	196.79
AP0807	15	701.50	63.637552	63.637552	0.000000	197.12
AP0807	16	701.61	22.750243	22.750243	0.000000	197.23
AP0807	17	701.78	11.741714	11.741714	0.000000	197.40

Crack speed of the fracturing specimens in the batch -1

SampleNo	Pic	HangTime A	Net tot Crk Speed	Net Left Tot Speed	Net right Tot Speed	Manual Time
AP0808	00	1140.88				0.00
AP0808	01	1151.78	0.000000	0.000000	0.000000	125.00
AP0808	02	1215.99	0.212800	0.212800	0.000000	189.21
AP0808	03	1225.68	-0.176687	-0.176687	0.000000	198.90
AP0808	04	1235.28	-0.177840	-0.177840	0.000000	208.50
AP0808	05	1250.18	0.031650	0.031650	0.000000	223.40
AP0808	06	1259.08	-1.258868	-1.258868	0.000000	232.30
AP0808	08	1265.58	0.946148	0.833578	0.000000	238.80
AP0808	09	1266.23	12.798832	13.924535	-1.125704	239.45
AP0808	10	1267.28	-5.575791	-9.314957	0.000000	240.50
AP0808	11	1273.66	0.073175	-0.347427	0.420601	246.88
AP0808	12	1276.19	-1.267324	-0.586764	-0.680560	249.41
AP0808	13	1283.00	2.157566	1.113151	0.507185	256.22
AP0808	14	1290.38	2.215206	2.682493	0.028449	263.60
AP0808	15	1295.53	-0.768936	-0.626786	-0.142150	268.75
AP0808	16	1300.00	-0.097774	-0.808430	0.710656	273.22
AP0808	17	1305.49	3.728434	3.731347	-0.002913	278.71
AP0808	18	1309.18	-9.049398	-8.523658	-0.525740	282.40

Crack speed of the fracturing specimens in the batch -1

SampleNo	Pic	HangTime A	Net tot Crk Speed	Net Left Tot Speed	Net right Tot Speed	Manual Time
AP0809	00	19.19				0.00
AP0809	02	459.53	0.000000	0.000000	0.000000	20.00
AP0809	03	461.28	0.846561	0.846561	0.000000	21.75
AP0809	04	462.29	4.406795	4.406795	0.000000	22.76
AP0809	07	465.58	-1.909640	-1.909640	0.000000	26.05
AP0809	08	466.28	-0.028568	-0.028568	0.000000	26.75
AP0809	09	466.73	9.894369	9.894369	0.000000	27.20
AP0809	10	467.38	5.124377	5.124377	0.000000	27.85
AP0809	11	467.63	-13.323381	-13.323381	0.000000	28.10
AP0809	12	468.29	16.900584	16.900584	0.000000	28.76
AP0809	13	468.83	2.013064	2.013064	0.000000	29.30
AP0809	14	468.98	2.465777	2.465777	0.000000	29.45
AP0809	15	469.23	-13.383227	-13.383227	0.000000	29.70
AP0809	16	470.23	4.071274	4.071274	0.000000	30.70
AP0809	17	472.92	4.554262	4.554262	0.000000	33.39
AP0809	18	475.23	-0.321964	-0.321964	0.000000	35.70
AP0809	19	477.19	-0.564243	-0.564243	0.000000	37.66
AP0809	20	478.23	0.381885	0.381885	0.000000	38.70
AP0809	21	479.32	6.105271	6.105271	0.000000	39.79
AP0809	23	481.92	4.350040	4.350040	0.000000	42.39
AP0809	24	483.51	2.687771	-2.203913	0.000000	43.98
AP0809	25	485.53	-1.036489	1.163731	-2.200220	46.00
AP0809	26	488.63	8.678549	7.961703	0.716846	49.10
AP0809	27	489.30	24.443982	8.965817	15.478165	49.77
AP0809	28	490.23	-20.585362	-28.951260	8.365899	50.70
AP0809	29	491.67	-2.627944	0.200913	-2.828857	52.14
AP0809	30	492.33	10.601327	10.044748	0.556579	52.80
AP0809	31	492.54	-73.964074	-10.514449	-63.449625	53.01
AP0809	32	494.54	12.772388	1.849876	10.922512	55.01
AP0809	33	495.63	0.628386	-0.390910	1.019296	56.10
AP0809	34	495.73	59.687816	26.356512	33.331304	56.20
AP0809	35	495.99	7.299209	10.148053	-2.848843	56.46
AP0809	36	496.04	-59.434673	-59.397772	-0.036901	56.51
AP0809	37	496.18	87.761549	8.357272	79.404277	56.65
AP0809	38	496.60	-12.505264	-7.201193	-5.304071	57.07
AP0809	39	496.83	6.524548	3.303936	3.220612	57.30
AP0810	00	0.00				14.70
AP0810	13	486.59	0.000000	0.000000	0.000000	501.29
AP0810	14	486.98	-17.933602	0.000000	-17.933602	501.68
AP0810	15	488.08	-0.309211	0.000000	-0.309211	502.78
AP0810	16	491.00	-0.130314	0.000000	-0.130314	505.70
AP0810	17	493.00	0.164625	0.000000	0.164625	507.70

Crack speed of the fracturing specimens in the batch -1

SampleNo	Pic	HangTime A	Net tot Crk Speed	Net Left Tot Speed	Net right Tot Speed	Manual Time
AP0812	00	168.28				0.00
AP0812	02	196.76	0.000000	0.000000	0.000000	24.00
AP0812	03	196.78	84.202203	84.202203	0.000000	24.02
AP0812	04	196.84	-94.177212	-94.177212	0.000000	24.08
AP0812	05	197.03	9.153494	9.153494	0.000000	24.27
AP0812	06	198.30	2.514390	2.514390	0.000000	25.54
AP0812	07	198.68	1.498309	1.498309	0.000000	25.92
AP0812	08	199.43	-1.225427	-1.225427	0.000000	26.67
AP0812	09	199.68	8.455690	8.455690	0.000000	26.92
AP0812	10	200.03	-4.029285	-4.029285	0.000000	27.27
AP0812	11	200.90	2.445312	2.445312	0.000000	28.14
AP0812	12	201.28	-0.811519	-0.811519	0.000000	28.52
AP0812	13	203.28	1.059412	1.059412	0.000000	30.52
AP0812	14	204.18	-1.538904	-1.538904	0.000000	31.42
AP0812	15	205.08	2.305615	2.305615	0.000000	32.32
AP0812	16	205.78	3.245782	3.245782	0.000000	33.02
AP0812	17	205.90	-27.584231	-27.584231	0.000000	33.14
AP0812	18	206.08	205.205512	205.205512	0.000000	33.32
AP0812	19	207.09	-4.477385	-4.477385	0.000000	34.33
AP0812	20	207.29	4.458872	4.458872	0.000000	34.53
AP0812	21	207.30	43.290451	43.290451	0.000000	34.54
AP0812	22	207.59	0.726255	0.726255	0.000000	34.83
AP0812	23	207.78	1.440036	1.440036	0.000000	35.02
AP0812	24	208.08	1.576879	1.576879	0.000000	35.32
AP0813	00	95.29				0.00
AP0813	02	128.93	0.000000	0.000000	0.000000	28.00
AP0813	03	130.68	1.248677	0.000000	1.248677	29.75
AP0813	04	132.39	6.950618	0.000000	6.950618	31.46
AP0813	05	135.54	0.014143	0.000000	0.014143	34.61
AP0813	06	136.57	9.647294	0.000000	9.647294	35.64
AP0813	07	136.88	3.777888	0.000000	3.777888	35.95
AP0813	08	137.04	-46.626947	0.000000	-46.626947	36.11
AP0813	09	137.68	17.432936	0.000000	17.432936	36.75
AP0813	10	138.04	24.543864	0.000000	24.543864	37.11
AP0813	11	140.29	-1.290678	0.000000	-1.290678	39.36
AP0813	12	142.68	0.459437	0.000000	0.459437	41.75
AP0813	13	143.28	-6.863468	0.000000	-6.863468	42.35
AP0813	14	143.50	16.856794	0.000000	16.856794	42.57
AP0813	15	143.91	-11.610922	0.000000	-11.610922	42.98
AP0813	16	144.69	10.910594	0.000000	4.737754	43.76
AP0813	17	145.04	6.210438	1.058201	5.152237	44.11
AP0813	18	145.57	4.905155	4.905155	0.000000	44.64
AP0813	19	148.07	-1.915315	-1.035612	-0.879703	47.14
AP0813	20	148.57	-5.949423	-10.391777	4.442354	47.64
AP0813	21	149.57	61.137842	0.000000	54.841546	48.64
AP0813	22	149.67	-429.171983	-11.111111	-418.060870	48.74
AP0813	23	149.79	5.469637	-6.172840	11.642477	48.86

Crack speed of the fracturing specimens in the batch -1

SampleNo	Pic	HangTime A	Net tot Crk Speed	Net Left Tot Speed	Net right Tot Speed	Manual Time
AP0814	00	1948.93				0.00
AP0814	02	2151.33	0.000000	0.000000	0.000000	350.00
AP0814	03	2151.63	0.000000	0.000000	0.000000	350.30
AP0814	04	2152.07	-0.304100	-0.304100	0.000000	350.74
AP0814	05	2155.44	1.031558	1.031558	0.000000	354.11
AP0814	07	2165.17	-0.096022	-0.096022	0.000000	363.84
AP0814	08	2167.36	0.872510	0.872510	0.000000	366.03
AP0814	09	2170.44	-0.236143	-0.236143	0.000000	369.11
AP0814	10	2175.90	0.900636	0.900636	0.000000	374.57
AP0814	11	2181.18	0.137630	0.137630	0.000000	379.85
AP0814	12	2190.32	-0.119202	-0.119202	0.000000	388.99
AP0814	13	2196.54	-0.040185	-0.040185	0.000000	395.21
AP0814	14	2201.75	0.829479	0.829479	0.000000	400.42
AP0814	15	2206.29	0.315438	0.315438	0.000000	404.96
AP0814	16	2206.54	-15.801725	-15.801725	0.000000	405.21
AP0814	17	2206.85	9.683192	9.683192	0.000000	405.52
AP0814	18	2210.29	0.136692	0.136692	0.000000	408.96
AP0814	19	2216.29	0.599624	0.599624	0.000000	414.96
AP0814	21	2224.69	0.313656	0.313656	0.000000	423.36
AP0814	22	2226.44	0.410217	0.410217	0.000000	425.11
AP0814	23	2230.33	0.000000	0.000000	0.000000	429.00
AP0814	24	2235.44	0.000000	0.000000	0.000000	434.11
AP0814	25	2245.29	0.036487	0.036487	0.000000	443.96
AP0814	26	2245.29	311.694268	311.694268	0.000000	443.96
AP0814	27	2250.49	-0.138019	-0.138019	0.000000	449.16
AP0814	28	2255.63	0.080386	0.080386	0.000000	454.30
AP0814	29	2260.68	0.156140	0.156140	0.000000	459.35
AP0814	30	2265.33	0.720829	0.720829	0.000000	464.00
AP0814	31	2270.39	-0.283340	-0.283340	0.000000	469.06
AP0814	32	2275.33	-0.144763	-0.144763	0.000000	474.00
AP0814	34	2285.44	0.083848	0.083848	0.000000	484.11
AP0814	35	2290.29	0.570715	0.570715	0.000000	488.96
AP0814	36	2295.90	0.444962	0.444962	0.000000	494.57
AP0814	37	2305.39	-0.112910	-0.112910	0.000000	504.06
AP0814	38	2310.66	0.931279	0.931279	0.000000	509.33
AP0814	39	2315.33	-0.229471	-0.229471	0.000000	514.00
AP0814	40	2320.44	0.139761	0.139761	0.000000	519.11
AP0814	41	2325.39	-0.116633	-0.116633	0.000000	524.06
AP0814	42	2330.33	0.288363	0.288363	0.000000	529.00
AP0814	43	2335.63	0.067313	0.067313	0.000000	534.30
AP0814	45	2345.47	-0.072487	-0.072487	0.000000	544.14
AP0814	46	2350.94	-0.024354	-0.024354	0.000000	549.61
AP0814	47	2355.88	0.487411	0.487411	0.000000	554.55
AP0814	48	2360.33	-0.591204	-0.591204	0.000000	559.00
AP0814	49	2367.50	0.168211	0.168211	0.000000	566.17
AP0814	50	2371.33	-0.092837	-0.092837	0.000000	570.00
AP0814	51	2375.33	0.054756	0.054756	0.000000	574.00
AP0814	52	2386.79	0.675350	0.675350	0.000000	585.46

Crack speed of the fracturing specimens in the batch -1

SampleNo	Pic	HangTime A	Net tot Crk Speed	Net Left Tot Speed	Net right Tot Speed	Manual Time
AP0814	53	2395.29	-0.041596	-0.041596	0.000000	593.96
AP0814	55	2405.32	0.226364	0.226364	0.000000	603.99
AP0814	56	2410.79	-0.156253	-0.156253	0.000000	609.46
AP0814	57	2415.29	-0.314606	-0.314606	0.000000	613.96
AP0814	58	2420.33	1.112123	1.112123	0.000000	619.00
AP0814	59	2426.57	0.227731	0.227731	0.000000	625.24
AP0814	60	2431.04	-0.905493	-0.905493	0.000000	629.71
AP0814	61	2436.16	0.777573	0.777573	0.000000	634.83
AP0814	62	2440.22	-0.087068	-0.087068	0.000000	638.89
AP0814	63	2445.38	0.137057	0.137057	0.000000	644.05
AP0814	64	2450.38	-0.241809	-0.241809	0.000000	649.05
AP0814	65	2450.66	1.265105	1.265105	0.000000	649.33
AP0814	66	2450.99	2.590355	2.590355	0.000000	649.66
AP0814	67	2451.29	1.179770	1.179770	0.000000	649.96
AP0814	68	2452.09	0.262804	0.262804	0.000000	650.76
AP0814	69	2452.09	-12.273937	-12.273937	0.000000	650.76
AP0814	70	2452.18	-7.205922	-7.205922	0.000000	650.85
AP0814	71	2452.39	-4.356003	-4.356003	0.000000	651.06
AP0814	72	2453.19	-0.185697	-0.185697	0.000000	651.86
AP0814	73	2455.32	0.401563	0.401563	0.000000	653.99
AP0814	74	2459.38	-0.508362	-0.508362	0.000000	658.05
AP0815	00	68.26				0.00
AP0815	02	73.11	0.000000	0.000000	0.000000	325.00
AP0815	03	73.11	-3887.045375	-3887.045400	0.000000	325.00
AP0815	04	73.11	4025.723741	4025.723740	0.000000	325.00
AP0815	05	73.14	-10.271998	-10.271998	0.000000	325.03
AP0815	06	73.25	-0.156287	-0.156287	0.000000	325.14
AP0815	07	73.30	29.732354	29.732354	0.000000	325.19
AP0815	08	73.36	12.301913	12.301913	0.000000	325.25
AP0815	09	73.42	-29.387378	-29.387378	0.000000	325.31
AP0815	10	74.01	1.104268	1.104268	0.000000	325.90
AP0815	11	74.06	14.679044	14.679044	0.000000	325.95
AP0815	12	74.31	8.677583	8.677583	0.000000	326.20
AP0815	13	74.41	1.697765	1.697765	0.000000	326.30
AP0815	14	75.00	1.122322	1.122322	0.000000	326.89

Crack speed of the fracturing specimens in the batch -1

SampleNo	Pic	HangTime A	Net tot Crk Speed	Net Left Tot Speed	Net right Tot Speed	Manual Time
AR0801	00	1085.30				0.00
AR0801	02	1430.38	0.000000	0.000000	0.000000	350.00
AR0801	03	1435.39	0.660729	0.000000	0.660729	355.01
AR0801	05	1445.64	0.363071	0.000000	0.363071	365.26
AR0801	06	1450.46	1.620643	0.000000	1.620643	370.08
AR0801	07	1451.45	0.410722	0.000000	0.410722	371.07
AR0801	08	1454.24	-0.395654	0.000000	-0.395654	373.86
AR0801	09	1455.59	0.765050	0.000000	0.765050	375.21
AR0801	10	1458.99	1.096046	0.000000	-0.976433	378.61
AR0801	11	1460.39	0.262549	-0.264178	0.526728	380.01
AR0801	12	1465.99	0.332616	0.395056	-0.062440	385.61
AR0801	13	1468.58	0.282754	-0.429000	0.711755	388.20
AR0801	14	1470.58	-0.898996	-0.167377	-0.731619	390.20
AR0801	15	1473.77	0.095876	0.221042	-0.125166	393.39
AR0801	16	1475.30	-0.392709	-1.182999	0.790289	394.92
AR0801	17	1480.58	0.399784	0.484501	-0.084717	400.20
AR0801	18	1485.74	-0.718884	-0.503881	-0.215002	405.36
AR0801	19	1490.53	0.538902	0.311060	0.227842	410.15
AR0801	20	1496.14	0.622636	0.136049	0.486587	415.76
AR0801	22	1505.39	-0.137898	0.037494	-0.175391	425.01
AR0801	23	1510.39	0.460816	0.226018	0.234798	430.01
AR0801	24	1515.48	-0.363299	-0.149315	-0.213984	435.10
AR0801	25	1520.49	0.148895	-0.069422	0.218318	440.11
AR0801	26	1530.39	0.072485	-0.077003	0.149488	450.01
AR0801	27	1535.33	0.087027	0.224724	-0.137697	454.95
AR0801	28	1540.69	0.130602	0.000000	0.130602	460.31
AR0801	29	1550.39	0.071546	0.038154	0.033391	470.01
AR0801	30	1555.30	0.608003	0.305172	0.302831	474.92
AR0801	32	1565.64	0.869823	0.466959	0.402864	485.26
AR0801	33	1570.54	-0.834678	-0.295051	-0.539627	490.16
AR0801	34	1580.54	0.111575	-0.040121	0.151696	500.16
AR0801	35	1583.99	0.223198	0.214097	0.009101	503.61
AR0801	36	1584.39	5.369471	-0.055676	5.425147	504.01
AR0801	37	1584.99	-3.148385	0.000000	-3.148385	504.61
AR0801	38	1585.08	116.208059	4.351834	111.856224	504.70
AR0801	39	1585.39	2.562881	2.477067	0.085814	505.01
AR0801	40	1590.77	-0.087762	-0.215531	0.127769	510.39
AR0801	41	1595.98	0.423726	0.213026	0.210699	515.60
AR0801	42	1600.98	0.840953	0.157499	0.683454	520.60
AR0801	43	1605.77	-0.472626	-0.314342	-0.158284	525.39
AR0801	44	1610.48	0.788362	-0.156845	0.945207	530.10
AR0801	45	1615.49	-0.973689	-0.152214	-0.821475	535.11
AR0801	46	1625.39	0.451993	0.077030	0.374964	545.01
AR0801	47	1635.69	0.830731	0.645990	0.184741	555.31
AR0801	48	1636.88	-0.682808	0.000000	-0.682808	556.50
AR0801	49	1637.14	15.927136	-19.796413	35.723549	556.76

Crack speed of the fracturing specimens in the batch -1

SampleNo	Pic	HangTime A	Net tot Crk Speed	Net Left Tot Speed	Net right Tot Speed	Manual Time
BP0808	00	0.00				0.00
BP0808	06	139.38	0.000000	0.000000	0.000000	80.00
BP0808	07	142.53	1.828723	1.828723	0.000000	83.15
BP0808	08	145.68	3.889315	3.889315	0.000000	86.30
BP0808	09	164.58	0.052202	0.052202	0.000000	105.20
BP0810	00	0.00				0.00
BP0810	01	137.83	0.000000	0.000000	0.000000	20.00
BP0810	02	145.09	0.258868	0.000000	0.258868	27.26
BP0810	03	146.53	1.272961	0.000000	1.272961	28.70
BP0810	04	146.87	9.859181	0.000000	9.859181	29.04
BP0810	05	147.97	-0.348017	0.000000	-0.348017	30.14
BP0810	06	149.09	10.583351	0.000000	10.583351	31.26
BP0810	07	149.59	2.225888	0.000000	2.225888	31.76
BP0810	08	150.29	-24.882169	0.000000	-24.882169	32.46
BP0810	09	151.29	16.769243	0.000000	16.769243	33.46
BP0810	10	154.37	7.334724	0.000000	7.334724	36.54
BP0810	11	155.79	-5.486986	0.000000	-5.486986	37.96
BP0810	12	156.19	-19.522845	0.000000	-19.522845	38.36
BP0810	13	157.39	6.865499	0.000000	6.865499	39.56
BP0810	14	157.58	123.260170	0.000000	123.260170	39.75
BP0810	15	157.59	-2275.735083	0.000000	-2275.735100	39.76
BP0811	00	0.00				0.00
BP0811	07	106.39	0.000000	0.000000	0.000000	20.00
BP0811	08	107.39	-3.378766	-1.491973	-1.886792	21.00
BP0811	09	108.79	1.899108	1.612274	0.286834	22.40
BP0811	10	111.99	1.758023	0.822192	0.935831	25.60
BP0811	11	112.77	-1.935172	0.967586	-2.902758	26.38
BP0811	12	115.29	0.012010	0.301895	-0.289884	28.90
BP0811	13	119.39	0.643332	0.275963	0.367369	33.00
BP0811	14	119.69	-26.439549	5.076950	-31.516498	33.30
BP0811	15	121.79	7.022975	3.069696	3.953279	35.40
BP0811	16	123.97	2.593859	2.591183	0.002676	37.58
BP0812	00	0.00				0.00
BP0812	04	109.57	0.000000	0.000000	0.000000	20.00
BP0812	05	109.99	-0.918245	17.051207	-17.969452	20.42
BP0812	06	110.03	-132.352002	-132.352000	0.000000	20.46
BP0812	07	110.53	33.256772	11.369979	0.000000	20.96
BP0812	08	112.39	-3.251013	-0.816442	-2.434571	22.82
BP0812	09	113.29	6.705984	3.351686	3.354298	23.72
BP0812	10	113.53	64.483379	29.892184	34.591195	23.96
BP0812	11	114.57	3.317750	8.750960	-5.433210	25.00
BP0812	12	115.33	-9.890472	-1.933136	-7.957335	25.76
BP0812	13	118.57	-0.831013	1.032486	-1.863499	29.00
BP0812	14	121.53	-1.229932	-1.229932	0.000000	31.96
BP0812	15	122.03	2.738563	2.738563	0.000000	32.46
BP0812	16	122.63	-37.180139	-37.180139	0.000000	33.06
BP0812	17	125.57	-1.924248	-1.924248	0.000000	36.00

Crack speed of the fracturing specimens in the batch -1

SampleNo	Pic	HangTime A	Net tot Crk Speed	Net Left Tot Speed	Net right Tot Speed	Manual Time
BP0813	00	0.00				0.00
BP0813	01	110.03	0.000000	0.000000	0.000000	300.00
BP0813	02	110.58	22.855844	0.000000	16.408177	300.55
BP0813	03	113.18	-1.012593	0.946834	-1.959427	303.15
BP0813	04	113.28	15.371814	3.691283	11.680531	303.25
BP0813	05	114.43	-1.323306	0.040718	-1.364024	304.40
BP0813	06	117.37	1.616991	0.547836	1.069156	307.34
BP0813	07	130.03	-0.217129	-0.093316	-0.123813	320.00
BP0813	08	135.28	-0.242219	-0.091452	-0.150768	325.25
BP0813	09	140.93	0.960055	0.542532	0.417523	330.90
BP0813	10	145.39	-1.298071	-0.769147	-0.528925	335.36
BP0813	11	151.09	0.490043	0.213689	0.276354	341.06
BP0813	12	160.39	0.406440	0.617985	-0.211546	350.36
BP0813	13	170.39	-0.133013	-0.016376	-0.116637	360.36
BP0814	00	0.00				0.00
BP0814	01	110.03	0.000000	0.000000	0.000000	300.00
BP0814	02	383.28	-0.047360	0.000000	-0.047360	573.25
BP0814	03	417.53	0.057249	0.000000	0.057249	607.50
BP0814	04	422.03	0.784314	0.000000	0.784314	612.00
BP0814	05	429.97	0.347197	0.000000	0.347197	619.94
BP0814	06	436.39	0.060511	0.000000	0.060511	626.36
BP0814	07	448.93	0.156331	0.000000	0.156331	638.90
BP0814	08	449.53	0.801174	0.000000	0.801174	639.50
BP0814	09	449.53	318.283840	0.000000	318.283840	639.50
BP0814	10	449.58	-32.294928	0.000000	-32.294928	639.55
BP0814	11	449.84	-1.667090	0.000000	-1.667090	639.81
BP0814	12	449.84	246.137316	0.000000	246.137316	639.81
BP0814	13	450.09	39.502900	0.000000	39.502900	640.06
BP0814	14	450.28	-6.295620	0.000000	-6.295620	640.25
BP0814	15	450.93	4.860395	0.000000	4.860395	640.90
BP0814	16	450.98	-15.647110	0.000000	-15.647110	640.95
BP0814	17	462.53	0.136124	0.000000	0.136124	652.50
BP0814	18	479.09	0.264979	0.000000	0.264979	669.06
BP0814	19	496.43	-0.048813	0.000000	-0.048813	686.40
BP0814	20	525.35	0.139051	0.000000	0.139051	715.32
BP0814	21	535.58	0.042406	0.000000	0.042406	725.55
BP0814	22	544.38	0.018893	0.000000	0.018893	734.35
BP0814	23	550.59	0.234665	0.000000	0.234665	740.56
BP0814	24	551.90	-0.030563	0.000000	-0.030563	741.87
BP0814	25	553.08	0.290733	0.000000	0.290733	743.05
BP0814	26	567.93	0.543794	0.000000	0.543794	757.90
BP0814	27	569.78	0.365584	0.000000	0.365584	759.75

Crack speed of the fracturing specimens in the batch -1

SampleNo	Pic	HangTime A	Net tot Crk Speed	Net Left Tot Speed	Net right Tot Speed	Manual Time
BR0801	00	0.00				0.00
BR0801	01	482.09	0.000000	0.000000	0.000000	320.00
BR0801	02	483.09	-2.427531	-2.427531	0.000000	321.00
BR0801	03	484.39	0.547764	0.547764	0.000000	322.30
BR0801	04	507.59	0.316438	0.316438	0.000000	345.50
BR0801	05	520.89	0.053167	0.053167	0.000000	358.80
BR0801	06	530.79	-0.203305	-0.203305	0.000000	368.70
BR0801	07	539.29	0.194631	0.194631	0.000000	377.20
BR0801	08	564.29	-0.053135	-0.053135	0.000000	402.20
BR0801	09	581.93	0.380862	0.380862	0.000000	419.84
BR0801	10	612.29	-0.017471	-0.017471	0.000000	450.20
BR0801	11	626.09	-1.167055	-1.167055	0.000000	464.00
BR0801	12	626.64	20.242549	0.000000	0.000000	464.55
BR0801	13	626.88	35.298653	35.298653	0.000000	464.79
BR0801	14	627.19	7.802800	7.802800	0.000000	465.10
BR0801	15	627.38	-18.356220	-18.356220	0.000000	465.29
BR0801	16	627.58	-0.373825	-0.373825	0.000000	465.49
BR0801	17	627.59	3205.463343	52.283604	0.000000	465.50
BR0801	18	627.69	27.179917	-12.005730	39.185647	465.60
BR0801	19	627.88	2.209981	6.856665	-4.646684	465.79
BR0801	20	634.38	0.371434	-0.858839	1.230273	472.29
BR0801	21	646.98	0.845695	0.225358	0.620336	484.89
BR0801	22	728.48	-0.140616	0.043218	-0.183834	566.39
BR0801	23	764.38	0.195202	-0.116053	0.311255	602.29
BR0801	24	820.49	-0.329571	-0.150648	-0.178922	658.40
BR0801	25	838.33	1.369302	0.192272	1.177031	676.24
BR0801	26	845.59	-3.286472	0.148515	-3.434987	683.50
BR0801	27	860.59	0.422345	-0.102356	0.524701	698.50
BR0801	28	868.98	-0.870164	-0.030681	-0.839483	706.89
BR0801	29	870.98	6.518005	2.903117	3.614888	708.89
BR0801	30	872.89	-2.360930	-0.953604	-1.407325	710.80
BR0801	31	873.49	-0.347943	-6.236677	5.888733	711.40
BR0802	00	0.00				0.00
BR0802	01	594.89	0.000000	0.000000	0.000000	300.00
BR0802	02	599.73	0.077967	0.000000	0.077967	304.84
BR0802	03	609.58	0.000000	0.000000	0.000000	314.69
BR0802	04	618.53	0.088823	0.000000	0.088823	323.64
BR0802	05	619.39	1.376112	0.000000	1.376112	324.50
BR0802	06	619.53	2.615876	0.000000	2.615876	324.64
BR0802	07	624.39	-0.089434	0.000000	-0.089434	329.50
BR0802	08	635.28	-0.106086	0.000000	-0.106086	340.39
BR0802	09	639.09	-0.177727	0.000000	-0.177727	344.20
BR0802	10	640.93	2.008700	0.000000	2.008700	346.04
BR0802	11	645.43	1.346892	0.000000	1.346892	350.54
BR0802	12	648.33	0.427455	0.000000	0.427455	353.44
BR0802	13	650.29	2.850103	0.000000	2.850103	355.40
BR0802	14	652.03	0.471267	0.000000	0.471267	357.14
BR0802	15	655.33	0.000000	0.000000	0.000000	360.44

Crack speed of the fracturing specimens in the batch -1

SampleNo	Pic	HangTime A	Net tot Crk Speed	Net Left Tot Speed	Net right Tot Speed	Manual Time
BR0802	17	665.03	0.187015	0.000000	0.187015	370.14
BR0802	18	670.34	0.005200	0.000000	0.005200	375.45
BR0802	19	676.09	-0.059399	0.000000	-0.059399	381.20
BR0802	20	680.23	4.439858	0.000000	4.439858	385.34
BR0802	21	681.39	-12.117105	0.000000	-12.117105	386.50
BR0802	22	685.59	6.315648	0.000000	6.315648	390.70
BR0802	23	690.99	-2.603052	0.000000	-2.603052	396.10
BR0802	24	715.39	0.190613	0.000000	0.190613	420.50
BR0802	25	718.78	2.264008	0.000000	2.264008	423.89
BR0802	26	722.29	-2.249095	0.000000	-2.249095	427.40
BR0802	27	722.39	18.360396	0.000000	18.360396	427.50
BR0802	28	729.53	0.299791	0.000000	0.299791	434.64
BR0802	29	735.34	-0.258252	0.000000	-0.258252	440.45
CP0801	00	145.30				0.00
CP0801	01	155.87	0.000000	0.000000	0.000000	90.00
CP0801	02	165.80	0.238097	0.238097	0.000000	99.93
CP0801	03	171.59	0.071046	0.071046	0.000000	105.72
CP0801	04	181.15	0.368548	0.368548	0.000000	115.28
CP0801	05	193.24	-0.097162	-0.097162	0.000000	127.37
CP0801	06	203.27	0.274733	0.274733	0.000000	137.40
CP0801	07	207.37	-0.669001	-0.669001	0.000000	141.50
CP0801	08	212.59	0.598391	0.598391	0.000000	146.72
CP0801	09	214.46	0.000000	0.000000	0.000000	148.59
CP0801	10	215.99	0.510699	0.510699	0.000000	150.12
CP0801	11	219.37	0.352942	0.352942	0.000000	153.50
CP0801	12	221.92	1.998365	1.998365	0.000000	156.05
CP0801	13	224.39	-1.109765	-1.109765	0.000000	158.52
CP0801	14	225.37	-0.405283	-0.405283	0.000000	159.50
CP0801	15	228.55	0.862165	0.862165	0.000000	162.68
CP0801	16	229.87	-2.074947	-2.074947	0.000000	164.00
CP0801	17	230.87	0.001606	0.001606	0.000000	165.00
CP0801	18	231.93	1.844877	1.844877	0.000000	166.06
CP0801	19	232.99	0.018048	0.018048	0.000000	167.12
CP0801	20	234.18	2.637804	2.637804	0.000000	168.31
CP0801	21	235.37	-3.641152	-3.641152	0.000000	169.50
CP0801	22	235.58	41.222944	41.222944	0.000000	169.71
CP0801	23	236.68	-2.847953	-2.847953	0.000000	170.81
CP0801	25	245.29	-0.047652	-0.047652	0.000000	179.42
CP0801	26	250.34	-0.232411	-0.232411	0.000000	184.47
CP0801	27	255.37	-0.233272	-0.233272	0.000000	189.50
CP0801	28	258.59	0.364713	0.364713	0.000000	192.72
CP0801	29	260.46	0.416399	0.416399	0.000000	194.59

Crack speed of the fracturing specimens in the batch -1

SampleNo	Pic	HangTime A	Net tot Crk Speed	Net Left Tot Speed	Net right Tot Speed	Manual Time
CP0802	00	377.98				0.00
CP0802	01	380.09	0.000000	0.000000	0.000000	30.00
CP0802	02	385.74	0.280091	0.280091	0.000000	35.65
CP0802	03	391.18	-0.434987	-0.434987	0.000000	41.09
CP0802	04	391.29	17.827714	17.827714	0.000000	41.20
CP0802	05	394.39	0.013251	0.013251	0.000000	44.30
CP0802	06	395.87	1.561891	1.561891	0.000000	45.78
CP0802	07	400.20	0.180913	0.180913	0.000000	50.11
CP0802	08	403.09	1.365311	1.365311	0.000000	53.00
CP0802	09	405.43	-2.015871	-2.015871	0.000000	55.34
CP0802	10	407.59	0.725515	0.725515	0.000000	57.50
CP0802	11	410.19	1.663572	1.663572	0.000000	60.10
CP0802	12	412.18	-2.363678	-2.363678	0.000000	62.09
CP0802	13	415.37	4.428046	4.428046	0.000000	65.28
CP0802	14	416.89	-4.109286	-4.109286	0.000000	66.80
CP0802	16	425.48	0.043780	0.043780	0.000000	75.39
CP0802	17	430.18	0.414111	0.414111	0.000000	80.09
CP0802	18	435.18	-0.308173	-0.308173	0.000000	85.09
CP0802	19	440.18	-0.860553	-0.860553	0.000000	90.09
CP0802	20	477.37	0.094182	0.094182	0.000000	127.28
CP0802	22	485.30	-0.247056	-0.247056	0.000000	135.21
CP0802	23	486.87	1.496965	1.496965	0.000000	136.78
CP0802	24	487.79	0.850353	0.850353	0.000000	137.70
CP0802	25	488.37	6.206991	6.206991	0.000000	138.28
CP0802	26	490.06	-1.189443	-1.189443	0.000000	139.97
CP0802	27	490.46	-9.781677	-9.781677	0.000000	140.37
CP0802	28	490.98	12.052472	12.052472	0.000000	140.89
CP0802	29	491.30	-2.279090	-2.279090	0.000000	141.21
CP0802	30	492.38	2.899264	2.899264	0.000000	142.29
CP0802	31	495.27	-0.532536	-0.532536	0.000000	145.18
CP0802	32	498.43	2.104849	2.104849	0.000000	148.34
CP0802	33	502.87	0.272423	0.272423	0.000000	152.78
CP0802	34	510.27	0.692196	0.692196	0.000000	160.18
CP0802	35	511.24	0.836314	0.836314	0.000000	161.15
CP0802	36	515.48	-0.170135	-0.170135	0.000000	165.39
CP0802	37	518.39	-0.425494	-0.425494	0.000000	168.30
CP0802	38	520.66	0.862207	0.862207	0.000000	170.57
CP0802	39	525.16	0.435495	0.435495	0.000000	175.07
CP0802	40	530.15	-0.296656	-0.296656	0.000000	180.06
CP0803	00	342.94				0.00
CP0803	19	405.58	0.000000	0.000000	0.000000	45.00
CP0803	20	405.59	-76.895997	0.000000	-76.895997	45.01
CP0803	21	405.59	-308.667516	0.000000	-308.667520	45.01
CP0803	22	405.59	0.000000	0.000000	0.000000	45.01
CP0803	23	405.78	2.024291	0.000000	2.024291	45.20
CP0803	25	405.99	23.827467	0.000000	23.827467	45.41
CP0803	26	410.39	-0.961253	0.000000	-0.961253	49.81
CP0803	27	415.28	0.160152	0.000000	0.160152	54.70

Crack speed of the fracturing specimens in the batch -1

SampleNo	Pic	HangTime A	Net tot Crk Speed	Net Left Tot Speed	Net right Tot Speed	Manual Time
CP0803	29	425.28	0.421544	0.000000	0.421544	64.70
CP0803	30	430.34	0.157449	0.000000	0.157449	69.76
CP0803	31	435.28	0.077729	0.000000	0.077729	74.70
CP0803	32	440.18	0.317965	0.000000	0.317965	79.60
CP0803	33	445.28	1.294958	0.000000	1.294958	84.70
CP0803	34	450.34	0.385060	0.000000	0.385060	89.76
CP0803	35	454.18	2.639406	0.000000	2.639406	93.60
CP0804	00	0.00				0.00
CP0804	01	140.38	0.000000	0.000000	0.000000	50.00
CP0804	02	185.50	-0.185263	0.024468	-0.209732	95.12
CP0804	03	189.89	0.000960	-0.581585	0.582545	99.51
CP0804	04	197.39	0.679528	0.677543	0.001985	107.01
CP0804	05	202.44	-0.567888	-0.059221	-0.508668	112.06
CP0804	06	205.28	3.333365	-0.381473	3.714838	114.90
CP0804	07	208.39	-2.480811	-0.139685	-2.341126	118.01
CP0804	08	210.02	-2.875282	1.583588	-4.458871	119.64
CP0804	09	215.26	2.705164	0.138005	2.567159	124.88
CP0804	10	219.16	1.048819	0.301489	0.747330	128.78
CP0804	11	220.19	-9.228279	-3.934455	-5.293824	129.81
CP0804	12	225.28	-0.287758	0.356537	-0.644294	134.90
CP0804	13	230.16	1.939189	0.520198	1.418991	139.78
CP0804	14	235.28	0.139565	0.638541	-0.498977	144.90
CP0804	16	245.23	-0.696907	-0.331616	-0.365292	154.85
CP0804	17	250.44	-0.133353	-0.271372	0.138019	160.06
CP0804	18	255.10	0.772308	-0.711431	1.483739	164.72
CP0804	19	260.39	-0.817888	0.762481	-1.580369	170.01
CP0804	20	265.29	-0.086367	-0.158289	0.071922	174.91
CP0804	21	270.26	1.176976	-0.067267	1.244244	179.88
CP0804	22	275.00	-0.225335	-0.225335	0.000000	184.62
CP0804	23	280.09	-1.131412	0.154939	-1.286351	189.71
CP0804	24	285.06	-0.102653	-0.322152	0.219499	194.68
CP0804	25	290.09	1.613503	0.455182	1.158321	199.71
CP0804	26	294.89	0.071190	-0.079036	0.150226	204.51
CP0804	27	295.00	-69.384259	-6.580817	-62.803442	204.62
CP0804	29	302.93	1.420058	1.282831	0.137227	212.55
CP0804	30	303.16	-45.800334	-42.649798	-3.150536	212.78
CP0804	31	305.44	-0.320370	0.317496	-0.637866	215.06
CP0804	32	310.39	0.440000	0.366549	0.073451	220.01
CP0804	33	313.68	-0.441747	-0.661950	0.220203	223.30
CP0804	34	315.57	-0.959508	-0.189907	-0.769601	225.19
CP0804	35	315.83	2.860608	0.063405	2.797203	225.45
CP0804	36	316.19	4.995578	0.955174	4.040404	225.81
CP0804	37	318.39	-0.498009	0.822922	-1.320930	228.01
CP0804	38	318.50	-16.238486	-29.459457	13.220970	228.12
CP0804	39	319.00	5.788084	5.793694	-0.005611	228.62
CP0804	40	319.68	12.293768	2.665050	9.628718	229.30
CP0804	41	320.08	-12.664808	-5.392761	-7.272047	229.70
CP0804	42	320.85	4.751656	2.390612	2.361044	230.47

Crack speed of the fracturing specimens in the batch -1

SampleNo	Pic	HangTime A	Net tot Crk Speed	Net Left Tot Speed	Net right Tot Speed	Manual Time
CP0804	43	325.39	-4.241283	-0.332679	-3.908603	235.01
CP0804	44	331.00	-0.726472	-0.713051	-0.013421	240.62
CP0804	45	335.34	0.530111	0.781472	-0.251362	244.96
CP0804	46	339.69	-0.278358	-0.696331	0.417973	249.31
CP0804	47	339.94	-2.617296	-2.647402	0.030106	249.56
CP0805	00	42.28				0.00
CP0805	10	121.18	0.000000	0.000000	0.000000	113.90
CP0805	11	122.58	2.475946	0.000000	2.475946	115.30
CP0805	12	127.28	-1.073462	0.000000	-1.073462	120.00
CP0805	13	128.28	-0.543173	0.000000	-0.543173	121.00
CP0805	14	130.28	-0.637406	0.000000	-0.637406	123.00
CP0805	15	132.08	5.943157	0.000000	5.943157	124.80
CP0805	16	134.28	0.166949	0.000000	0.166949	127.00
CP0805	17	135.57	0.612856	0.000000	0.612856	128.29
CP0805	18	145.28	1.125832	0.000000	1.125832	138.00
CP0805	19	147.28	0.139435	0.000000	0.139435	140.00
CP0805	20	150.39	0.791210	0.000000	0.791210	143.11
CP0805	21	153.18	1.135747	0.000000	1.135747	145.90
CP0805	22	155.28	1.221309	0.000000	1.221309	148.00
CP0805	23	157.83	2.100975	0.000000	2.100975	150.55
CP0805	24	160.38	0.385500	0.000000	0.385500	153.10
CP0805	25	162.68	0.768275	0.000000	0.768275	155.40
CP0805	26	165.44	0.870742	0.000000	0.870742	158.16
CP0805	27	167.84	0.928779	0.000000	0.928779	160.56
CP0805	28	169.18	2.287613	0.000000	2.287613	161.90
CP0805	29	169.88	-5.934409	0.000000	-5.934409	162.60
CP0805	30	170.04	3.483091	0.000000	3.483091	162.76
CP0805	31	170.29	-5.361230	0.000000	-5.361230	163.01
CP0805	32	171.18	2.528618	0.000000	2.528618	163.90
CP0805	33	173.94	-0.653279	0.000000	-0.653279	166.66
CP0805	34	174.08	56.720982	0.000000	56.720982	166.80
CP0805	35	174.19	2.402722	0.000000	2.402722	166.91
CP0805	36	174.36	-31.412539	0.000000	-31.412539	167.08
CP0805	37	174.38	253.553937	0.000000	253.553937	167.10
CP0805	38	175.07	-0.120409	0.000000	-0.120409	167.79
CP0806	00	138.90				0.00
CP0806	04	215.53	0.000000	0.000000	0.000000	50.00
CP0806	05	220.19	0.091740	0.091740	0.000000	54.66
CP0806	06	222.00	0.430302	0.430302	0.000000	56.47
CP0806	07	226.03	-0.193262	-0.193262	0.000000	60.50
CP0806	08	230.34	0.000000	0.000000	0.000000	64.81
CP0806	09	235.37	-0.072178	-0.072178	0.000000	69.84
CP0806	12	242.69	0.000000	0.000000	0.000000	77.16
CP0806	13	245.49	0.122297	0.122297	0.000000	79.96
CP0806	14	247.69	0.024955	0.024955	0.000000	82.16
CP0806	15	249.59	0.025149	0.025149	0.000000	84.06

Crack speed of the fracturing specimens in the batch -1

SampleNo	Pic	HangTime A	Net tot Crk Speed	Net Left Tot Speed	Net right Tot Speed	Manual Time
CP0807	00	22.64				0.00
CP0807	07	154.29	0.000000	0.000000	0.000000	50.00
CP0807	08	161.08	0.127284	0.127284	0.000000	56.79
CP0807	09	167.59	-0.029022	-0.029022	0.000000	63.30
CP0807	10	175.39	0.034356	0.034356	0.000000	71.10
CP0807	12	185.39	0.591813	0.591813	0.000000	81.10
CP0807	13	190.59	0.096566	0.096566	0.000000	86.30
CP0807	14	195.49	0.014532	0.014532	0.000000	91.20
CP0807	15	200.38	0.146762	0.146762	0.000000	96.09
CP0807	16	205.39	-0.065046	-0.065046	0.000000	101.10
CP0807	17	205.39	65.176261	65.176261	0.000000	101.10
CP0807	18	210.39	0.091857	0.091857	0.000000	106.10
CP0807	19	215.38	-0.092041	-0.092041	0.000000	111.09
CP0807	20	220.64	0.800944	0.800944	0.000000	116.35
CP0807	21	225.74	0.384171	0.384171	0.000000	121.45
CP0807	22	230.95	0.164738	0.164738	0.000000	126.66
CP0807	23	235.03	0.078758	0.078758	0.000000	130.74
CP0807	25	243.38	0.000000	0.000000	0.000000	139.09
CP0808	00	150.08				0.00
CP0808	14	206.18	0.000000	0.000000	0.000000	30.00
CP0808	15	206.29	-2.329358	0.000000	-2.329358	30.11
CP0808	16	206.48	-11.412960	0.000000	-11.412960	30.30
CP0808	17	206.68	10.152727	0.000000	10.152727	30.50
CP0808	18	206.83	-24.445877	0.000000	-24.445877	30.65
CP0808	19	210.79	1.324554	0.000000	1.324554	34.61
CP0808	20	215.39	-0.329030	0.000000	-0.329030	39.21
CP0808	21	220.30	0.239997	0.000000	0.239997	44.12
CP0808	22	225.48	0.948263	0.000000	0.948263	49.30
CP0808	23	225.68	1.964458	0.000000	1.964458	49.50
CP0808	24	225.79	0.618923	0.000000	0.618923	49.61
CP0808	25	225.80	229.438756	0.000000	229.438756	49.62
CP0808	26	225.99	64.781248	0.000000	64.781248	49.81
CP0808	27	226.29	-5.458046	0.000000	-5.458046	50.11
CP0808	28	226.48	6.910978	0.000000	6.910978	50.30
CP0808	29	228.29	-0.073761	0.000000	-0.073761	52.11
CP0808	30	230.30	0.227779	0.000000	0.227779	54.12
CP0808	31	235.98	0.080966	0.000000	0.080966	59.80
CP0810	00	0.00				0.00
CP0810	05	89.54	0.000000	0.000000	0.000000	10.00
CP0810	06	92.96	-0.025077	-0.025077	0.000000	13.42
CP0810	07	95.36	2.323536	2.323536	0.000000	15.82
CP0810	08	95.58	-0.547222	-0.547222	0.000000	16.04
CP0810	09	95.77	0.000000	0.000000	0.000000	16.23
CP0810	10	95.93	3.243091	3.243091	0.000000	16.39
CP0810	11	96.33	1.258883	1.258883	0.000000	16.79
CP0810	12	96.52	-4.495456	-4.495456	0.000000	16.98
CP0810	13	96.86	10.134847	10.134847	0.000000	17.32
CP0810	14	97.08	6.691565	6.691565	0.000000	17.54

Crack speed of the fracturing specimens in the batch -1

SampleNo	Pic	HangTime A	Net tot Crk Speed	Net Left Tot Speed	Net right Tot Speed	Manual Time
CP0810	15	97.34	2.453660	2.453660	0.000000	17.80
CP0810	16	97.48	122.182614	-70.667990	0.000000	17.94
CP0810	17	97.56	51.797748	63.106589	-24.701699	18.02
CP0810	18	97.59	-60.758291	-149.521540	76.858485	18.05
CP0810	19	98.51	1.702348	3.688662	-1.670878	18.97
CP0810	20	100.34	2.434963	-0.237082	2.318306	20.80
CP0810	21	102.09	-0.575109	-0.652433	1.097732	22.55
CP0810	22	103.68	3.894370	0.752435	3.141935	24.14
CP0810	23	103.85	-11.660049	4.164285	-15.824334	24.31
CP0810	24	105.39	-3.308864	-7.301921	3.993058	25.85
CP0811	00	0.00				0.00
CP0811	02	188.25	0.000000	0.000000	0.000000	8.00
CP0811	03	188.38	3.370994	2.232520	1.138475	8.13
CP0811	04	188.49	20.939180	10.813920	10.125260	8.24
CP0811	05	188.59	-18.691444	-11.371337	-7.320107	8.34
CP0811	06	189.07	0.744424	-0.109162	0.853586	8.82
CP0811	07	189.57	0.000000	0.000000	0.000000	9.32
CP0811	08	190.15	2.848552	-1.080392	3.928944	9.90
CP0811	09	190.65	4.669566	2.031732	2.637834	10.40
CP0811	10	191.29	3.577271	0.562904	3.014367	11.04
CP0811	11	192.57	-0.090663	-0.710247	0.619584	12.32
CP0811	12	193.09	-2.611919	-1.748907	-0.863012	12.84
CP0811	13	193.57	-3.330521	-4.050803	0.720282	13.32
CP0811	14	194.55	4.102101	0.000000	4.102101	14.30
CP0811	15	196.09	-0.052466	0.000000	-0.052466	15.84
CP0811	16	196.59	0.161594	0.000000	0.161594	16.34
CP0811	17	200.25	1.470449	0.000000	1.470449	20.00
CP0811	18	202.54	-0.027629	0.000000	-0.027629	22.29
CP0811	19	204.33	0.707895	0.000000	0.707895	24.08
CP0811	20	204.65	25.081850	0.000000	25.081850	24.40
CP0811	21	204.72	17.634935	0.000000	17.634935	24.47
CP0811	22	204.76	8.658075	0.000000	8.658075	24.51
CP0811	23	205.18	7.040207	0.000000	7.040207	24.93
CP0811	24	205.57	-9.689323	0.000000	-9.689323	25.32
CP0811	25	205.86	8.072751	0.000000	8.072751	25.61
CP0811	26	206.33	-2.984266	0.000000	-2.984266	26.08
CP0811	27	212.36	0.373729	0.000000	0.373729	32.11
CP0812	00	1729.97				0.00
CP0812	08	1751.63	0.000000	0.000000	0.000000	8.00
CP0812	09	1751.68	14.760692	0.000000	14.760692	8.05
CP0812	10	1752.09	33.602315	0.000000	33.602315	8.46
CP0812	11	1752.50	-2.876101	0.000000	-2.876101	8.87
CP0812	12	1753.28	25.214258	0.000000	25.214258	9.65
CP0812	13	1757.66	-4.055686	0.000000	-4.055686	14.03
CP0812	14	1757.75	-16.806360	0.000000	-16.806360	14.12
CP0812	15	1758.25	2.259344	0.000000	2.259344	14.62
CP0812	16	1758.69	5.004164	0.000000	5.004164	15.06
CP0812	17	1759.59	2.906698	0.000000	2.906698	15.96

Crack speed of the fracturing specimens in the batch -1

SampleNo	Pic	HangTime A	Net tot Crk Speed	Net Left Tot Speed	Net right Tot Speed	Manual Time
CP0812	20	1764.25	1.607664	0.000000	-1.607664	20.62
CP0812	21	1770.49	0.845511	0.000000	0.845511	26.86
CP0812	20	1764.25	1.607664	0.000000	1.607664	20.62
CP0812	21	1770.49	0.845511	0.000000	0.845511	26.86
CP0812	22	1774.09	0.609307	0.000000	0.609307	30.46
CP0812	23	1775.50	0.294659	0.000000	0.294659	31.87
CP0812	24	1775.53	0.868429	0.000000	0.868429	31.90
CP0812	25	1776.16	2.903397	0.000000	2.903397	32.53
CP0812	26	1776.47	1.165269	0.000000	1.165269	32.84
CP0812	27	1776.94	-4.825689	0.000000	-4.825689	33.31
CP0812	28	1777.16	10.200052	0.000000	10.200052	33.53
CP0812	29	1777.38	-3.283899	0.000000	-3.283899	33.75
CP0812	30	1777.59	7.062425	0.000000	7.062425	33.96
CP0812	31	1777.69	414.232614	0.000000	414.232614	34.06
CP0812	32	1777.75	-29.494691	0.000000	-29.494691	34.12
CP0812	33	1777.85	17.637928	0.000000	17.637928	34.22
CP0813	00	189.84				0.00
CP0813	03	213.08	0.000000	0.000000	0.000000	8.00
CP0813	04	213.18	36.117940	0.000000	36.117940	8.10
CP0813	05	213.39	-15.294257	0.000000	-15.294257	8.31
CP0813	06	213.40	121.100918	0.000000	121.100918	8.32
CP0813	07	213.69	6.858589	0.000000	6.858589	8.61
CP0813	08	213.90	9.523810	0.000000	9.523810	8.82
CP0813	09	213.93	-40.000000	0.000000	-40.000000	8.85
CP0813	10	213.93	404.702803	0.000000	404.702803	8.85
CP0813	11	214.03	31.902404	0.000000	31.902404	8.95
CP0813	12	214.18	5.241637	0.000000	5.241637	9.10
CP0813	13	214.43	-11.174579	0.000000	-11.174579	9.35
CP0813	14	216.58	6.327284	0.000000	6.327284	11.50
CP0813	15	217.93	1.474062	0.000000	1.474062	12.85
CP0813	16	220.34	-1.489742	0.000000	-1.489742	15.26
CP0813	17	223.53	2.886089	0.000000	2.886089	18.45
CP0813	18	225.34	-0.434608	0.000000	-0.434608	20.26
CP0813	19	228.93	2.453345	0.000000	2.453345	23.85
CP0813	20	230.34	0.000000	0.000000	0.000000	25.26
CP0813	21	235.68	0.904231	0.000000	0.904231	30.60
CP0813	22	239.93	0.563987	0.000000	0.563987	34.85
CP0814	00	100.85				0.00
CP0814	02	410.57	0.000000	0.000000	0.000000	100.00
CP0814	03	412.35	0.443835	0.443835	0.000000	101.78
CP0814	04	412.85	-0.618890	-0.618890	0.000000	102.28
CP0814	05	413.09	8.447638	8.447638	0.000000	102.52
CP0814	06	414.35	1.994927	1.994927	0.000000	103.78
CP0814	07	417.97	-0.421322	-0.421322	0.000000	107.40
CP0814	09	425.29	0.103545	0.103545	0.000000	114.72
CP0814	10	430.44	-0.244259	-0.244259	0.000000	119.87
CP0814	11	435.36	0.196801	0.196801	0.000000	124.79

Crack speed of the fracturing specimens in the batch -1

SampleNo	Pic	HangTime A	Net tot Crk Speed	Net Left Tot Speed	Net right Tot Speed	Manual Time
CP0815	00	187.34				0.00
CP0815	02	355.15	0.000000	0.000000	0.000000	100.00
CP0815	04	362.37	0.016679	0.000000	0.016679	107.22
CP0815	05	365.34	1.899469	0.000000	1.899469	110.19
CP0815	06	370.43	0.000000	0.000000	0.000000	115.28
CP0815	07	375.34	0.685916	0.000000	0.685916	120.19
CP0815	08	380.58	0.423638	0.000000	0.423638	125.43
CP0815	09	385.26	0.726530	0.000000	0.726530	130.11
CP0815	10	390.29	6.491274	0.000000	6.491274	135.14
CP0815	11	395.25	-6.537650	0.000000	-6.537650	140.10
CP0815	12	400.34	-0.218377	0.000000	-0.218377	145.19
CP0815	13	405.76	0.290496	0.000000	0.290496	150.61
CP0815	14	410.53	-0.251572	0.000000	-0.251572	155.38
CP0815	16	425.97	0.298845	0.000000	0.298845	170.82
CP0815	17	430.37	0.556847	0.000000	0.556847	175.22
CP0815	18	435.34	-0.337671	0.000000	-0.337671	180.19
CP0815	19	440.37	0.325333	0.000000	0.325333	185.22
CP0815	20	446.25	-0.526051	0.000000	-0.526051	191.10
CP0815	21	450.31	0.687908	0.000000	0.687908	195.16
CP0815	22	460.34	0.018844	0.000000	0.018844	205.19
CP0815	23	465.53	0.722685	0.000000	0.722685	210.38
CP0815	25	486.03	0.004888	0.000000	0.004888	230.88
CP0815	26	495.31	-0.134717	0.000000	-0.134717	240.16
CP0815	27	500.50	0.334411	0.000000	0.334411	245.35
CP0815	28	505.59	-0.170521	0.000000	-0.170521	250.44
CP0815	29	510.31	0.103009	0.000000	0.103009	255.16
CP0815	30	520.56	-0.094725	0.000000	-0.094725	265.41
CP0815	31	530.33	0.216730	0.000000	0.216730	275.18
CP0815	32	530.81	-5.619358	0.000000	-5.619358	275.66
CP0815	33	535.97	0.542785	0.000000	0.542785	280.82
CR0801	00	183.57				0.00
CR0801	02	240.35	0.000000	0.000000	0.000000	75.00
CR0801	04	433.16	0.010998	0.010998	0.000000	267.81
CR0801	06	462.44	0.001053	0.001053	0.000000	297.09
CR0801	07	470.97	0.377459	0.377459	0.000000	305.62
CR0801	08	475.39	0.568942	0.568942	0.000000	310.04
CR0801	10	485.41	0.229172	0.229172	0.000000	320.06
CR0801	11	490.39	-0.504642	-0.504642	0.000000	325.04
CR0801	12	495.25	0.201003	0.201003	0.000000	329.90
CR0801	13	497.15	0.026211	0.026211	0.000000	331.80
CR0801	14	500.35	-0.123543	-0.123543	0.000000	335.00
CR0801	15	500.39	2.222767	2.222767	0.000000	335.04
CR0801	16	505.35	0.459697	0.459697	0.000000	340.00
CR0801	17	505.79	-9.860239	-9.860239	0.000000	340.44
CR0801	18	510.39	0.544494	0.544494	0.000000	345.04
CR0801	19	514.13	0.295374	0.295374	0.000000	348.78
CR0801	20	514.59	-4.937417	-4.937417	0.000000	349.24
CR0801	21	514.94	15.867622	15.867622	0.000000	349.59

Crack speed of the fracturing specimens in the batch -1

SampleNo	Pic	HangTime A	Net tot Crk Speed	Net Left Tot Speed	Net right Tot Speed	Manual Time
CR0801	22	515.10	-25.820657	-25.820657	0.000000	349.75
CR0801	23	515.19	5.051203	5.051203	0.000000	349.84
CR0801	24	515.29	86.037428	86.037428	0.000000	349.94
CR0801	25	515.35	6.544004	6.544004	0.000000	350.00
CR0801	26	515.39	-73.839013	-73.839013	0.000000	350.04
CR0801	27	515.44	84.074978	84.074978	0.000000	350.09
CR0801	28	515.47	146.109503	146.109503	0.000000	350.12
CR0801	29	515.57	44.771309	44.771309	0.000000	350.22
CR0801	30	515.73	-6.994620	-6.994620	0.000000	350.38
CR0801	31	516.07	-2.558847	-2.558847	0.000000	350.72
CR0801	32	516.35	-1.199000	-1.199000	0.000000	351.00
CR0801	33	518.25	0.161807	0.161807	0.000000	352.90
CR0801	34	518.47	3.636364	3.636364	0.000000	353.12
CR0801	35	519.39	-1.721574	-1.721574	0.000000	354.04
CR0801	36	520.09	1.205286	1.205286	0.000000	354.74
CR0801	37	520.57	0.766030	0.766030	0.000000	355.22
CR0801	38	523.35	-0.111288	-0.111288	0.000000	358.00
CR0801	39	525.29	0.391540	0.391540	0.000000	359.94
CR0801	40	530.35	-0.075260	-0.075260	0.000000	365.00
CR0801	41	533.16	-0.464318	-0.464318	0.000000	367.81
CR0801	42	535.33	0.437133	0.437133	0.000000	369.98
CR0801	43	538.29	1.447222	1.447222	0.000000	372.94
CR0801	45	543.86	0.386017	0.386017	0.000000	378.51
CR0801	46	545.35	-0.335596	-0.335596	0.000000	380.00
CR0801	47	550.29	0.178344	0.178344	0.000000	384.94
CR0801	48	555.39	-0.234247	-0.234247	0.000000	390.04
CR0801	49	556.59	0.090408	0.090408	0.000000	391.24
CR0802	00	0.00				0.00
CR0802	08	245.55	0.000000	0.000000	0.000000	100.00
CR0802	09	250.59	0.648404	0.000000	0.648404	105.04
CR0802	10	260.74	-0.177420	0.000000	-0.177420	115.19
CR0802	11	265.49	0.004435	0.000000	0.004435	119.94
CR0802	12	270.79	0.099927	0.000000	0.099927	125.24
CR0802	13	275.39	0.021919	0.000000	0.021919	129.84
CR0802	14	285.87	0.056701	0.000000	0.056701	140.32
CR0802	15	295.49	4.102380	0.000000	4.102380	149.94
CR0802	16	299.93	1.357379	0.000000	1.357379	154.38
CR0802	19	301.09	-0.344359	0.000000	-0.344359	155.54
CR0802	20	302.09	0.399457	0.000000	0.399457	156.54
CR0802	21	302.53	90.817385	0.000000	90.817385	156.98
CR0802	22	303.29	-0.519286	0.000000	-0.519286	157.74
CR0802	23	305.58	0.004354	0.000000	0.004354	160.03
CR0802	24	310.39	0.336663	0.000000	0.336663	164.84
CR0802	25	320.37	12.505133	0.000000	12.505133	174.82
CR0802	26	325.48	-0.154009	0.000000	-0.154009	179.93
CR0802	27	330.37	-0.004210	0.000000	-0.004210	184.82
CR0802	28	335.39	-0.078151	0.000000	-0.078151	189.84
CR0802	29	340.39	-32.083212	0.000000	-32.083212	194.84

Crack speed of the fracturing specimens in the batch -1

SampleNo	Pic	HangTime A	Net tot Crk Speed	Net Left Tot Speed	Net right Tot Speed	Manual Time
CR0802	30	345.38	-7.686093	0.000000	-7.686093	199.83
CR0802	31	351.27	-0.172012	0.000000	-0.172012	205.72
CR0802	32	355.53	0.466048	0.000000	0.466048	209.98
CR0802	33	355.93	2.363786	0.000000	2.363786	210.38
CR0802	35	363.39	-0.010669	0.000000	-0.010669	217.84
CR0802	36	365.49	-0.436872	0.000000	-0.436872	219.94
CR0802	37	370.43	0.094175	0.000000	0.094175	224.88
CR0802	38	375.59	-0.031752	0.000000	-0.031752	230.04
CR0802	39	380.42	0.466933	0.000000	0.466933	234.87
CR0802	40	385.37	0.092092	0.000000	0.092092	239.82
CR0802	41	390.55	-0.258608	0.000000	-0.258608	245.00
CR0802	42	400.37	0.403164	0.000000	0.403164	254.82
CR0802	43	410.37	-0.091033	0.000000	-0.091033	264.82
CR0802	45	430.39	0.040523	0.000000	0.040523	284.84
CR0802	46	440.43	0.046311	0.000000	0.046311	294.88
CR0802	47	450.42	0.213001	0.000000	0.213001	304.87
CR0802	48	460.35	-0.022381	0.000000	-0.022381	314.80
CR0802	49	470.74	0.019321	0.000000	0.019321	325.19
CR0802	51	490.37	0.083210	0.000000	0.083210	344.82
CR0802	52	501.15	-0.019578	0.000000	-0.019578	355.60
CR0802	53	520.34	0.075873	0.000000	0.075873	374.79
CR0802	54	530.33	-0.236202	0.000000	-0.236202	384.78
CR0802	55	551.37	0.265269	0.000000	0.265269	405.82
CR0802	56	565.37	0.130231	0.000000	0.130231	419.82
DP0802	00	0.00				0.00
DP0802	01	167.25	0.000000	0.000000	0.000000	30.00
DP0802	02	179.99	-0.032756	-0.055083	0.022327	42.74
DP0802	03	184.25	0.082366	0.082366	0.000000	47.00
DP0802	04	185.68	0.000000	0.000000	0.000000	48.43
DP0802	05	188.85	0.110687	-0.110687	0.221374	51.60
DP0802	06	203.29	0.098397	0.122696	-0.024299	66.04
DP0802	07	235.93	0.031718	0.010219	0.021500	98.68
DP0802	08	252.78	0.021648	0.021648	0.000000	115.53
DP0802	09	294.93	-0.050276	-0.058601	0.008324	157.68
DP0803	00	0.00				0.00
DP0803	02	132.02	0.000000	0.000000	0.000000	25.00
DP0803	03	135.79	0.065152	0.000000	0.065152	28.77
DP0803	04	141.18	-0.063845	0.000000	-0.063845	34.16
DP0803	05	142.47	1.605344	0.000000	1.605344	35.45
DP0803	06	146.37	-0.353959	0.000000	-0.353959	39.35
DP0803	07	149.29	0.000000	0.000000	0.000000	42.27
DP0803	08	152.52	0.427381	0.000000	0.427381	45.50
DP0803	09	155.23	0.134136	0.000000	0.134136	48.21
DP0803	10	160.50	-0.068977	0.000000	-0.068977	53.48
DP0803	11	168.47	-0.132074	0.000000	-0.132074	61.45
DP0803	12	183.49	0.140164	0.000000	0.140164	76.47
DP0803	13	232.80	-0.014231	0.000000	-0.014231	125.78
DP0803	14	266.03	-0.062523	0.000000	-0.062523	159.01

Crack speed of the fracturing specimens in the batch -1

SampleNo	Pic	HangTime A	Net tot Crk Speed	Net Left Tot Speed	Net right Tot Speed	Manual Time
DP0804	00	0.00				0.00
DP0804	02	194.53	0.000000	0.000000	0.000000	25.00
DP0804	03	203.36	0.626848	0.000000	0.626848	33.83
DP0804	04	206.53	2.560062	0.000000	2.560062	37.00
DP0804	05	208.59	-1.816171	0.000000	-1.816171	39.06
DP0804	06	217.53	0.161723	0.000000	0.161723	48.00
DP0804	07	226.33	0.805285	0.000000	0.805285	56.80
DP0804	08	243.59	0.972042	0.000000	0.972042	74.06
DP0804	09	320.64	-0.557993	0.000000	-0.557993	151.11
DP0804	10	326.59	0.300295	0.000000	0.300295	157.06
DP0804	11	338.36	0.231086	0.000000	0.231086	168.83
DP0806	00	0.00				0.00
DP0806	01	134.56	0.000000	0.000000	0.000000	20.00
DP0806	02	138.55	-0.101284	0.000000	-0.101284	23.99
DP0806	03	150.29	0.410006	0.000000	0.410006	35.73
DP0806	04	163.55	-0.353240	0.000000	-0.353240	48.99
DP0806	05	176.55	0.138159	0.000000	0.138159	61.99
DP0806	06	190.58	0.141392	0.000000	0.141392	76.02
DP0806	07	222.03	0.208456	0.000000	0.208456	107.47
DP0806	08	222.55	0.390878	0.000000	0.390878	107.99
DP0806	09	235.29	0.038490	0.000000	0.038490	120.73
DP0806	10	238.38	-1.873631	0.000000	-1.873631	123.82
DP0808	00	0.00				0.00
DP0808	02	159.55	0.000000	0.000000	0.000000	20.00
DP0808	03	161.39	0.546314	0.342156	0.204158	21.84
DP0808	04	162.09	0.051940	0.519442	-0.467502	22.54
DP0808	05	165.30	0.294057	-0.007672	0.301729	25.75
DP0808	06	177.57	0.055254	0.055254	0.000000	38.02
DP0808	07	182.19	0.011147	0.149956	-0.138809	42.64
DP0808	08	185.75	-0.109686	-0.289826	0.180140	46.20
DP0808	09	187.37	0.445848	0.636902	-0.191055	47.82
DP0808	10	194.97	0.267352	0.182024	0.085328	55.42
DP0808	11	205.55	0.401161	0.330902	0.070258	66.00
DP0808	12	223.03	0.117262	0.003810	0.113452	83.48
DP0808	13	244.37	-0.004597	0.025725	-0.030322	104.82
DP0808	14	269.35	0.165197	0.153449	0.011749	129.80
DP0808	15	276.93	-0.449647	-0.315485	-0.134162	137.38
DP0808	16	277.93	-5.346911	-3.115320	-2.231591	138.38
DP0808	17	282.03	0.767457	0.533522	0.233935	142.48
DP0808	18	301.03	-0.244375	-0.223436	-0.020939	161.48
DP0812	00	0.00				0.00
DP0812	24	71.83	0.000000	0.000000	0.000000	73.49
DP0812	25	74.83	-0.270770	0.334663	-0.605432	76.49
DP0812	26	75.24	-37.490182	-35.960505	-1.529677	76.90
DP0812	27	75.59	16.833236	26.540092	-9.706856	77.25
DP0812	28	76.34	0.446428	18.320836	-17.874408	78.00
DP0812	29	82.55	-3.658639	-3.658639	0.000000	84.21
DP0812	30	88.19	0.092726	0.092726	0.000000	89.85
DP0812	31	95.49	-0.170214	-0.170214	0.000000	97.15

Crack speed of the fracturing specimens in the batch -1

SampleNo	Pic	HangTime A	Net tot Crk Speed	Net Left Tot Speed	Net right Tot Speed	Manual Time
DP0813	00	0.00				0.00
DP0813	02	133.39	0.000000	0.000000	0.000000	5.00
DP0813	03	134.08	-0.665550	0.000000	-0.665550	5.69
DP0813	04	134.25	199.434144	0.000000	199.434144	5.86
DP0813	05	135.29	-0.613152	0.000000	-0.613152	6.90
DP0813	06	136.55	1.067438	0.000000	1.067438	8.16
DP0813	07	140.55	8.853601	0.000000	8.853601	12.16
DP0813	08	142.53	-22.310196	0.000000	-22.310196	14.14
DP0813	09	145.39	-1.715130	0.000000	-1.715130	17.00
DP0813	10	147.25	-0.097075	0.000000	-0.097075	18.86
DP0813	11	150.15	1.262065	0.000000	1.262065	21.76
DP0813	12	156.69	0.242868	0.000000	0.242868	28.30
DP0813	13	167.69	0.021838	0.000000	0.021838	39.30
DP0814	00	0.00				0.00
DP0814	02	309.53	0.000000	0.000000	0.000000	100.00
DP0814	03	324.58	-0.006952	-0.006952	0.000000	115.05
DP0814	04	331.08	0.051045	0.051045	0.000000	121.55
DP0814	05	345.09	0.022092	0.022092	0.000000	135.56
DP0814	07	364.08	-0.016299	-0.016299	0.000000	154.55
DP0814	08	371.05	0.000000	0.000000	0.000000	161.52
DP0814	09	410.49	0.008472	0.008472	0.000000	200.96
DP0814	10	413.79	0.320512	0.320512	0.000000	204.26
DP0814	11	437.28	-0.045027	-0.045027	0.000000	227.75
DP0814	12	431.59	-0.114822	0.063903	0.000000	222.06
DP0814	13	438.58	0.048495	0.048495	0.000000	229.05
DP0814	14	479.45	0.009191	0.000000	0.009191	269.92
DP0814	15	611.29	0.010230	0.007714	0.002517	401.76
DP0814	16	628.38	0.018111	0.059506	-0.041395	418.85
DP0814	17	649.53	-0.089300	-0.091589	0.002288	440.00
DP0814	18	750.39	-0.001147	-0.004028	0.002881	540.86
DP0815	00	0.00				0.00
DP0815	03	503.53	0.000000	0.000000	0.000000	100.00
DP0815	04	514.88	-0.061829	0.000000	0.000000	111.35
DP0815	05	516.99	0.171781	0.000000	0.000000	113.46
DP0815	06	521.59	0.304482	0.000000	0.000000	118.06
DP0815	07	522.23	-1.658316	0.000000	0.000000	118.70
DP0815	08	522.48	0.042768	0.000000	0.000000	118.95
DP0815	09	522.53	0.000000	0.000000	0.000000	119.00
DP0815	10	525.28	-0.769438	-0.769438	0.000000	121.75
DP0815	11	547.28	0.015949	0.015949	0.000000	143.75
DP0815	12	574.53	0.051505	0.051505	0.000000	171.00
DP0815	13	583.73	-0.076278	-0.076278	0.000000	180.20
DP0815	14	602.38	0.037628	0.037628	0.000000	198.85
DP0815	15	607.93	-0.063221	-0.063221	0.000000	204.40
DP0815	16	609.08	0.610221	0.610221	0.000000	205.55

Crack speed of the fracturing specimens in the batch -1

SampleNo	Pic	HangTime A	Net tot Crk Speed	Net Left Tot Speed	Net right Tot Speed	Manual Time
DR0801	00	0.00				0.00
DR0801	03	234.27	0.000000	0.000000	0.000000	100.00
DR0801	04	235.38	-2.212739	0.000000	0.000000	101.11
DR0801	07	269.24	0.062176	0.000000	0.000000	134.97
DR0801	08	293.53	0.043336	0.000000	0.000000	159.26
DR0801	09	311.39	0.019646	0.019646	0.000000	177.12
DR0801	10	320.83	0.188788	0.188788	0.000000	186.56
DR0801	11	328.27	-0.002799	-0.002799	0.000000	194.00
DR0801	12	336.37	0.086558	0.086558	0.000000	202.10
DR0801	13	345.20	-0.119098	-0.119098	0.000000	210.93
DR0801	15	370.39	0.029926	0.029926	0.000000	236.12
DR0801	16	380.39	-0.138969	-0.138969	0.000000	246.12
DR0801	17	400.24	0.087551	0.087551	0.000000	265.97
DR0801	18	410.03	0.146274	0.146274	0.000000	275.76
DR0801	20	455.34	-0.046969	-0.046969	0.000000	321.07
DR0801	21	461.64	0.393001	0.393001	0.000000	327.37
DR0801	22	472.08	-0.033309	-0.033309	0.000000	337.81
DR0801	23	500.64	-0.110991	-0.110991	0.000000	366.37
DR0801	24	507.39	0.572685	0.572685	0.000000	373.12
DR0801	25	592.27	-0.003559	-0.003559	0.000000	458.00
DR0801	26	642.19	0.006938	0.006938	0.000000	507.92
DR0801	27	666.93	-0.086022	-0.086022	0.000000	532.66
DR0801	28	810.48	-0.009624	-0.009624	0.000000	676.21
DR0802	00	0.00				0.00
DR0802	02	234.48	0.000000	0.000000	0.000000	80.00
DR0802	03	237.09	0.909150	0.000000	0.909150	82.61
DR0802	05	245.43	-0.040645	0.000000	-0.040645	90.95
DR0802	06	250.27	0.492183	0.000000	0.492183	95.79
DR0802	07	255.93	-0.600550	0.000000	-0.600550	101.45
DR0802	08	262.63	0.202378	0.000000	0.202378	108.15
DR0802	09	265.27	0.517628	0.000000	0.517628	110.79
DR0802	10	270.27	0.743641	0.000000	-0.002121	115.79
DR0802	11	275.27	-0.130343	-0.064830	-0.065513	120.79
DR0802	12	280.37	-0.402238	-0.667581	0.265343	125.89
DR0802	13	285.24	-0.419432	0.000000	-0.419432	130.76
DR0802	14	290.27	0.344324	0.000000	0.344324	135.79
DR0802	15	295.37	0.258607	0.000000	0.258607	140.89
DR0802	17	305.37	-0.203390	0.000000	-0.203390	150.89
DR0802	18	310.34	0.409235	0.000000	0.409235	155.86
DR0802	19	315.37	0.000000	0.000000	0.000000	160.89
DR0802	20	320.59	0.389636	0.000000	0.389636	166.11
DR0802	21	326.09	-0.491566	0.000000	-0.491566	171.61
DR0802	22	330.24	-0.165354	0.000000	-0.165354	175.76
DR0802	23	335.24	1.597864	0.000000	1.597864	180.76
DR0802	24	340.43	-0.420872	0.000000	-0.420872	185.95
DR0802	25	355.30	0.209233	0.000000	0.209233	200.82
DR0802	27	365.27	0.141188	0.000000	0.141188	210.79
DR0802	28	370.37	0.081622	0.000000	0.081622	215.89

Crack speed of the fracturing specimens in the batch -1

SampleNo	Pic	HangTime A	Net tot Crk Speed	Net Left Tot Speed	Net right Tot Speed	Manual Time
DR0802	29	375.30	-0.372714	0.000000	-0.372714	220.82
DR0802	30	380.27	0.914374	0.000000	0.914374	225.79
DR0802	31	385.37	-0.871860	0.000000	-0.871860	230.89
DR0802	32	390.43	0.196082	0.000000	0.196082	235.95
DR0802	33	395.37	-0.005111	0.000000	-0.005111	240.89
DR0802	34	400.37	0.006859	0.000000	0.006859	245.89
DR0802	35	405.43	0.527062	0.000000	0.527062	250.95
DR0802	37	425.49	-0.154889	0.000000	-0.154889	271.01
DR0802	38	430.59	0.285705	0.000000	0.285705	276.11
DR0802	39	435.37	-0.125068	0.000000	-0.125068	280.89
DR0802	40	440.27	0.708386	0.000000	0.708386	285.79
DR0802	41	445.43	0.287120	0.000000	0.287120	290.95
DR0802	42	450.43	-0.657854	0.000000	-0.657854	295.95
DR0802	43	455.33	0.262782	0.000000	0.262782	300.85
DR0802	44	455.59	5.261111	0.000000	5.261111	301.11
DR0802	45	460.37	0.160284	0.000000	0.160284	305.89
DR0802	46	465.37	-0.088774	0.000000	-0.088774	310.89
DR0802	47	470.27	0.391986	0.000000	0.391986	315.79
DR0802	48	475.37	0.312276	0.000000	0.312276	320.89
DR0802	50	485.27	0.766548	0.000000	0.766548	330.79
DR0802	51	490.30	-1.555534	0.000000	-1.555534	335.82
DR0802	52	495.49	0.261825	0.000000	0.261825	341.01
DR0802	53	500.68	-0.184261	0.000000	-0.184261	346.20
DR0802	54	505.99	0.054511	0.000000	0.054511	351.51
DR0802	55	507.79	-0.911438	0.000000	-0.911438	353.31
DR0802	56	510.49	0.233502	0.000000	0.233502	356.01
DR0802	57	515.69	-0.357651	0.000000	-0.357651	361.21
DR0802	58	520.39	0.659274	0.000000	0.659274	365.91
DR0802	59	525.30	0.056817	0.000000	0.056817	370.82
DR0802	61	550.38	0.082205	0.000000	0.082205	395.90

Tot - Total
Crk - Crack
Manual Time - Time read using a stop watch
Hang Time A - Time read from the hanging watch

Time to failure states, crack speeds at these events, lowest speed (due to crack closure) and duration of frature

Specimen No.	Time to crack initiation - s	Net Speed at Crack initiation - mm/s	Time to catastrophic failure - s	Catastrophic speed - mm/s	Lowest speed indicated - mm/s	Duration of fracture - s
AP0801	100.00	6.269737	100.98	1040.944062	-1021.102983	0.98
AP0804	125.00	26.045544	126.87	3493.776132	-1451.418201	1.87
AP0805	0.00	4.453437	3.84	54.377508	-12.424344	3.84
AP0807	150.00	11.041578	197.12	63.637552	-35.345498	47.12
AP0808	125.00	0.212800	239.45	12.798832	-9.049398	114.45
AP0809	20.00	0.846561	56.65	87.761549	-73.964074	36.65
AP0810	501.29	-17.933602	507.70	0.164625	-17.933602	6.41
AP0813	28.00	1.248677	48.64	61.137842	-429.171983	20.64
AP0814	350.00	-0.304100	443.96	311.694268	-15.801725	93.96
AP0815	325.00	-3887.045375	325.19	29.732354	-3887.045375	0.19
AR0801	350.00	0.660729	504.70	116.208059	-3.148385	154.70
BP0808	80.00	1.828723	86.30	3.889315	0.052202	6.30
BP0810	20.00	0.258868	39.75	123.260170	-2275.735083	19.75
BP0811	20.00	-3.378766	35.40	7.022975	-26.439549	15.40
BP0812	20.00	-0.918245	23.96	64.483379	-132.352002	3.96
BP0813	300.00	22.855844	300.55	22.855844	-1.323306	0.55
BP0814	300.00	-0.047360	639.50	318.283840	-32.294928	339.50
BR0801	320.00	-2.427531	465.50	3205.463343	-18.356220	145.50
BR0802	300.00	0.077967	427.50	18.360396	-12.117105	127.50
CP0801	90.00	0.238097	169.71	41.222944	-3.641152	79.71
CP0802	30.00	0.280091	41.20	17.827714	-9.781677	11.20
CP0803	45.00	-76.895997	45.41	23.827467	-308.667516	0.41
CP0804	50.00	-0.185263	229.30	12.293768	-69.384259	179.30
CP0805	113.90	2.475946	167.10	253.553937	-31.412539	53.20
CP0806	50.00	0.091740	56.47	0.430302	-0.193262	6.47
CP0807	50.00	0.127284	101.10	65.176261	-0.092041	51.10
CP0808	30.00	-2.329358	49.62	229.438756	-24.445877	19.62
CP0810	10.00	-0.025077	17.94	122.182614	-60.758291	7.94
CP0811	8.00	3.370994	24.40	25.081850	-18.691444	16.40
CP0812	8.00	14.760692	34.06	414.232614	-29.494691	26.06
CP0813	8.00	36.117940	8.85	404.702803	-40.000000	0.85
CP0814	100.00	0.443835	102.52	8.447638	-0.618890	2.52
CP0815	100.00	0.016679	135.14	6.491274	-6.537650	35.14
CR0801	75.00	0.010998	350.12	146.109503	-73.839013	275.12
CR0802	100.00	0.648404	156.98	90.817385	-32.083212	56.98
DP0802	30.00	-0.032756	51.60	0.110687	-0.050276	21.60
DP0803	25.00	0.065152	35.45	1.605344	-0.353959	10.45
DP0804	25.00	0.626848	37.00	2.560062	-1.816171	12.00
DP0806	20.00	-0.101284	35.73	0.410006	-1.873631	15.73
DP0808	20.00	0.546314	142.48	0.767457	-5.346911	122.48
DP0812	73.49	-0.270770	77.25	16.833236	-37.490182	3.76
DP0813	5.00	-0.665550	5.86	199.434144	-22.310196	0.86
DP0814	100.00	-0.006952	204.26	0.320512	-0.114822	104.26
DP0815	100.00	-0.061829	205.55	0.610221	-1.658316	105.55
DR0801	100.00	-2.212739	373.12	0.572685	-2.212739	273.12
DR0802	80.00	0.909150	301.11	5.261111	-1.555534	221.11

Chart 1- Input and desired output data used for training the ANN model for fracture toughness, before randomizing														
Spec. No	ROL- m/s	Crk Len. m	Len. m	Hght - m	Width m	Volume m3	Uncrked Vol. m3	Hght*Wdth *Effc. Len. m3	Cracked Volume m3	Height* Wdth m2	Crack Length *Wdth m2	(Hght-Crk Len.) *Wdth m2	FT - Pa	Normalised FT - Pa
X08AP01	0.0025	0.041	1	0.09	0.045	0.00405	0.002205	0.0011899	0.001845	0.00405	0.001845	0.002205	172738.27	3.97134296
X08AP02	0.0025	0.041	1	0.09	0.045	0.00405	0.002205	0.0011899	0.001845	0.00405	0.001845	0.002205	79725.352	1.83292748
X08AP03	0.0025	0.041	1	0.09	0.045	0.00405	0.002205	0.0011899	0.001845	0.00405	0.001845	0.002205	78396.594	1.80237864
X08AP04	0.0025	0.041	1	0.09	0.045	0.00405	0.002205	0.0011899	0.001845	0.00405	0.001845	0.002205	44291.863	1.01829306
X08AP09	0.01	0.041	1	0.09	0.045	0.00405	0.002205	0.0011899	0.001845	0.00405	0.001845	0.002205	110729.66	2.54573281
X08AP10	0.01	0.041	1	0.09	0.045	0.00405	0.002205	0.0011899	0.001845	0.00405	0.001845	0.002205	97442.102	2.24024482
X08AP11	0.01	0.041	1	0.09	0.045	0.00405	0.002205	0.0011899	0.001845	0.00405	0.001845	0.002205	155021.53	3.56402597
X08AP14	0.000625	0.041	1	0.09	0.045	0.00405	0.002205	0.0011899	0.001845	0.00405	0.001845	0.002205	100099.62	2.30134248
X08AP15	0.000625	0.041	1	0.09	0.045	0.00405	0.002205	0.0011899	0.001845	0.00405	0.001845	0.002205	99656.688	2.29115931
X08BP02	0.0025	0.025	0.6	0.054	0.027	0.00087	0.0004698	0.000257	0.000405	0.00146	0.000675	0.000783	64282.75	1.477894
X08BP03	0.0025	0.025	0.6	0.054	0.027	0.00087	0.0004698	0.000257	0.000405	0.00146	0.000675	0.000783	37400.875	0.85986565
X08BP04	0.0025	0.025	0.6	0.054	0.027	0.00087	0.0004698	0.000257	0.000405	0.00146	0.000675	0.000783	52594.98	1.20918606
X08BP05	0.0025	0.025	0.6	0.054	0.027	0.00087	0.0004698	0.000257	0.000405	0.00146	0.000675	0.000783	25713.102	0.59115765
X08BP09	0.01	0.025	0.6	0.054	0.027	0.00087	0.0004698	0.000257	0.000405	0.00146	0.000675	0.000783	46166.703	1.06139662
X08BP10	0.01	0.025	0.6	0.054	0.027	0.00087	0.0004698	0.000257	0.000405	0.00146	0.000675	0.000783	39738.43	0.91360726
X08BP11	0.01	0.025	0.6	0.054	0.027	0.00087	0.0004698	0.000257	0.000405	0.00146	0.000675	0.000783	105189.96	2.41837214
X08BP14	0.000625	0.025	0.6	0.054	0.027	0.00087	0.0004698	0.000257	0.000405	0.00146	0.000675	0.000783	42075.984	0.96734885
X08BP15	0.000625	0.025	0.6	0.054	0.027	0.00087	0.0004698	0.000257	0.000405	0.00146	0.000675	0.000783	70126.641	1.6122481
X08CP01	0.0025	0.025	0.3	0.027	0.014	0.00011	8.1E-06	3.213E-05	0.0001013	0.00036	0.000338	0.000027	48053.387	1.10477247
X08CP02	0.0025	0.025	0.3	0.027	0.014	0.00011	8.1E-06	3.213E-05	0.0001013	0.00036	0.000338	0.000027	26210.941	0.60260322
X08CP03	0.0025	0.025	0.3	0.027	0.014	0.00011	8.1E-06	3.213E-05	0.0001013	0.00036	0.000338	0.000027	33200.523	0.76329736
X08CP04	0.0025	0.025	0.3	0.027	0.014	0.00011	8.1E-06	3.213E-05	0.0001013	0.00036	0.000338	0.000027	54169.273	1.24537988
X08CP05	0.0025	0.025	0.3	0.027	0.014	0.00011	8.1E-06	3.213E-05	0.0001013	0.00036	0.000338	0.000027	30579.43	0.70303707
X08CP09	0.01	0.025	0.3	0.027	0.014	0.00011	8.1E-06	3.213E-05	0.0001013	0.00036	0.000338	0.000027	45432.297	1.04451224
X08CP10	0.01	0.025	0.3	0.027	0.014	0.00011	8.1E-06	3.213E-05	0.0001013	0.00036	0.000338	0.000027	68148.445	1.56676834
X08CP11	0.01	0.025	0.3	0.027	0.014	0.00011	8.1E-06	3.213E-05	0.0001013	0.00036	0.000338	0.000027	26210.941	0.60260322
X08CP14	0.000625	0.025	0.3	0.027	0.014	0.00011	8.1E-06	3.213E-05	0.0001013	0.00036	0.000338	0.000027	12581.252	0.28924956
X08CP15	0.000625	0.025	0.3	0.027	0.014	0.00011	8.1E-06	3.213E-05	0.0001013	0.00036	0.000338	0.000027	22716.148	0.52225611
X08DP01	0.0025	0.006	0.15	0.014	0.006	1.2E-05	6.75E-06	3.57E-06	0.0000054	8.1E-05	0.000036	0.000045	21652.867	0.49781072
X08DP02	0.0025	0.006	0.15	0.014	0.006	1.2E-05	6.75E-06	3.57E-06	0.0000054	8.1E-05	0.000036	0.000045	30073.428	0.69140382
X08DP03	0.0025	0.006	0.15	0.014	0.006	1.2E-05	6.75E-06	3.57E-06	0.0000054	8.1E-05	0.000036	0.000045	22454.826	0.51624818

Spec. No	ROL- m/s	Crk Len. m	Len. m	Hght - m	Width m	Volume m3	Uncrked Vol. m3	Hght*Wdth *Effc. Len. m3	Cracked Volume m3	Height* Wdth m2	Crack Length *Wdth m2	(Hght-Crk Len.) *Wdth m2	FT - Pa	Normalised FT - Pa
X08DP04	0.0025	0.006	0.15	0.014	0.006	1.2E-05	6.75E-06	3.57E-06	0.0000054	8.1E-05	0.000036	0.000045	20048.951	0.46093586
X08DP05	0.0025	0.006	0.15	0.014	0.006	1.2E-05	6.75E-06	3.57E-06	0.0000054	8.1E-05	0.000036	0.000045	13031.818	0.2996083
X08DP09	0.01	0.006	0.15	0.014	0.006	1.2E-05	6.75E-06	3.57E-06	0.0000054	8.1E-05	0.000036	0.000045	17643.078	0.40562358
X08DP10	0.01	0.006	0.15	0.014	0.006	1.2E-05	6.75E-06	3.57E-06	0.0000054	8.1E-05	0.000036	0.000045	26063.637	0.59921663
X08DP11	0.01	0.006	0.15	0.014	0.006	1.2E-05	6.75E-06	3.57E-06	0.0000054	8.1E-05	0.000036	0.000045	17643.078	0.40562358
X08DP14	0.000625	0.006	0.15	0.014	0.006	1.2E-05	6.75E-06	3.57E-06	0.0000054	8.1E-05	0.000036	0.000045	8420.56	0.19359307
X08DP15	0.000625	0.006	0.15	0.014	0.006	1.2E-05	6.75E-06	3.57E-06	0.0000054	8.1E-05	0.000036	0.000045	17643.078	0.40562358
X12AP01	0.0025	0.041	1	0.09	0.045	0.00405	0.002205	0.0011899	0.001845	0.00405	0.001845	0.002205	127560.57	2.93268413
X12AP02	0.0025	0.041	1	0.09	0.045	0.00405	0.002205	0.0011899	0.001845	0.00405	0.001845	0.002205	42520.188	0.97756133
X12AP03	0.0025	0.041	1	0.09	0.045	0.00405	0.002205	0.0011899	0.001845	0.00405	0.001845	0.002205	159450.7	3.66585494
X12AP04	0.0025	0.041	1	0.09	0.045	0.00405	0.002205	0.0011899	0.001845	0.00405	0.001845	0.002205	59528.266	1.36858593
X12AP05	0.0025	0.041	1	0.09	0.045	0.00405	0.002205	0.0011899	0.001845	0.00405	0.001845	0.002205	79725.352	1.83292748
X12AP09	0.01	0.041	1	0.09	0.045	0.00405	0.002205	0.0011899	0.001845	0.00405	0.001845	0.002205	120473.87	2.76975713
X12AP10	0.01	0.041	1	0.09	0.045	0.00405	0.002205	0.0011899	0.001845	0.00405	0.001845	0.002205	155907.36	3.58439161
X12AP11	0.01	0.041	1	0.09	0.045	0.00405	0.002205	0.0011899	0.001845	0.00405	0.001845	0.002205	76536.336	1.75961034
X12AP14	0.000625	0.041	1	0.09	0.045	0.00405	0.002205	0.0011899	0.001845	0.00405	0.001845	0.002205	34547.656	0.79426866
X12AP15	0.000625	0.041	1	0.09	0.045	0.00405	0.002205	0.0011899	0.001845	0.00405	0.001845	0.002205	106300.47	2.4439033
X12BP01	0.0025	0.025	0.6	0.054	0.027	0.00087	0.0004698	0.000257	0.000405	0.00146	0.000675	0.000783	78892.469	1.81377907
X12BP02	0.0025	0.025	0.6	0.054	0.027	0.00087	0.0004698	0.000257	0.000405	0.00146	0.000675	0.000783	82281.922	1.89170436
X12BP03	0.0025	0.025	0.6	0.054	0.027	0.00087	0.0004698	0.000257	0.000405	0.00146	0.000675	0.000783	48153.625	1.10707699
X12BP04	0.0025	0.025	0.6	0.054	0.027	0.00087	0.0004698	0.000257	0.000405	0.00146	0.000675	0.000783	35063.32	0.80612404
X12BP05	0.0025	0.025	0.6	0.054	0.027	0.00087	0.0004698	0.000257	0.000405	0.00146	0.000675	0.000783	28050.654	0.64489919
X12BP09	0.01	0.025	0.6	0.054	0.027	0.00087	0.0004698	0.000257	0.000405	0.00146	0.000675	0.000783	81814.406	1.88095593
X12BP10	0.01	0.025	0.6	0.054	0.027	0.00087	0.0004698	0.000257	0.000405	0.00146	0.000675	0.000783	53763.758	1.23605688
X12BP11	0.01	0.025	0.6	0.054	0.027	0.00087	0.0004698	0.000257	0.000405	0.00146	0.000675	0.000783	88827.07	2.04218073
X12BP14	0.000625	0.025	0.6	0.054	0.027	0.00087	0.0004698	0.000257	0.000405	0.00146	0.000675	0.000783	51426.203	1.18231527
X12BP15	0.000625	0.025	0.6	0.054	0.027	0.00087	0.0004698	0.000257	0.000405	0.00146	0.000675	0.000783	50491.18	1.1608186
X12CP01	0.0025	0.013	0.3	0.027	0.014	0.00011	0.0000567	3.213E-05	5.265E-05	0.00036	0.000176	0.000189	52421.883	1.20520647
X12CP02	0.0025	0.013	0.3	0.027	0.014	0.00011	0.0000567	3.213E-05	5.265E-05	0.00036	0.000176	0.000189	43684.898	1.00433862
X12CP03	0.0025	0.013	0.3	0.027	0.014	0.00011	0.0000567	3.213E-05	5.265E-05	0.00036	0.000176	0.000189	26210.941	0.60260322
X12CP04	0.0025	0.013	0.3	0.027	0.014	0.00011	0.0000567	3.213E-05	5.265E-05	0.00036	0.000176	0.000189	14852.866	0.34147515
X12CP05	0.0025	0.013	0.3	0.027	0.014	0.00011	0.0000567	3.213E-05	5.265E-05	0.00036	0.000176	0.000189	30579.43	0.70303707

Spec. No	ROL- m/s	Crk Len. m	Len. m	Hght - m	Width m	Volume m3	Uncrked Vol. m3	Hght*Wdth *Effc. Len. m3	Cracked Volume m3	Height* Wdth m2	Crack Length *Wdth m2	(Hght-Crk Len.) *Wdth m2	FT - Pa	Normalised FT - Pa
X12CP09	0.01	0.013	0.3	0.027	0.014	0.00011	0.0000567	3.213E-05	5.265E-05	0.00036	0.000176	0.000189	56790.371	1.30564029
X12CP10	0.01	0.013	0.3	0.027	0.014	0.00011	0.0000567	3.213E-05	5.265E-05	0.00036	0.000176	0.000189	36695.316	0.84364448
X12CP11	0.01	0.013	0.3	0.027	0.014	0.00011	0.0000567	3.213E-05	5.265E-05	0.00036	0.000176	0.000189	38442.711	0.883818
X12CP14	0.000625	0.013	0.3	0.027	0.014	0.00011	0.0000567	3.213E-05	5.265E-05	0.00036	0.000176	0.000189	29705.732	0.68295029
X12CP15	0.000625	0.013	0.3	0.027	0.014	0.00011	0.0000567	3.213E-05	5.265E-05	0.00036	0.000176	0.000189	64653.652	1.48642123
X12DP01	0.0025	0.006	0.15	0.014	0.006	1.2E-05	6.75E-06	3.57E-06	0.0000054	8.1E-05	0.000036	0.000045	33222.105	0.76379355
X12DP02	0.0025	0.006	0.15	0.014	0.006	1.2E-05	6.75E-06	3.57E-06	0.0000054	8.1E-05	0.000036	0.000045	23919.916	0.54993136
X12DP03	0.0025	0.006	0.15	0.014	0.006	1.2E-05	6.75E-06	3.57E-06	0.0000054	8.1E-05	0.000036	0.000045	28792.492	0.66195443
X12DP04	0.0025	0.006	0.15	0.014	0.006	1.2E-05	6.75E-06	3.57E-06	0.0000054	8.1E-05	0.000036	0.000045	28792.492	0.66195443
X12DP05	0.0025	0.006	0.15	0.014	0.006	1.2E-05	6.75E-06	3.57E-06	0.0000054	8.1E-05	0.000036	0.000045	14396.246	0.33097722
X12DP09	0.01	0.006	0.15	0.014	0.006	1.2E-05	6.75E-06	3.57E-06	0.0000054	8.1E-05	0.000036	0.000045	28792.492	0.66195443
X12DP10	0.01	0.006	0.15	0.014	0.006	1.2E-05	6.75E-06	3.57E-06	0.0000054	8.1E-05	0.000036	0.000045	24362.879	0.56011531
X12DP11	0.01	0.006	0.15	0.014	0.006	1.2E-05	6.75E-06	3.57E-06	0.0000054	8.1E-05	0.000036	0.000045	18825.861	0.43281638
X12DP14	0.000625	0.006	0.15	0.014	0.006	1.2E-05	6.75E-06	3.57E-06	0.0000054	8.1E-05	0.000036	0.000045	19490.303	0.44809225
X12DP15	0.000625	0.006	0.15	0.014	0.006	1.2E-05	6.75E-06	3.57E-06	0.0000054	8.1E-05	0.000036	0.000045	28792.492	0.66195443
X20AP01	0.0025	0.041	1	0.09	0.045	0.00405	0.002205	0.0011899	0.001845	0.00405	0.001845	0.002205	106300.47	2.4439033
X20AP02	0.0025	0.041	1	0.09	0.045	0.00405	0.002205	0.0011899	0.001845	0.00405	0.001845	0.002205	81497.031	1.87365931
X20AP03	0.0025	0.041	1	0.09	0.045	0.00405	0.002205	0.0011899	0.001845	0.00405	0.001845	0.002205	125434.55	2.88380575
X20AP04	0.0025	0.041	1	0.09	0.045	0.00405	0.002205	0.0011899	0.001845	0.00405	0.001845	0.002205	169549.25	3.89802581
X20AP05	0.0025	0.041	1	0.09	0.045	0.00405	0.002205	0.0011899	0.001845	0.00405	0.001845	0.002205	59528.266	1.36858593
X20AP09	0.01	0.041	1	0.09	0.045	0.00405	0.002205	0.0011899	0.001845	0.00405	0.001845	0.002205	106743.39	2.45408631
X20AP10	0.01	0.041	1	0.09	0.045	0.00405	0.002205	0.0011899	0.001845	0.00405	0.001845	0.002205	95670.422	2.19951297
X20AP11	0.01	0.041	1	0.09	0.045	0.00405	0.002205	0.0011899	0.001845	0.00405	0.001845	0.002205	61122.77	1.40524441
X20AP14	0.000625	0.041	1	0.09	0.045	0.00405	0.002205	0.0011899	0.001845	0.00405	0.001845	0.002205	105148.88	2.41742774
X20AP15	0.000625	0.041	1	0.09	0.045	0.00405	0.002205	0.0011899	0.001845	0.00405	0.001845	0.002205	82382.859	1.89402496
X20BP01	0.0025	0.025	0.6	0.054	0.027	0.00087	0.0004698	0.000257	0.000405	0.00146	0.000675	0.000783	414.661	0.00953327
X20BP02	0.0025	0.025	0.6	0.054	0.027	0.00087	0.0004698	0.000257	0.000405	0.00146	0.000675	0.000783	392.149	0.00901571
X20BP03	0.0025	0.025	0.6	0.054	0.027	0.00087	0.0004698	0.000257	0.000405	0.00146	0.000675	0.000783	254.171	0.00584352
X20BP04	0.0025	0.025	0.6	0.054	0.027	0.00087	0.0004698	0.000257	0.000405	0.00146	0.000675	0.000783	363.101	0.00834788
X20BP05	0.0025	0.025	0.6	0.054	0.027	0.00087	0.0004698	0.000257	0.000405	0.00146	0.000675	0.000783	413.935	0.00951658
X20BP09	0.01	0.025	0.6	0.054	0.027	0.00087	0.0004698	0.000257	0.000405	0.00146	0.000675	0.000783	294.112	0.00676179
X20BP10	0.01	0.025	0.6	0.054	0.027	0.00087	0.0004698	0.000257	0.000405	0.00146	0.000675	0.000783	508.341	0.01168703

Spec. No	ROL- m/s	Crk Len. m	Len. m	Hght - m	Width m	Volume m3	Uncrked Vol. m3	Hght*Wdth *Effc. Len. m3	Cracked Volume m3	Height* Wdth m2	Crack Length *Wdth m2	(Hght-Crk Len.) *Wdth m2	FT - Pa	Normalised FT - Pa
X20BP11	0.01	0.025	0.6	0.054	0.027	0.00087	0.0004698	0.000257	0.000405	0.00146	0.000675	0.000783	588.224	0.01352358
X20BP14	0.000625	0.025	0.6	0.054	0.027	0.00087	0.0004698	0.000257	0.000405	0.00146	0.000675	0.000783	312.267	0.00717918
X20BP15	0.000625	0.025	0.6	0.054	0.027	0.00087	0.0004698	0.000257	0.000405	0.00146	0.000675	0.000783	275.957	0.0063444
X20CP01	0.0025	0.013	0.3	0.027	0.014	0.00011	0.0000567	3.213E-05	5.265E-05	0.00036	0.000176	0.000189	281.022	0.00646084
X20CP02	0.0025	0.013	0.3	0.027	0.014	0.00011	0.0000567	3.213E-05	5.265E-05	0.00036	0.000176	0.000189	141.165	0.00324546
X20CP03	0.0025	0.013	0.3	0.027	0.014	0.00011	0.0000567	3.213E-05	5.265E-05	0.00036	0.000176	0.000189	199.983	0.00459771
X20CP04	0.0025	0.013	0.3	0.027	0.014	0.00011	0.0000567	3.213E-05	5.265E-05	0.00036	0.000176	0.000189	113.716	0.00261439
X20CP05	0.0025	0.013	0.3	0.027	0.014	0.00011	0.0000567	3.213E-05	5.265E-05	0.00036	0.000176	0.000189	198.676	0.00456767
X20CP09	0.01	0.013	0.3	0.027	0.014	0.00011	0.0000567	3.213E-05	5.265E-05	0.00036	0.000176	0.000189	241.81	0.00555934
X20CP10	0.01	0.013	0.3	0.027	0.014	0.00011	0.0000567	3.213E-05	5.265E-05	0.00036	0.000176	0.000189	169.921	0.00390657
X20CP11	0.01	0.013	0.3	0.027	0.014	0.00011	0.0000567	3.213E-05	5.265E-05	0.00036	0.000176	0.000189	141.165	0.00324546
X20CP14	0.000625	0.013	0.3	0.027	0.014	0.00011	0.0000567	3.213E-05	5.265E-05	0.00036	0.000176	0.000189	130.708	0.00300505
X20CP15	0.000625	0.013	0.3	0.027	0.014	0.00011	0.0000567	3.213E-05	5.265E-05	0.00036	0.000176	0.000189	130.708	0.00300505
X20DP01	0.0025	0.006	0.15	0.014	0.006	1.2E-05	6.75E-06	3.57E-06	0.0000054	8.1E-05	0.000036	0.000045	25864.848	0.59464637
X20DP02	0.0025	0.006	0.15	0.014	0.006	1.2E-05	6.75E-06	3.57E-06	0.0000054	8.1E-05	0.000036	0.000045	32023.145	0.73622883
X20DP05	0.0025	0.006	0.15	0.014	0.006	1.2E-05	6.75E-06	3.57E-06	0.0000054	8.1E-05	0.000036	0.000045	19706.551	0.4530639
X20DP09	0.01	0.006	0.15	0.014	0.006	1.2E-05	6.75E-06	3.57E-06	0.0000054	8.1E-05	0.000036	0.000045	27096.506	0.62296283
X20DP10	0.01	0.006	0.15	0.014	0.006	1.2E-05	6.75E-06	3.57E-06	0.0000054	8.1E-05	0.000036	0.000045	27096.506	0.62296283
X20DP11	0.01	0.006	0.15	0.014	0.006	1.2E-05	6.75E-06	3.57E-06	0.0000054	8.1E-05	0.000036	0.000045	32023.145	0.73622883
X20DP14	0.000625	0.006	0.15	0.014	0.006	1.2E-05	6.75E-06	3.57E-06	0.0000054	8.1E-05	0.000036	0.000045	22169.869	0.50969687
X20DP15	0.000625	0.006	0.15	0.014	0.006	1.2E-05	6.75E-06	3.57E-06	0.0000054	8.1E-05	0.000036	0.000045	21677.205	0.49837027
Y08AP26	0.01	0.041	1	0.09	0.045	0.00405	0.002205	0.0011899	0.001845	0.00405	0.001845	0.002205	79725.352	1.83292748
Y08AP30	0.000625	0.041	1	0.09	0.045	0.00405	0.002205	0.0011899	0.001845	0.00405	0.001845	0.002205	66437.797	1.52743965
Y08BP20	0.0025	0.025	0.6	0.054	0.027	0.00087	0.0004698	0.000257	0.000405	0.00146	0.000675	0.000783	58438.863	1.34353998
Y08BP26	0.01	0.025	0.6	0.054	0.027	0.00087	0.0004698	0.000257	0.000405	0.00146	0.000675	0.000783	75970.523	1.746602
Y08BP30	0.000625	0.025	0.6	0.054	0.027	0.00087	0.0004698	0.000257	0.000405	0.00146	0.000675	0.000783	44413.535	1.02109037
Y08CP20	0.0025	0.025	0.3	0.027	0.014	0.00011	8.1E-06	3.213E-05	0.0001013	0.00036	0.000338	0.000027	30579.43	0.70303707
Y08CP26	0.01	0.025	0.3	0.027	0.014	0.00011	8.1E-06	3.213E-05	0.0001013	0.00036	0.000338	0.000027	21842.449	0.50216931
Y08CP30	0.000625	0.013	0.3	0.027	0.014	0.00011	0.0000567	3.213E-05	5.265E-05	0.00036	0.000176	0.000189	14328.647	0.32942308
Y08DP20	0.0025	0.006	0.15	0.014	0.006	1.2E-05	6.75E-06	3.57E-06	0.0000054	8.1E-05	0.000036	0.000045	17643.078	0.40562358
Y08DP26	0.01	0.006	0.15	0.014	0.006	1.2E-05	6.75E-06	3.57E-06	0.0000054	8.1E-05	0.000036	0.000045	17643.078	0.40562358
Y08DP30	0.000625	0.006	0.15	0.014	0.006	1.2E-05	6.75E-06	3.57E-06	0.0000054	8.1E-05	0.000036	0.000045	17643.078	0.40562358

Spec. No	ROL- m/s	Crk Len. m	Len. m	Hght - m	Width m	Volume m3	Uncrked Vol. m3	Hght*Wdth *Effc. Len. m3	Cracked Volume m3	Height* Wdth m2	Crack Length *Wdth m2	(Hght-Crk Len.) *Wdth m2	FT - Pa	Normalised FT - Pa
Y12AP20	0.0025	0.041	1	0.09	0.045	0.00405	0.002205	0.0011899	0.001845	0.00405	0.001845	0.002205	77067.844	1.77182999
Y12AP26	0.01	0.041	1	0.09	0.045	0.00405	0.002205	0.0011899	0.001845	0.00405	0.001845	0.002205	57579.422	1.32378099
Y12AP30	0.000625	0.041	1	0.09	0.045	0.00405	0.002205	0.0011899	0.001845	0.00405	0.001845	0.002205	58465.258	1.34414682
Y12BP20	0.0025	0.025	0.6	0.054	0.027	0.00087	0.0004698	0.000257	0.000405	0.00146	0.000675	0.000783	39738.43	0.91360726
Y12BP26	0.01	0.025	0.6	0.054	0.027	0.00087	0.0004698	0.000257	0.000405	0.00146	0.000675	0.000783	70126.641	1.6122481
Y12BP30	0.000625	0.025	0.6	0.054	0.027	0.00087	0.0004698	0.000257	0.000405	0.00146	0.000675	0.000783	42075.984	0.96734885
Y12CP20	0.0025	0.013	0.3	0.027	0.014	0.00011	0.0000567	3.213E-05	5.265E-05	0.00036	0.000176	0.000189	22716.148	0.52225611
Y12CP26	0.01	0.013	0.3	0.027	0.014	0.00011	0.0000567	3.213E-05	5.265E-05	0.00036	0.000176	0.000189	59411.465	1.36590061
Y12CP30	0.000625	0.013	0.3	0.027	0.014	0.00011	0.0000567	3.213E-05	5.265E-05	0.00036	0.000176	0.000189	22716.148	0.52225611
Y12DP20	0.0025	0.006	0.15	0.014	0.006	1.2E-05	6.75E-06	3.57E-06	0.0000054	8.1E-05	0.000036	0.000045	14396.246	0.33097722
Y12DP26	0.01	0.006	0.15	0.014	0.006	1.2E-05	6.75E-06	3.57E-06	0.0000054	8.1E-05	0.000036	0.000045	14396.246	0.33097722
Y12DP30	0.000625	0.006	0.15	0.014	0.006	1.2E-05	6.75E-06	3.57E-06	0.0000054	8.1E-05	0.000036	0.000045	19490.303	0.44809225
Y20AP20	0.0025	0.041	1	0.09	0.045	0.00405	0.002205	0.0011899	0.001845	0.00405	0.001845	0.002205	111969.84	2.57424501
Y20AP26	0.01	0.041	1	0.09	0.045	0.00405	0.002205	0.0011899	0.001845	0.00405	0.001845	0.002205	132875.59	3.05487931
Y20AP30	0.000625	0.041	1	0.09	0.045	0.00405	0.002205	0.0011899	0.001845	0.00405	0.001845	0.002205	107186.31	2.4642693
Y20BP20	0.0025	0.025	0.6	0.054	0.027	0.00087	0.0004698	0.000257	0.000405	0.00146	0.000675	0.000783	726.202	0.01669576
Y20BP26	0.01	0.025	0.6	0.054	0.027	0.00087	0.0004698	0.000257	0.000405	0.00146	0.000675	0.000783	408.489	0.00939138
Y20BP30	0.000625	0.025	0.6	0.054	0.027	0.00087	0.0004698	0.000257	0.000405	0.00146	0.000675	0.000783	530.128	0.01218792
Y20CP20	0.0025	0.013	0.3	0.027	0.014	0.00011	0.0000567	3.213E-05	5.265E-05	0.00036	0.000176	0.000189	392.124	0.00901514
Y20CP26	0.01	0.013	0.3	0.027	0.014	0.00011	0.0000567	3.213E-05	5.265E-05	0.00036	0.000176	0.000189	226.125	0.00519873
Y20CP30	0.000625	0.013	0.3	0.027	0.014	0.00011	0.0000567	3.213E-05	5.265E-05	0.00036	0.000176	0.000189	254.881	0.00585985
Y20DP20	0.0025	0.006	0.15	0.014	0.006	1.2E-05	6.75E-06	3.57E-06	0.0000054	8.1E-05	0.000036	0.000045	31530.48	0.7249022
Y20DP26	0.01	0.006	0.15	0.014	0.006	1.2E-05	6.75E-06	3.57E-06	0.0000054	8.1E-05	0.000036	0.000045	32023.145	0.73622883
Y20DP30	0.000625	0.006	0.15	0.014	0.006	1.2E-05	6.75E-06	3.57E-06	0.0000054	8.1E-05	0.000036	0.000045	21677.205	0.49837027
Z08AP40	0.0025	0.041	1	0.09	0.045	0.00405	0.002205	0.0011899	0.001845	0.00405	0.001845	0.002205	106300.47	2.4439033
Z08AP41	0.0025	0.041	1	0.09	0.045	0.00405	0.002205	0.0011899	0.001845	0.00405	0.001845	0.002205	119588.03	2.74939129
Z08AP46	0.01	0.041	1	0.09	0.045	0.00405	0.002205	0.0011899	0.001845	0.00405	0.001845	0.002205	35433.492	0.81463449
Z08AP50	0.000625	0.041	1	0.09	0.045	0.00405	0.002205	0.0011899	0.001845	0.00405	0.001845	0.002205	99656.688	2.29115931
Z08BP40	0.0025	0.025	0.6	0.054	0.027	0.00087	0.0004698	0.000257	0.000405	0.00146	0.000675	0.000783	90580.242	2.08248707
Z08BP41	0.0025	0.025	0.6	0.054	0.027	0.00087	0.0004698	0.000257	0.000405	0.00146	0.000675	0.000783	52594.98	1.20918606
Z08BP46	0.000625	0.025	0.6	0.054	0.027	0.00087	0.0004698	0.000257	0.000405	0.00146	0.000675	0.000783	49673.039	1.14200911
Z08BP50	0.000625	0.025	0.6	0.054	0.027	0.00087	0.0004698	0.000257	0.000405	0.00146	0.000675	0.000783	80645.633	1.85408522

Spec. No	ROL- m/s	Crk Len. m	Len. m	Hght - m	Width m	Volume m3	Uncrked Vol. m3	Hght*Wdth *Effc. Len. m3	Cracked Volume m3	Height* Wdth m2	Crack Length *Wdth m2	(Hght-Crk Len.) *Wdth m2	FT - Pa	Normalised FT - Pa
Z08CP40	0.0025	0.025	0.3	0.027	0.014	0.00011	8.1E-06	3.213E-05	0.0001013	0.00036	0.000338	0.000027	45432.297	1.04451224
Z08CP41	0.0025	0.025	0.3	0.027	0.014	0.00011	8.1E-06	3.213E-05	0.0001013	0.00036	0.000338	0.000027	15289.715	0.35151853
Z08CP46	0.01	0.025	0.3	0.027	0.014	0.00011	8.1E-06	3.213E-05	0.0001013	0.00036	0.000338	0.000027	26210.941	0.60260322
Z08CP50	0.000625	0.013	0.3	0.027	0.014	0.00011	0.0000567	3.213E-05	5.265E-05	0.00036	0.000176	0.000189	26210.941	0.60260322
Z08DP40	0.0025	0.006	0.15	0.014	0.006	1.2E-05	6.75E-06	3.57E-06	0.0000054	8.1E-05	0.000036	0.000045	36088.113	0.82968457
Z08DP41	0.0025	0.006	0.15	0.014	0.006	1.2E-05	6.75E-06	3.57E-06	0.0000054	8.1E-05	0.000036	0.000045	14034.267	0.32265513
Z08DP46	0.01	0.006	0.15	0.014	0.006	1.2E-05	6.75E-06	3.57E-06	0.0000054	8.1E-05	0.000036	0.000045	8821.539	0.20281179
Z08DP50	0.000625	0.006	0.15	0.014	0.006	1.2E-05	6.75E-06	3.57E-06	0.0000054	8.1E-05	0.000036	0.000045	17643.078	0.40562358
Z12AP40	0.0025	0.041	1	0.09	0.045	0.00405	0.002205	0.0011899	0.001845	0.00405	0.001845	0.002205	60945.605	1.40117129
Z12AP41	0.0025	0.041	1	0.09	0.045	0.00405	0.002205	0.0011899	0.001845	0.00405	0.001845	0.002205	63780.285	1.46634206
Z12AP46	0.01	0.041	1	0.09	0.045	0.00405	0.002205	0.0011899	0.001845	0.00405	0.001845	0.002205	44469.031	1.02236625
Z12AP50	0.000625	0.041	1	0.09	0.045	0.00405	0.002205	0.0011899	0.001845	0.00405	0.001845	0.002205	106300.47	2.4439033
Z12BP40	0.0025	0.025	0.6	0.054	0.027	0.00087	0.0004698	0.000257	0.000405	0.00146	0.000675	0.000783	36232.094	0.83299477
Z12BP41	0.0025	0.025	0.6	0.054	0.027	0.00087	0.0004698	0.000257	0.000405	0.00146	0.000675	0.000783	67789.086	1.55850649
Z12BP46	0.01	0.025	0.6	0.054	0.027	0.00087	0.0004698	0.000257	0.000405	0.00146	0.000675	0.000783	37400.875	0.85986565
Z12BP50	0.000625	0.025	0.6	0.054	0.027	0.00087	0.0004698	0.000257	0.000405	0.00146	0.000675	0.000783	43104.508	0.99099515
Z12CP40	0.0025	0.013	0.3	0.027	0.014	0.00011	0.0000567	3.213E-05	5.265E-05	0.00036	0.000176	0.000189	41937.504	0.96416512
Z12CP41	0.0025	0.013	0.3	0.027	0.014	0.00011	0.0000567	3.213E-05	5.265E-05	0.00036	0.000176	0.000189	55916.672	1.28555349
Z12CP46	0.01	0.013	0.3	0.027	0.014	0.00011	0.0000567	3.213E-05	5.265E-05	0.00036	0.000176	0.000189	31453.129	0.72312386
Z12CP50	0.000625	0.013	0.3	0.027	0.014	0.00011	0.0000567	3.213E-05	5.265E-05	0.00036	0.000176	0.000189	22716.148	0.52225611
Z12DP40	0.0025	0.006	0.15	0.014	0.006	1.2E-05	6.75E-06	3.57E-06	0.0000054	8.1E-05	0.000036	0.000045	14396.246	0.33097722
Z12DP41	0.0025	0.006	0.15	0.014	0.006	1.2E-05	6.75E-06	3.57E-06	0.0000054	8.1E-05	0.000036	0.000045	23919.916	0.54993136
Z12DP46	0.01	0.006	0.15	0.014	0.006	1.2E-05	6.75E-06	3.57E-06	0.0000054	8.1E-05	0.000036	0.000045	4872.576	0.11202307
Z12DP50	0.000625	0.006	0.15	0.014	0.006	1.2E-05	6.75E-06	3.57E-06	0.0000054	8.1E-05	0.000036	0.000045	19490.303	0.44809225
Z20AP40	0.0025	0.041	1	0.09	0.045	0.00405	0.002205	0.0011899	0.001845	0.00405	0.001845	0.002205	124017.22	2.85122064
Z20AP41	0.0025	0.041	1	0.09	0.045	0.00405	0.002205	0.0011899	0.001845	0.00405	0.001845	0.002205	26575.117	0.61097582
Z20AP46	0.01	0.041	1	0.09	0.045	0.00405	0.002205	0.0011899	0.001845	0.00405	0.001845	0.002205	39862.676	0.91646374
Z20AP50	0.000625	0.041	1	0.09	0.045	0.00405	0.002205	0.0011899	0.001845	0.00405	0.001845	0.002205	59351.098	1.36451274
Z20BP40	0.0025	0.025	0.6	0.054	0.027	0.00087	0.0004698	0.000257	0.000405	0.00146	0.000675	0.000783	450.245	0.01035137
Z20BP41	0.0025	0.025	0.6	0.054	0.027	0.00087	0.0004698	0.000257	0.000405	0.00146	0.000675	0.000783	234.2	0.00538438
Z20BP46	0.01	0.025	0.6	0.054	0.027	0.00087	0.0004698	0.000257	0.000405	0.00146	0.000675	0.000783	588.224	0.01352358
Z20BP50	0.000625	0.025	0.6	0.054	0.027	0.00087	0.0004698	0.000257	0.000405	0.00146	0.000675	0.000783	334.053	0.00768005

Spec. No	ROL- m/s	Crk Len. m	Len. m	Hght - m	Width m	Volume m3	Uncrked Vol. m3	Hght*Wdth *Effc. Len. m3	Cracked Volume m3	Height* Wdth m2	Crack Length *Wdth m2	(Hght-Crk Len.) *Wdth m2	FT - Pa	Normalised FT - Pa
Z20CP40	0.0025	0.013	0.3	0.027	0.014	0.00011	0.0000567	3.213E-05	5.265E-05	0.00036	0.000176	0.000189	483.62	0.01111868
Z20CP41	0.0025	0.013	0.3	0.027	0.014	0.00011	0.0000567	3.213E-05	5.265E-05	0.00036	0.000176	0.000189	198.676	0.00456767
Z20CP46	0.01	0.013	0.3	0.027	0.014	0.00011	0.0000567	3.213E-05	5.265E-05	0.00036	0.000176	0.000189	368.597	0.00847424
Z20CP50	0.000625	0.013	0.3	0.027	0.014	0.00011	0.0000567	3.213E-05	5.265E-05	0.00036	0.000176	0.000189	130.708	0.00300505
Z20DP40	0.0025	0.006	0.15	0.014	0.006	1.2E-05	6.75E-06	3.57E-06	0.0000054	8.1E-05	0.000036	0.000045	39413.102	0.9061278
Z20DP41	0.0025	0.006	0.15	0.014	0.006	1.2E-05	6.75E-06	3.57E-06	0.0000054	8.1E-05	0.000036	0.000045	39413.102	0.9061278
Z20DP46	0.01	0.006	0.15	0.014	0.006	1.2E-05	6.75E-06	3.57E-06	0.0000054	8.1E-05	0.000036	0.000045	32023.145	0.73622883
Z20DP50	0.000625	0.006	0.15	0.014	0.006	1.2E-05	6.75E-06	3.57E-06	0.0000054	8.1E-05	0.000036	0.000045	16011.572	0.3681144

Desired and network outputs of training data sets

Chart 2 - Training, desired and network outputs		
Spec. No.	Normalised FT - Pa	FT Network output - Pa
X12DP04	0.66195443	0.458994478
X20BP01	0.00953327	0.853312433
X20DP02	0.73622883	0.458994478
X12AP02	0.97756133	1.982278705
Z20DP46	0.73622883	0.624333382
X12BP01	1.81377907	0.853312433
Z08CP41	0.35151853	0.645701706
Y12BP30	0.96734885	0.896797061
X20AP05	1.36858593	1.982278705
X08CP15	0.52225611	0.639326215
Z12BP41	1.55850649	0.853312433
X12BP03	1.10707699	0.853312433
Z20BP50	0.00768005	0.896797061
X08AP11	3.56402597	2.219578266
X12BP02	1.89170436	0.853312433
X12DP11	0.43281638	0.624333382
Z08BP41	1.20918606	0.853312433
Y12CP20	0.52225611	0.609021306
Y12DP26	0.33097722	0.624333382
Y08BP30	1.02109037	0.896797061
X20CP15	0.00300505	0.600313544
Y12AP20	1.77182999	1.982278705
X08CP09	1.04451224	0.660379171
X20CP05	0.00456767	0.609021306
Z12CP40	0.96416512	0.609021306
X20CP10	0.00390657	0.651621222
X20CP11	0.00324546	0.651621222
Z12DP46	0.11202307	0.624333382
X08AP02	1.83292748	1.982278705
X12AP14	0.79426866	2.037235498
X08DP10	0.59921663	0.624333382
Y12CP26	1.36590061	0.651621222
Z08CP46	0.60260322	0.660379171
X12CP03	0.60260322	0.609021306
X12BP15	1.1608186	0.896797061
Z20DP40	0.9061278	0.458994478
X08BP14	0.96734885	0.896797061
X08DP15	0.40562358	0.439865947
Y20BP30	0.01218792	0.896797061
X08CP01	1.10477247	0.645701706
Y20BP26	0.00939138	0.91926378
Z20AP40	2.85122064	1.982278705
Z08AP41	2.74939129	1.982278705
Y12AP30	1.34414682	2.037235498
Y20DP26	0.73622883	0.624333382

Desired and network outputs of training data sets

Spec. No.	Normalised FT - Pa	FT Network output - Pa
Z08AP40	2.4439033	1.982278705
X20DP14	0.50969687	0.439865947
X08DP05	0.2996083	0.458994478
X12AP03	3.66585494	1.982278705
X08DP09	0.40562358	0.624333382
X08CP03	0.76329736	0.645701706
Y20AP26	3.05487931	2.219578266
X08CP02	0.60260322	0.645701706
X08AP03	1.80237864	1.982278705
X08CP10	1.56676834	0.660379171
X12DP14	0.44809225	0.439865947
X08CP05	0.70303707	0.645701706
Z08DP41	0.32265513	0.458994478
Z20CP40	0.01111868	0.609021306
Z12BP46	0.85986565	0.91926378
X08BP03	0.85986565	0.853312433
Z20AP50	1.36451274	2.037235498
Z20BP46	0.01352358	0.91926378
Y08DP26	0.40562358	0.624333382
X12CP11	0.883818	0.651621222
X20BP02	0.00901571	0.853312433
X08CP04	1.24537988	0.645701706
X12BP05	0.64489919	0.853312433
X20BP15	0.0063444	0.896797061
X12AP09	2.76975713	2.219578266
Z12AP41	1.46634206	1.982278705
Z20DP50	0.3681144	0.439865947
Y12BP20	0.91360726	0.853312433
Z20BP41	0.00538438	0.853312433
X08DP04	0.46093586	0.458994478
X20DP05	0.4530639	0.458994478
X12CP14	0.68295029	0.600313544
X08DP03	0.51624818	0.458994478
X20CP04	0.00261439	0.609021306
X12DP01	0.76379355	0.458994478
X12DP02	0.54993136	0.458994478
X12DP03	0.66195443	0.458994478
X08AP14	2.30134248	2.037235498
X08DP02	0.69140382	0.458994478
Y08CP30	0.32942308	0.600313544
X12CP02	1.00433862	0.609021306
X20AP09	2.45408631	2.219578266
X08BP09	1.06139662	0.91926378
X20BP04	0.00834788	0.853312433
X08BP15	1.6122481	0.896797061
Z12BP50	0.99099515	0.896797061

Desired and network outputs of training data sets

Spec. No.	Normalised FT - Pa	FT Network output - Pa
Z08DP40	0.82968457	0.458994478
X12DP09	0.66195443	0.624333382
X20CP01	0.00646084	0.609021306
X20AP03	2.88380575	1.982278705
X20CP03	0.00459771	0.609021306
Y12BP26	1.6122481	0.91926378
X08BP11	2.41837214	0.91926378
X08AP09	2.54573281	2.219578266
Z12CP50	0.52225611	0.600313544
Y12CP30	0.52225611	0.600313544
Z12AP50	2.4439033	2.037235498
Z20CP50	0.00300505	0.600313544
Y08DP20	0.40562358	0.458994478
X08BP05	0.59115765	0.853312433
X08DP01	0.49781072	0.458994478
Z08AP46	0.81463449	2.219578266
Y08CP20	0.70303707	0.645701706
X12CP10	0.84364448	0.651621222
Z08BP50	1.85408522	0.896797061
Y08DP30	0.40562358	0.439865947
Z12CP41	1.28555349	0.609021306
Z08BP40	2.08248707	0.853312433
Z12AP46	1.02236625	2.219578266
X12AP11	1.75961034	2.219578266
Y08AP26	1.83292748	2.219578266

Related to Figure 8-3 and Table 8-5

Desired and network outputs of cross validation data sets

Chart 3 - Cross Validation desired and network outputs		
Sper No	Normalised FT - Pa	FT Network output - Pa
X12BP10	1.236056877	0.91926378
X20AP14	2.417427739	2.037235498
Z20AP46	0.916463741	2.219578266
X20BP05	0.009516582	0.853312433
X20AP15	1.894024957	2.037235498
Y20DP20	0.724902203	0.458994478
X20BP10	0.011687025	0.91926378
X20AP11	1.405244406	2.219578266
Y08CP26	0.502169311	0.660379171
X12BP11	2.042180733	0.91926378
X12CP01	1.20520647	0.609021306
X12BP04	0.80612404	0.853312433
X12BP14	1.182315267	0.896797061
Y20BP20	0.016695763	0.853312433
Z12DP50	0.448092246	0.439865947
X20CP09	0.005559338	0.651621222
Y20DP30	0.498370265	0.439865947
X20CP02	0.003245457	0.609021306
X12AP15	2.443903303	2.037235498
Z08BP46	1.142009111	0.896797061
X12AP01	2.932684129	1.982278705
X20BP03	0.005843524	0.853312433
Z20BP40	0.010351368	0.853312433
Y08BP26	1.746602003	0.91926378
X08AP15	2.291159307	2.037235498
X08AP10	2.240244819	2.219578266
Z20AP41	0.61097582	1.982278705
Y20AP20	2.574245011	1.982278705
Z08DP50	0.405623578	0.439865947
X12CP09	1.305640291	0.651621222
Y08BP20	1.343539983	0.853312433
X08DP14	0.193593072	0.439865947
Y12DP30	0.448092246	0.439865947
Z08AP50	2.291159307	2.037235498
X12CP04	0.341475147	0.609021306
X08BP02	1.477893997	0.853312433

169

Desired and network outputs of Testing data sets

Chart 4 - (test) Forecasted, desired and network outputs		
Spec No.	Normalised FT Pa	FT Network output Pa
X08BP04	1.20918606	0.853312433
X20AP01	2.4439033	1.982278705
X20DP15	0.49837027.	0.439865947
X20AP02	1.87365931	1.982278705
X08CP14	0.28924956	0.639326215
X08CP11	0.60260322	0.660379171
Z20CP41	0.00456767	0.609021306
Y20CP30	0.00585985	0.600313544
X12AP10	3.58439161	2.219578266
Z12BP40	0.83299477	0.853312433
X12AP05	1.83292748	1.982278705
Y20AP30	2.4642693	2.037235498
X20DP01	0.59464637	0.458994478
X12AP04	1.36858593	1.982278705
X20BP14	0.00717918	0.896797061
Z12CP46	0.72312386	0.651621222
Z12DP40	0.33097722	0.458994478
X20AP10	2.19951297	2.219578266
X08AP04	1.01829306	1.982278705
X20CP14	0.00300505	0.600313544
X20DP10	0.62296283	0.624333382
Z08DP46	0.20281179	0.624333382
Z12DP41	0.54993136	0.458994478
X08BP10	0.91360726	0.91926378
X08AP01	3.97134296	1.982278705
X20BP11	0.01352358	0.91926378
X12DP05	0.33097722	0.458994478
Y20CP26	0.00519873	0.651621222
Z08CP40	1.04451224	0.645701706
X20DP09	0.62296283	0.624333382
X20BP09	0.00676179	0.91926378
Y12AP26	1.32378099	2.219578266
Y20CP20	0.00901514	0.609021306
X20AP04	3.89802581	1.982278705
Z12AP40	1.40117129	1.982278705
Z08CP50	0.60260322	0.600313544
Z20DP41	0.9061278	0.458994478
X20DP11	0.73622883	0.624333382
X08DP11	0.40562358	0.624333382
Z20CP46	0.00847424	0.651621222
Y08AP30	1.52743965	2.037235498
X12DP15	0.66195443	0.439865947
X12BP09	1.88095593	0.91926378
X12CP15	1.48642123	0.600313544
X12CP05	0.70303707	0.609021306
Y12DP20	0.33097722	0.458994478
X12DP10	0.56011531	0.624333382